The Synthesis and Photochemistry of Nitric Oxide containing Organometallic Compounds of Iron.

A Thesis presented for the degree of Master of Science

by

Kieran Maher B. Sc. (Hons.)

under the supervision of Dr. Mary Pryce and Prof. Conor Long

at

DUBLIN CITY UNIVERSITY
School of Chemical Sciences
December 2001

...another average day in the lab

"If we can live in our modern world with the ancient dreams that have always stirred us, then our work will have been done"

Sigurd F. Olson

Declaration

I hereby certify that this material, which I now submit for assessment on the programme of study leading to the award of M. Sc. is entirely my own work and has not been taken from the work of others save and to the extent that such work has been cited and acknowledged within the text of my work.

Signed: Kieran Mackey **ID No.:** 98970631

Date: 11th February 02

Dedication

To my parents, for the support, patience and love that will be hard to repay.

Acknowledgements

I would like to offer my sincerest gratitude to my supervisors Dr. Mary Pryce and Prof. Conor Long for the opportunity to carry out the research, for their support, advice, guidance and assistance throughout the last couple of years.

My thanks to all the technical staff, Mick, Maurice, Ambrose, Damien, Vinny, Veronica and John for their very generous help in various ways.

I would like to thank Dr. Siobhan O' Keeffe, easily the post-doc with the best musical taste in the world, for her help, advice and assistance. Thanks to those who were there when I arrived, Peter, Davnat and (Dr.) Bronagh, for showing me the way to do things, some more textbook than others, but you have to live and learn. Thanks to Peter for the education on sectarianism, Jane's Defence Weekly, The Who/Meatloaf (easy mistake) and the merits of Scottish/Celtic football (though I'll probably never learn). Thanks to Davnat for the advice, friendship and good training. Thanks to Kevin Kincaid for his help and advice, especially in relation to computers (goes without saying) and life in the big bad world. Thanks to Karl (the big lump), Kevin (ninja boy) and Jennifer (quiet but deadly sarcastic) for the laughs, the entertainment, the few quiet ales and the help. Thanks to Johnny for knowing way too much about UV and music. Thanks to Claire for the Cooley peninsula, and all those dodgy farmer stories. I consider myself lucky to have met all of you.

Thanks to the old AG07 gang, Ben, Colm, Ger, Ollie, honorary member Carol and last but certainly not least Mairead (one of the good ones). It was a pretty good introduction to post grad life. Thank you all. Thanks to everybody in X246, Adrian (thanks for all the laughs, they were good old times), Dec, Helen, Marco (Dr. Duati, - the time will come one day when you might beat me at squash, though I may retire), (Dr.) Moss, (Dr.) Scott, Wes, the Fiona's (twice the fun). For the rest of my year who have made it this far or further, Rob, Ray, Jenny, Edna, the best of luck. Thanks for the laughs. Thanks to Darren, Dave (David) Savage, Lorraine, Eimear and the other countless other post grads for the laughs and the good times.

To the most important person in my life, Sabrina, thank you for your love, support, friendship, and patience. I know it hasn't always been easy watching me trying to do this. Thanks for the good times, the better times and everything in between. Thank you for coming along when you did, your (our?) timing was perfect.

Thanks to my parents, for their support, psychological, financial and a million other ways. Thanks for believing in me, and for the sacrifices made to allow us kids to study. Thanks to Declan and Anne-Marie. Special thanks to Dec, for always showing me the way and being a good older brother to a pesky little brother.

I dedicate this thesis to you all.

Table of Contents

Chapter 1

The Synthesis and Photochemistry of Nitric Oxide containing Organometallic Compounds of Iron.

Kieran Maher

Abstract

Nitric oxide has been shown in the recent past to have an important role in many biological systems, including an essential role in neurotransmission, blood clotting, and in combating tumour cells and intracellular parasites. This thesis investigates the photochemistry of a series of compounds containing NO as a ligand. The aim of this work is to investigate the possibility that NO could be released under photochemical conditions at specific biological sites, thus providing a novel means of location specific therapy.

Chapter 1 is a general overview of the history of organometallic chemistry, including a description of the current bonding models in the type of complexes under investigation. This chapter also includes a literature survey of different types of organometallic compounds containing NO ligands, their chemistry and photochemistry.

Chapter 2 describes the photochemistry of compounds of the type (η^3-allyl) Fe $(CO)_2NO$, and (η^3-2-chloroallyl) Fe $(CO)_2NO$. Ultraviolet/visible monitored flash-photolysis studies and infrared monitored steady state photolysis were used to identify the primary photo-process, namely CO-loss. Matrix isolation was also used to investigate the photochemistry of (η^3-allyl) Fe $(CO)_2NO$ and to characterise the primary photoproducts. The photochemistry of (η^3-allyl) Fe $CO(NO)PPh_3$ and (η^3-allyl) Fe $(PPh_3)_2NO$ was also investigated. No evidence for loss of NO was observed with these systems however. The photochemistry of $Fe(PPh_3)_2(NO)_2$ is also described.

Chapter 3 contains the experimental procedures and techniques used in the synthesis and the analysis of the compounds used in this work

1 Introduction and Literature Survey

1.1 Introduction to Organometallic Chemistry

Organometallic chemistry can be defined as a study of the interaction of metallic molecules with organic and inorganic ligands. It can be regarded as an intermediate between classical inorganic and organic chemistry. Organometallic complexes have been known for almost two hundred years, with the first synthetic organometallic compound, $K[PtCl_3(C_2H_4)]$, prepared by the Danish pharmacist William C. Zeise in 1827, though the structure and nature of the bonding was unclear.[1] It was his fellow countryman, SM Jörgensen and Alfred Werner, from Switzerland, who between the 1870's and 1915, discovered many metal complexes and developed the theory of co-ordination complexes.

The first metal carbonyls $Ni(CO)_4$ and $Fe(CO)_5$, were discovered in 1890 and 1891 respectively, by Mond.[2] Mond subsequently developed an industrial process to isolate pure nickel by the thermal decomposition of $Ni(CO)_4$.

The development of organometallic chemistry has seen major advances in the past fifty years. These advances have stemmed from discoveries in the early 1950's, in particular the discovery of ferrocene by Kealy and Pauson.[3] They were the first to report the structure of ferrocene, they incorrectly assigned a σ-bonding structure. Somewhat surprisingly, two independent research groups, in London[4] and Munich[5] prepared and correctly assigned the sandwich structure of ferrocene at approximately the same time in 1952. For this discovery, Wilkinson and Fischer were jointly awarded the Nobel Prize for Chemistry in 1973. Since the 1950s,

organometallic chemistry has become a very active and wide-ranging field, marked by the discovery of new organometallic compounds along with their detailed structural and chemical characterisation, and their application as synthetic intermediates and catalysts in industrial processes.

1.2 Bonding in Organometallic Complexes

Transition metals can form complexes with a variety of neutral molecules, including carbon monoxide, isocyanides, nitric oxide, substituted phosphines, and various molecules with de-localised π-orbitals such as pyridine, 2,2'-bipyryidine and 1, 10-phenanthroline. The metal atoms in organometallic complexes are in low positive, zero, or negative formal oxidation states, with a partially filled d-orbital. The ligands mentioned above, in addition to having lone pairs, have the ability to stabilise low oxidation states, due to their vacant π*-orbitals. The lone pair forms a σ-bond with the metal. The vacant π*-orbitals of the ligand have the ability to accept electron density from filled metal d-orbitals. In this way, the bond between a metal and a ligand consists of both a σ-bond (donor-acceptor bond), with electron donation from the ligand to the metal, and a π-bond, with electron density transferring from the metal to the ligand (back bond).

1.2.1 Bonding in Metal-Carbonyl Complexes

The bonding of CO to a metal can be understood as consisting of a ligand to metal σ bond and metal to ligand π-backbonding. In order to form a metal carbonyl bond,

the metal must have vacant d-orbitals to accept the electrons donated by the CO molecule, but also occupied d-orbitals in order to donate electrons to the CO ligand. The ligand to metal σ bonding results from the lone pair of CO, localised around the carbon transferring its electron density to a vacant d-orbital of the metal, resulting in the formation of a donor-acceptor σ bond. This electron transfer makes the metal more electron rich. In order to compensate for this extra electron density, a metal d-orbital interacts with an empty π* orbital of the CO, thus relieving itself of the added electron density, and increasing the strength of the bond. This is shown in Figure 1.1 using a simple MO diagram.

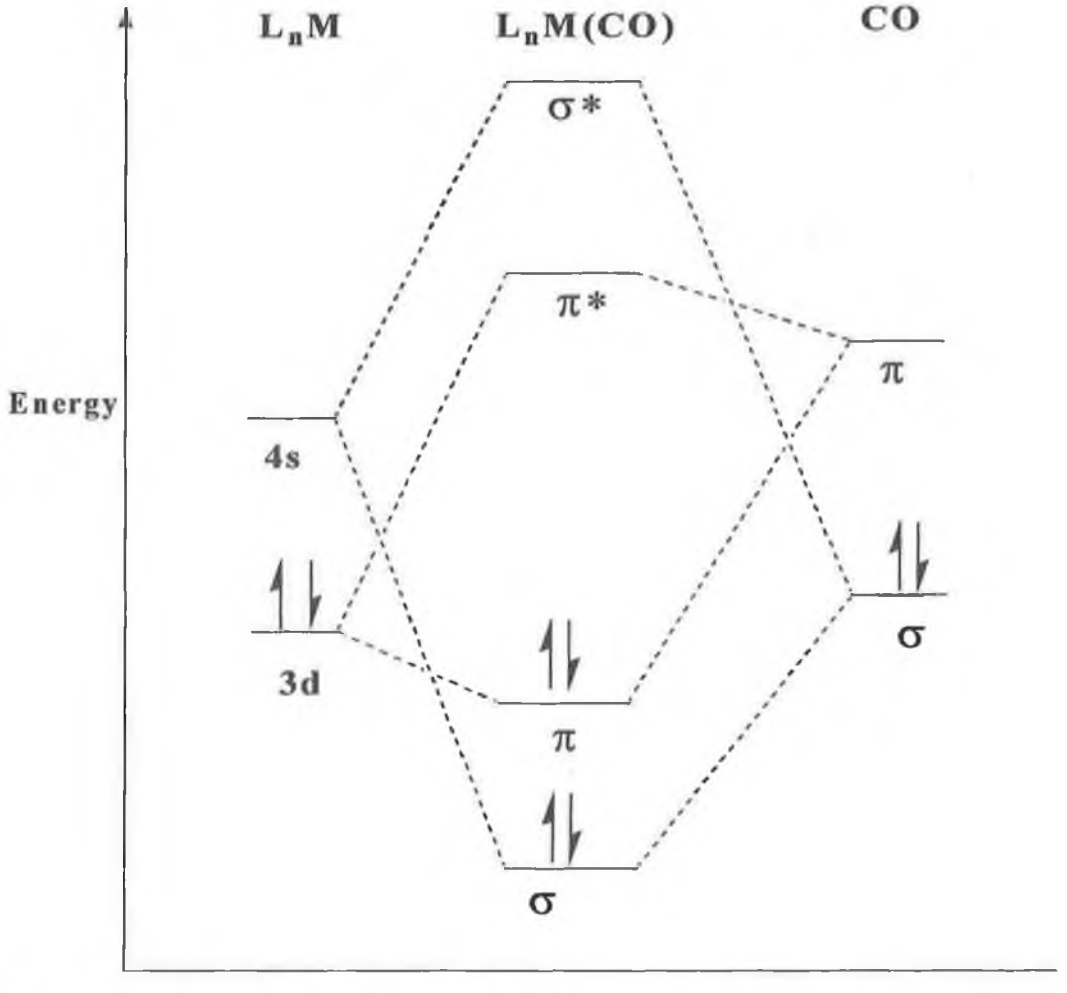

Figure 1.1 Molecular orbital diagram for $L_5M(CO)$.

The greater the backbonding, i.e. the greater the donation of electron density from the metal to the CO antibonding orbitals, the more the bond-order of CO is reduced. The extent of back donation from the metal to ligand affects the strength of the CO bond. The more back donation present the greater the strength of the M-C bond, as the π^* orbital of the CO is a bonding orbital with respect to the M-C. However, this π^* orbital is anti-bonding with respect to the C-O bond. When this orbital becomes more populated, the strength of the C-O bond is weakened and the bond length is increased. This has a direct effect upon the stretching frequencies of terminal CO groups in metal carbonyls, shifting them to lower frequency. We can therefore conclude that, the greater the M-CO π-backbonding the lower the frequency of CO stretching.

1.2.2 Bonding in Metal-Nitrosyl Complexes

1.2.2.1 Bonding in Nitric Oxide

The nitric oxide (NO) molecule is paramagnetic, due to the anti-bonding electron with the electron configuration of:

$$(\sigma_1)^2(\sigma_1^*)^2\ (\sigma_2)^2(\sigma_2^*)^2\ (\sigma_3)^2(\pi)^4(\pi^*)^1$$

The electron in the π^* orbital is lost relatively easily, to form the nitrosonium ion, NO^+. As this electron is removed from the π^*, anti-bonding orbital, the bond becomes stronger. The bond-order is increased from formally 2.5 (i.e. (10 bonding electrons – 5 anti- bonding electrons)/2 = 2.5) to 3 and the bond length is reduced

from 1.15 Å to 1.06 Å in NO^+. The molecular orbital diagram for NO is shown in Figure 1.2

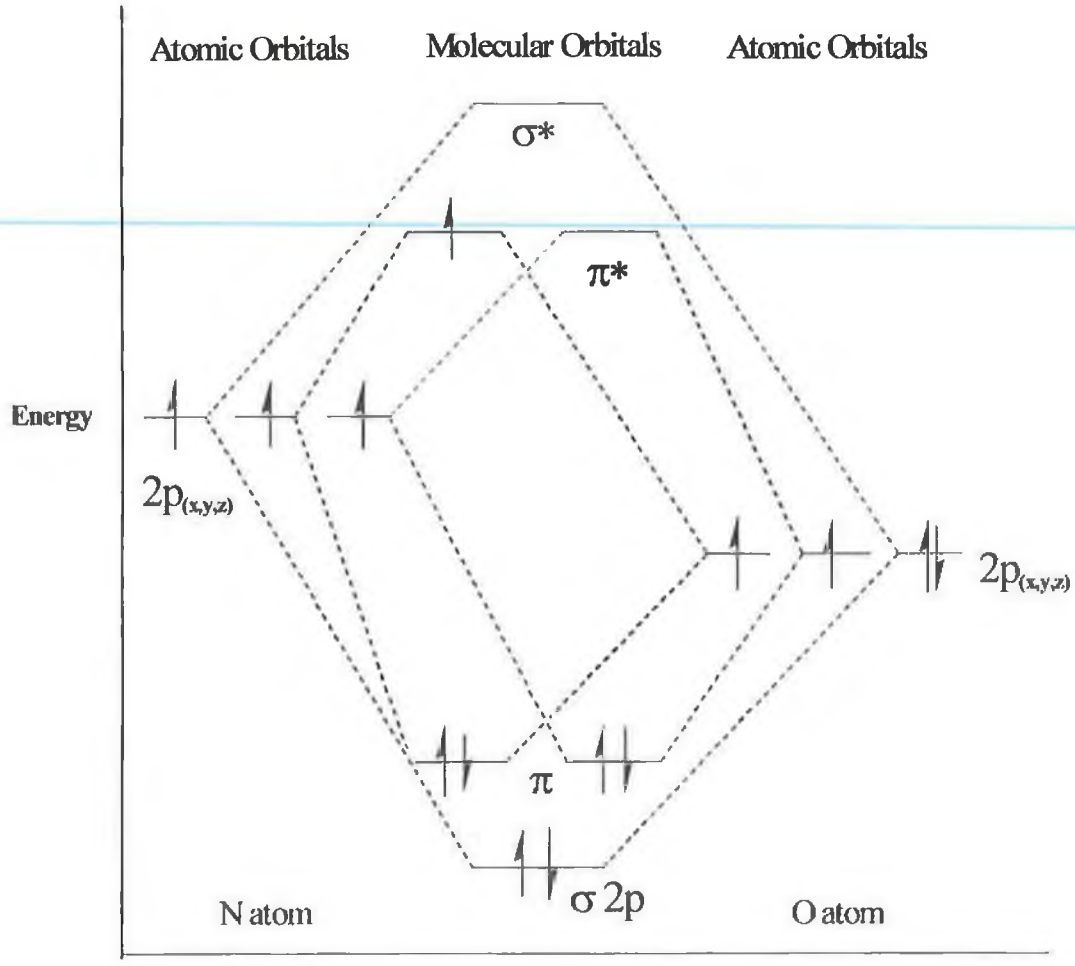

Figure 1.2 Molecular orbital diagram for NO molecule. Molecular orbitals arising from 1s and 2s electrons are excluded for simplicity.

1.2.2.2 Bonding in Metal-Nitrosyl Complexes

The bonding of NO to a metal is similar to that of a metal carbonyl bond, except that NO contains one more electron, occupying the π^* orbital. NO can form a bond with a metal in one of two configurations, as a result of this extra electron. It may be formally considered a three electron donor, resulting in a linear M-N-O configuration, or as a one electron donor resulting in a bent M-N-O configuration.

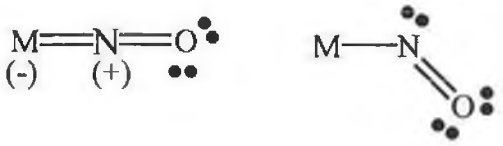

Figure 1.3 Linear and Bent forms of the M-N-O group.

As with a metal carbonyl bond, in order to form a metal nitrosyl bond, the metal must have vacant d-orbitals to accept the electrons donated by the NO molecule. It must also have occupied d-orbitals in order to donate electrons to the NO ligand. The ligand to metal σ bonding results from donation of the lone pair of NO to a vacant d-orbital of the metal, forming a donor-acceptor σ bond. This electron transfer makes the metal more electron rich. In order to compensate for this extra electron density, a metal d-orbital interacts with a π* orbital of the NO, thus relieving itself of the added electron density, and increasing the strength of the bond.

The idea that there is significant M-N π-backbonding is also supported by the vibration frequencies of M-N-O groups. Nitrogen monoxide, with it unpaired electron in a π* orbital, has a stretching frequency of 1860 cm^{-1}. Linear M-N-O groups in molecules with a small charge or no charge, have stretching frequencies between 1800 and 1900 cm^{-1}. This would indicate that between the metal d π orbital and the NO π* orbital, one electron pair is shared. Structural data suggests that M-CO and M-NO bonds are equally as strong, however substitution reactions on mixed metal carbonyl-nitrosyl compounds have yielded substitution of CO.[6]

As stated already the bent M-N-O group results from the NO being formally a one electron donor when bonding to the metal, with a lone pair localised on the nitrogen. Formally one lone-pair electron must have come from the metal, giving the NO^- co-ordination mode. The metal must have a suitable electronic configuration and partially filled co-ordination shell in order for the bond to form in this way. Transition metals, which are late in the series with a relatively large number of electrons, tend to adopt the bent mode. NO will also form single bonds to univalent groups such as alkyl radicals and halogens.

The bond angle for bent M-N-O is in the region of 120-140°, whereas in the linear M-N-O the bond angle is approximately 180°, depending on the circumstances. Examples of 'bent' M-N-O complexes include $[Co(NH_3)_5NO]Br_2$, $[Ir(CO)(Cl)(PPh_3)_2(NO)]^+$, and $IrCl_2(PPh_3)_2NO$. $[Ir(CO)(Cl)(PPh_3)_2(NO)]^+$ is formed by treating $Ir(CO)(Cl)(PPh_3)_2$ with NO^+PF_6.[7] $[Ir(CO)(Cl)(PPh_3)_2(NO)]^+$ can be considered to be an Ir^{III} compound where the Ir^I complex has donated two electrons to convert NO^+ to NO^-. The strength of the bent M-N-O is weaker than the linear M-N-O, as would be expected, due to the lower degree of backbonding in bent M-N-O.

1.2.3 Bonding in Metal-Allyl Complexes

Allyl ligands can be bound to a metal in either a de-localised π-bond or a σ-bond. The de-localised π form is considered as a three electron donor ligand, and the electron density is considered to be de-localised around the three carbon atoms.

This trihapto (η^3) form can be represented as a number of different resonance forms as shown in Figure 1.4.

Figure 1.4 Resonance forms of the unsubstituted trihapto allyl ligand.

In the trihapto form the bond angles of C-C-C is approximately 120°. The bond lengths of C-C in this form are between 1.35 and 1.4 Å. The monohapto (η^1) form is co-ordinated to the metal through only one of the carbons, forming a σ-bond between the carbon atom and the metal. It may be relatively facile to interchange between an η^1 allyl and an η^3 allyl groups.[8] (Figure 1.5).

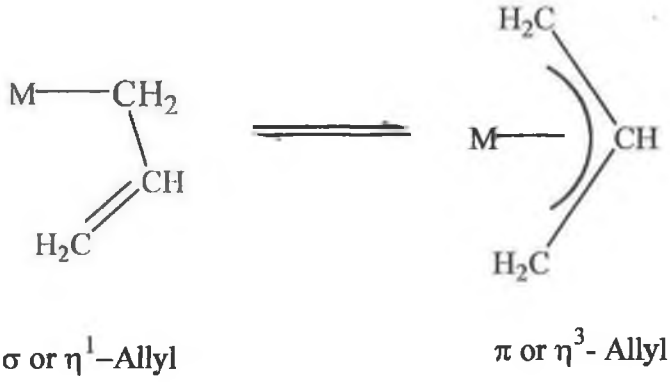

σ or η^1–Allyl π or η^3- Allyl

Figure 1.5 Transformation between η^1 allyl and η^3 allyl bound to a metal.

1.3 Study of Transients and Short lived Species

Photochemical processes involve the generation of molecules in their excited states and formation of highly reactive very short-lived intermediates. A variety of

techniques have been developed to detect the intermediates formed in photochemical reactions, some of which are described below. The advantages and disadvantages of some of the techniques are also discussed. Conventional spectrometers are not capable of recording spectra quickly enough to detect the intermediates of most photochemical reactions at room temperatures.

To counteract this fact, low temperature techniques (10-77 K) such as matrix isolation, were developed in the 1950's.[9] Due to the low temperature, the lifetime of the transient produced was prolonged so that a variety of conventional spectrometers could be used to identify the photo fragments. Solution phase flash photolysis involves the generation of a relatively high concentration of excited state molecules using a high intensity flash from a UV light source. [10] The concentration of excited molecules is measured by a second light source, at a wavelength that is absorbed by the species under investigation. Detection is most commonly by means of ultraviolet/visible (UV/vis) spectroscopy or Time Resolved infra red (TRIR) spectroscopy.

Pimentel,[11] using 'rapid scan spectroscopy' was the first to develop a method to record the infrared (IR) spectra of transient species. Today, the transients are generated by flash photolysis, and spectra recorded at different wavelengths across the absorption spectrum. Using a number of flashes, a 'point by point' spectrum may be built up corresponding to any particular time delay after the flash.

1.3.1 Low Temperature Matrix Isolation

As mentioned above, matrix isolation was developed in the early 1950's.[11] The method involves the trapping of a molecule at low temperature in a large excess of an inert solid, thus forming a matrix around the molecule. The molecule in question is surrounded by a large number of host matrix atoms or molecules in order to ensure bimolecular reactions of the molecules of interest do not occur. The most common matrix materials are the solid gases, such as the noble gases, methane and other gases such as CO and N_2. Frozen hydrocarbons and polymer films have also been used. Temperatures vary depending on the matrix material being used. Typically temperatures for a frozen gas matrix is between 10-20 K, whereas for the hydrocarbons or polymer films the temperature is maintained at 77 K. Following deposition of the sample in the matrix gas, the sample is photolysed to generate intermediates. The intermediates formed have much longer lifetimes at low temperature than they would in solution at room temperature, and can be investigated using a wide range of conventional spectroscopic techniques.

IR and UV/vis are the most commonly used techniques, but other techniques such as Raman,[12] electron spin resonance,[13] magnetic circular dichromism,[14] fluorescence,[15] and Mössbauer spectroscopy[16] have all been used in conjunction with matrix isolation to study organometallic species. Matrix isolation has proved especially effective in identifying transients of metal carbonyls. This is largely due to the intense ν_{CO} stretching bands in the IR region 2150 to 1750 cm^{-1}. When, for example free CO is generated from a metal carbonyl species, it will be observed at

approximately 2140 cm^{-1}, with corresponding depletion in the intensity of the parent CO band.

Matrix isolation does however have certain limitations. The restricted temperature range that is used and the limited diffusion possible, results in little, if any kinetic data being obtained. The solid matrix 'cage' can block certain photochemical pathways, which are observed in solution. For instance upon photolysis of $Mn_2(CO)_{10}$ in an N_2 matrix, only the CO loss product $Mn_2(CO)_9$ was observed. [17] No evidence for formation of $Mn(CO)_5$ radicals was observed, however in solution photolysis both these species were observed.[18] The other main problem with matrix isolation is that it cannot be easily used for charged species.

1.3.2 Solution Phase Flash Photolysis

Norrish and Porter were the first to develop the flash photolysis technique,[10] which ultimately led to their receiving the Nobel Prize. The basic technique involves the generation of excited state molecules using a high intensity pulse of light. The concentration of excited molecules is measured by a secondary light source, the monitoring beam, at a wavelength that is absorbed by the species under investigation. The advantages of using lasers as the light source are the short pulse duration, the monochromatic beam, and the high intensity of the beam. Detection is most commonly by means of UV/vis spectroscopy or TRIR spectroscopy. The time resolution of experiments is dependent on the duration of the flash. In the original studies,[11] the flash lamps used allowed pulses in the micro-second range, whereas now, pulsed lasers can produce flashes in the femto-second range.

1.3.2.1 Detection by UV/vis Spectroscopy

The transient species is generated as explained above in section 1.3.2, and by varying the monitoring wavelength, while maintaining the time-delay, a spectrum of the excited state may be built up point-by-point. UV/vis spectroscopy as a means of detection can be a very good source of kinetic data. The study of photochemical kinetics is possibly the most important method in determining the reaction mechanism. Understanding the properties of the transient is key to determining the rate and mechanism of the reaction. A kinetic study can lead to calculation of a rate constant for a given reaction in a particular set of conditions. UV/vis spectroscopy alone is unlikely to provide structural information for organometallic species, as the spectra are relatively insensitive to structural changes. In conjunction with other techniques however, it can be used to identify the fragments formed and the mechanism of a photochemical reaction. This lack of structural information is the major drawback of UV/vis detection.

1.3.2.2 Detection by TRIR Spectroscopy

Pimentel's rapid scan spectroscopy, the first method to record the IR spectra of transient species, was a modification of Norrish and Porter's flash photolysis technique.[11] Today, the transients are generated by flash photolysis, and spectra recorded at a particular wavelength using a tuneable IR spectrometer. This procedure is repeated at a number of different wavelengths across the spectral region of interest. In this way, a 'point by point' spectrum may be built up corresponding to any particular time delay after the flash. The spectra formed are

difference spectra, based upon the initial sample before photolysis. Therefore, if CO is generated from a metal carbonyl species, it will be observed at approximately 2140cm^{-1} (depending on solvent) as a positive absorption, and a corresponding depletion of the parent CO concentration will be observed as a negative absorption. Absorption bands due to solvents and bands due to species unaffected by photolysis do not register on a difference spectrum, as their absorbance remains constant throughout the experiment.

1.4 Chemistry of Nitric Oxide

Nitric Oxide (NO) is a relatively unstable, colourless gas. It is a 15e$^-$, paramagnetic, diatomic radical, having an electron in the π^* orbital. It is potentially toxic,[19] and is synthesised by both humans and animals. The reactions of NO and transition metals are of particular interest in biochemical systems, in surface chemistry and in the atmosphere.[20]

The discovery of NO was credited to Joseph Priestley in 1772, though his work was based largely upon the experiments of Mayow and Hayes.[21] NO was first prepared about 1620 by the Belgian scientist Jan Baptist van Helmont,[22] though he never isolated or studied it. Priestley used NO in his experiments, which investigated both combustion and respiration in plants. NO reacted with the oxygen produced by respiration to form NO_2, which is a red gas and so could be readily observed. From his experimental results Priestley concluded that air was comprised of about one fifth oxygen.[23]

The common commercial route to NO is by means of catalytic oxidation of ammonia, shown in Reaction 1.1. This is the first step in the Ostwald process, where ammonia is converted to nitric acid, for which Ostwald was awarded the Nobel Prize in 1909. This development led in turn to the large-scale synthesis of KNO_3 and NH_4NO_3, which were used in fertilisers and also in explosives.

$$4NH_3\,(g) + 5O_2(g) \xrightarrow[\sim 900°C]{\text{Pt-Rh catalyst}} 4NO\,(g) + 5H_2O\,(g)$$

Reaction 1.1 Catalytic Oxidation of NH_3 to form NO, the first step in the Ostwald Process in which nitric acid is produced industrially.

The biochemistry of NO has been extensively investigated in the past twenty years. NO has been found to play a role in neurotransmission in the central nervous system, in vasodilation - where blood pressure is decreased as a result of relaxation of the smooth muscle cells that overlay blood vessels - and the immune systems ability to kill tumour cells and intercellular parasites. Particularly, the binding of NO to heme iron centres in proteins has been shown to be a crucial step in enzymes' reactions to combat toxins and pathogens.

NO (and NO_2) is a by-product of the combustion of fossil fuels in the engines of automobiles, so there has been great interest in reactions involving NO and metal surfaces, in order to develop more efficient catalysts for use in catalytic converters.

The chemistry of NO is also a cause of concern in the atmosphere. NO is involved in reactions which cause depletion of the ozone layer in the ionosphere (upper

atmosphere). In the troposphere (lower atmosphere), in highly polluted areas, NO is implicated in production of smog (which also contains traces of metals such as titanium, lead, iron, zinc, and nickel) via photodissociation.[24] As already mentioned above, NO is produced by combustion in automobile engines, which can then react with air to form NO_2. In sunlight NO_2 undergoes dissociation to form NO and atomic O, as shown in Reaction 1.2. The potential reaction of O with O_2 to form O_3, ozone, is described by Reaction 1.3. Ozone is a strong oxidising agent. In the troposphere, ozone can damage plant life, is an irritant to eyes and can damage the respiratory systems of mammals.

Reaction 1.2 $NO_2(g) + h\upsilon \xrightarrow{393nm} NO(g) + O(g)$

Reaction 1.3 $O(g) + O_2(g) \longrightarrow O_3(g)$

On the other hand, in the upper atmosphere, NO reacts with ozone to form NO_2 and O_2 (Reaction 1.4). NO_2 then reacts with atomic O to regenerate NO and the cycle may continue (Reaction 1.5). In this way, NO effectively serves as a catalyst, increasing the rate of decomposition of ozone. Ozone may also react with elemental oxygen, resulting in O_2 (Reaction 1.6). Depletion of the ozone layer is a well-known, much publicised cause of concern, as ozone in the troposphere filters solar radiation of less than 300nm.[25]

Reaction 1.4 $O_3(g) + NO(g) \longrightarrow NO_2(g) + O_2(g)$

Reaction 1.5 $NO_2(g) + O(g) \longrightarrow NO(g) + O_2(g)$

Reaction 1.6 $O_3(g) + O(g) \longrightarrow O_2(g)$

Photochemistry of various Fe-NO complexes has been investigated,[26] primarily with biological functions in mind, however a variety of other potential uses have also been proposed. Fe-NO complexes such as nitroprussides, which undergo photo-isomerisation, are used as vasodilators to control blood pressure, but have also received interest due to their potential technical application in information storage systems.[27] It has been proposed that information could be optically written, read, stored and/or erased in such systems. [28] This holographic storage process is based on the excitation of crystalline materials to produce long-lived metastable electronic states.

1.4.1 Role of Nitric Oxide in Biological Systems

The very important role of NO in biology has only in the recent past begun to be fully appreciated. Prior to the 1980's research of NO's role in biological reactions was generally limited to a number of areas:

- as a stimulator of guanylyl cyclase
- it's role in the microbial nitrogen cycle
- it's properties as a food preservative
- it's role in carcinogenic compounds.

As early as 1916, it was reported that more nitrate was excreted in urine than was ingested, indicating an endogenous means of producing NO, [29] however the significance of this was not realised for more than 60 years.

In the intervening years, researchers believed that the nitrates present in the body were derived solely from dietary sources. In the 1950's research found that the body converts nitrites and nitrates from preserved foods to the nitrosation agent $[H_2ONO]^+$ ion, which in turn forms carcinogenic nitrosamines. [30] This led initially to a decrease in the amount of cured foodstuffs consumed. Further studies have set the daily tolerance limit at between 5 and 10g of $NaNO_2$ depending on body weight.[31] Though controversial, nitrites are still used as preservatives and do have some advantages. The addition of nitrite (and ascorbate, a reducing agent) has been shown to dramatically inhibit the growth of the organism responsible for botulism – *Clostridium botulinium*.[32] Addition of nitrite to meat also gives it a fresh red colour. In the absence of nitrite or nitrate, the myoglobin in meat is oxidised, causing the meat to darken, but by reacting with nitrite (Reaction 1.7), the myoglobin forms a red compound, nitrosyl heme, which retards the rate of oxidation.[33]

Reaction 1.7 $O_2Fe^{II}Mb + NO \longrightarrow (NO)Fe^{II}Mb + O_2$

The biochemistry of NO has been extensively investigated in the past twenty years. To date, NO has been established as having a direct role in a range of different biological responses, the main ones being:

- immune system regulation
- cytotoxicity
- enzyme regulation

- vasodilation
- neurotransmission
- penile erection.

The definitive discovery by Tannenbaum and co-workers that both rats and humans excrete more urinary nitrate than they ingest, was the first step in establishing proof that NO was metabolised in the body. [34,35] Along with other research[36] suggesting inflammatory processes associated with fighting infection were responsible for increased levels of urinary nitrate, Tannenbaum found that nitrate levels in rat urine was increased by injection of endotoxin.[37] Endotoxin is a component of certain bacteria which is designed to trigger a reaction of the immune system.

It was then demonstrated that macrophages from mice who have previously been injected with a chemical agent, such as endotoxin, produce significantly more nitrites and nitrates than average.[38] Macrophages are a type of white blood cell, essential in the immune system. They are now known to be important in defence against tumours and infections. This established the link between the presence of macrophages - the defence cells – and the resultant increase in nitrate presence. The same study found that mice with specific, genetically determined macrophage deficiencies excreted fewer nitrates. By isolating cultures of macrophages, and treating them with endotoxin (and γ interferon, an immuno-hormone called a cytokine), the macrophages were suddenly stimulated to produce nitrates.[39] By selectively varying different aspects of the macrophage it was found that nitrates were not produced if L-arginine was absent. This suggested that an enzyme in the activated macrophages converted arginine into an intermediate, which was the

active cytotoxic agent in the macrophage's ability to kill tumour cells and infections, which itself was quickly converted to either nitrates or nitrites. In addition, if a secondary amine, such as morpholine was added to these activated macrophages, N-nitrosation occurred, suggesting that a more reactive oxide of nitrogen than a nitrate or nitrite was being formed.[40] This was subsequently proposed to be NO by Marletta and co-workers[41], though there has been much discussion of its identity and a variety of potential 'candidates' have been put forward. Peroxynitrite, $ONOO^-$, which can form from the reaction of superoxide O_2^- with NO in aqueous, alkaline solutions, has in the past also been proposed as the reactive agent[42]. However a recent study suggested that the evidence for the role of peroxynitrite in biological systems is both indirect and ambiguous. [43]

At the same time that the origin of nitrates in the body was being investigated, Hibbs and co-workers were investigating how macrophages could kill tumour cells and bacteria. They too proved that the tumour killing ability of the macrophages was removed if L-arginine was not present.[44] They found that this arginine dependent product inhibited the metabolism of tumour cells by interfering with enzymes containing iron-sulphur clusters in these cells. It was proposed that L-arginine was converted into nitrates and another amino acid, L-citrulline. In this way, Hibbs provided evidence that a specific enzyme, now known to be nitric oxide synthase (NOS), produced NO from L-arginine. Scheme 1.1 shows the formation of NO and L-citrulline from L-arginine. NO is catalysed by all nitric oxide synthases by a similar mechanism. The mechanism proposed involves the NADPH (nicotinamide-adenine dinucleotide phosphate) dependent, two-step mixed function oxidation of the guanidino nitrogen of arginine. The first step, a two electron

oxidation, is a hydroxylation to form N^G-hydroxy-L-arginine, which is an enzyme bound intermediate. Then electron removal occurs, followed by oxygen insertion and C-N bond scission to form L-citrulline and free-radical NO.

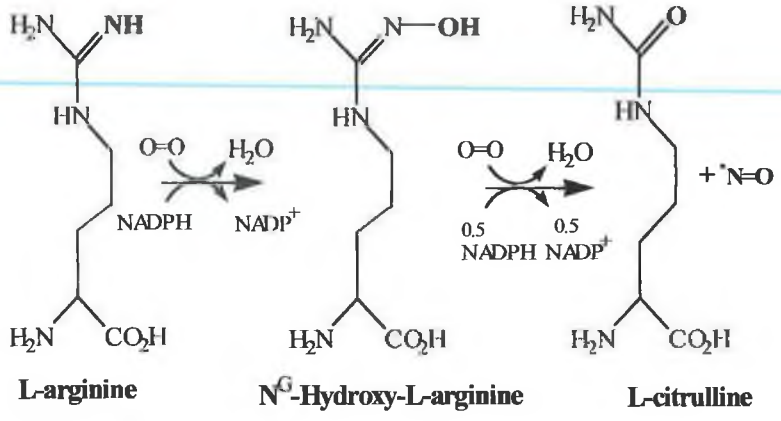

Scheme 1.1 Formation of NO and L-citrulline from L-arginine. Formally 1.5 molecules of NADPH and 2 molecules of O_2 are consumed in the reaction.

This study also identified an inhibitor of NOS, a methyl derivative of arginine, N^G-monomethyl-L-arginine, which blocked the formation of nitrates, and thus removed the macrophages ability to kill tumour cells.

Somewhat unwittingly, NO has been used for almost 150 years as a vasodilator, to reduce blood pressure. It was first reported in 1867 that amyl nitrate was an effective treatment for angina,[45] a heart condition, where the coronary arteries become constricted. Blood vessels consist of two main cell layers, the endothelial cell layer lining the lumen (inside of blood vessels) and the outer, smooth muscle cell layer. The relaxation and contraction of the smooth muscle layer controls the rate of blood flow through the blood vessels, and so controls blood pressure. For much of the past century, nitroglycerine has been used as treatment to control high

blood pressure and heart attacks. It was not until the 1970's that evidence was provided to explain what caused this very beneficial effect. Murad and co-workers[46] demonstrated that NO from NO-releasing agents such as nitroglycerine, and other organic nitrates could activate the soluble form of guanylyl cyclase, to induce vasodilation, though the organic nitrates themselves are not directly responsible for the effect. Subsequently it was shown that NO stimulated guanylyl cyclase by binding to the iron of the enzyme's heme group.[47] In 1980, it was discovered that the endothelial cells released a substance, which diffused into the overlying, smooth muscle cell layer and induced relaxation.[48] This substance was termed endothelial derived relaxation factor (EDRF). For a number of years EDRF proved particularly elusive to isolate and identify.

Eventually, in 1986 two groups simultaneously proposed that NO constituted the main part of EDRF.[49,50] Using chemiluminescence as the method of detection, ERDF was proven to be indistinguishable from NO.[51,52] NO is now regarded as the principle regulator of blood pressure. It is now theoretically possible to control and modify blood pressure, irrespective of whether a patient is suffering from high or low blood pressure. High blood pressure may be treated using a vasodilator such as nitroprusside, whereas low blood pressure could potentially be treated with an NOS inhibitor such as N^G-monomethyl-L-arginine (NMMA). Currently this is only a potential treatment, as reported animal studies indicate that high doses of NMMA may cause accelerated death due to depressed heart function.[53]

In 1988, Garthwaite and co-workers reported that cultured neurons taken from the cerebellar portion of a rat's brain released a labile substance - which behaved in a

similar way to ERDF (and turned out to be NO) - from the stimulated N-methyl-D-aspartate (NMDA) receptor.[54] This led to a series of studies into the role of NO in neurotransmission, as the NMDA receptor is important in the transmission of nerve impulses from cell to cell. In one study to isolate the ERDF-producing enzyme from the rat's brain, it was discovered that Ca^{2+} and calmodulin – a calcium binding regulatory protein - were necessary to maintain the activity of the enzyme.[55] This enzyme, an NOS, has since been isolated and sequenced.[56] This was the first nitric oxide synthase enzyme to be isolated. Crucial to the idea that NO was involved in neurotransmission, was the discovery that NOS was found almost exclusively in neurons, though neurons make up only approximately 15% of brain cells.[55] The other 85% of brain cells are called glia, and NOS enzymes were not detected in glial cells.

The mechanism of neurotransmission has been studied and is now better understood. Glutamate released from a stimulated neuron binds to an NMDA receptor on an adjacent neuron. This activates the receptor, causing a channel to open, which allows Ca^{2+} to enter the neuron. The Ca^{2+} can then bind to calmodulin, allowing it to associate with NOS. This in turn activates the NOS, which in the presence of oxygen and NADPH (as shown above in Scheme 1.1) can convert L-arginine to L-citrulline and NO. Though the chemical mechanism of NO's involvement in neurotransmission is relatively well understood, some of the roles that NO plays in neurotransmission are not fully known or understood.

It should be noted that there are different forms of nitric oxide synthase. As a result of the studies to isolate and sequence the different forms of NOS, there is now a

body of evidence to suggest that there are three main forms of NOS. The three types are similarly structured, but not identical, resulting in their different functions. The first is known as *inducible*, and is triggered by endotoxins or other inflammatory agents, causing NO to be produced by macrophages and other immune cells. This inducible form iNOS, functions independent of Ca^{2+} and calmodulin, unlike the other two types which are regarded as constitutive, by virtue of being present continuously. They produce smaller quantities of NO, which has the effect of acting as a messenger molecule, rather than as a defence mechanism. The two types are *brain*, bNOS, which is involved in neurotransmission and *endothelial* eNOS, which is involved in vasodilation.

NO has achieved public acclaim and some notoriety with the launch of the impotence drug, Viagra®. The cause was the crucial role that NO plays in penile erection in animals and humans. NO has been identified as the transmitter molecule which transmits the autonomic signal to the corpus cavernosum, causing it to dilate, and become engorged with blood, resulting in the penis becoming erect. It is estimated that up to 10 million men in the USA alone suffer from impotence, and Viagra® has done much to raise both the profile and share price of Pfizer, as well as bringing some general public awareness to one therapeutic effect of NO.

1.5 Chemistry of Allyl Iron-Nitrosyl Complexes

η^3-Allyl-dicarbonyl-nitrosyliron complexes have been known for almost forty years, and have been shown in that time to be versatile as reagents for organic transformations. One of their more useful roles is in carbonylation reactions to

prepare β,γ-unsaturated carbonyl compounds. Such carbonylation reactions are not limited to iron, but can occur with other metals such as nickel, cobalt and palladium. Allyl-dicarbonyl-nitrosyliron complexes have a characteristic dark red colour, are relatively air sensitive, but stable under an N_2 atmosphere at 0°C.

The first complex in this series, η^3-allyl-dicarbonyl-nitrosyliron, was reported in 1965.[57] η^3-Allyl-dicarbonyl-nitrosyliron and similar complexes were independently reported very soon after.[58] A number of groups synthesised allyl-$Fe(CO)_2NO$ by dehalogenation of a halo-η^3-allyl-tricarbonyliron complex, and subsequent reaction of the η^3-allyl-tricarbonyliron complex formed, with an atmosphere of nitric oxide. The reaction is shown in Scheme 1.2. The complex was also synthesised by treating η^3-allyl-dicarbonyl-triphenylphosphine-iron with nitric oxide, with loss of triphenylphosphine favoured rather than loss of CO.[58]

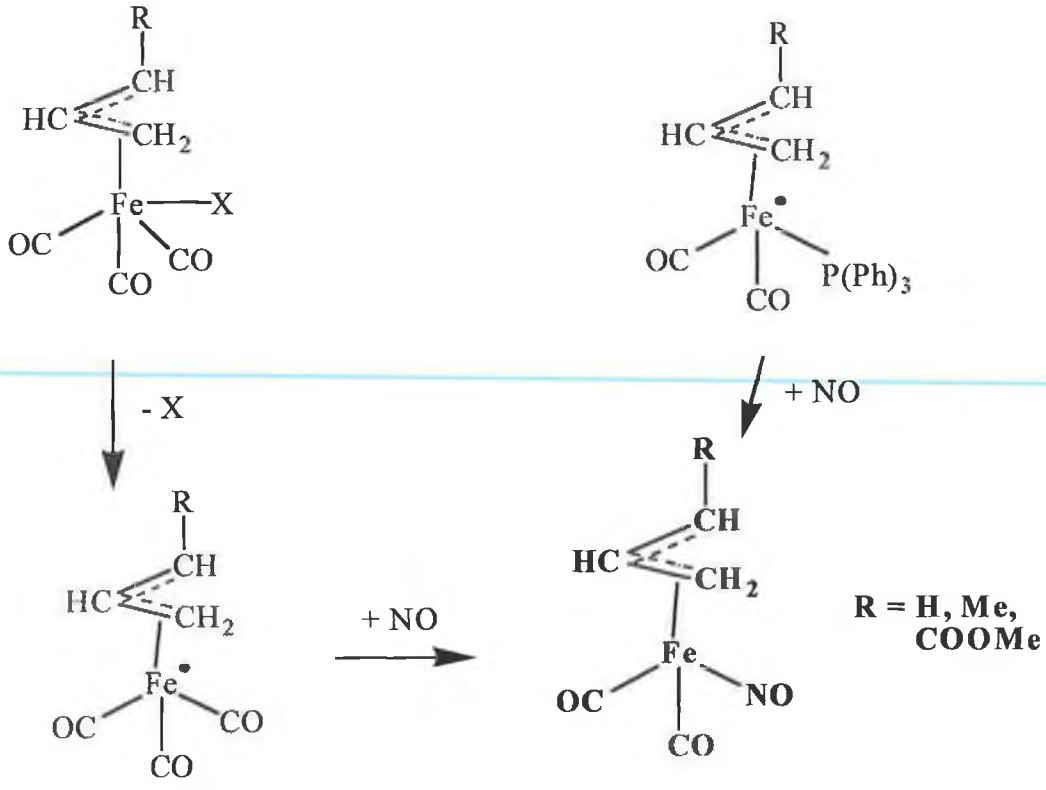

Scheme 1.2 Original schematic synthesis of η^3-allyl dicarbonyl-nitrosyliron by dehalogenation of a halo-η^3-allyl-tricarbonyliron and also by treating η^3-allyl-dicarbonyl-triphenylphosphine-iron with nitric oxide.[58]

Pauson and co-workers subsequently came up with a more general method of synthesising allyl-dicarbonyl-nitrosyliron complexes.[59] This synthesis involved generation of the salt $Na^+[Fe(CO)_3NO]^-$ from $Fe(CO)_5$ and $Na(NO)_2$, and this salt was allowed to react with a suitable allyl halide, in this case allyl bromide, to form the required η^3-allyl dicarbonyl-nitrosyliron. The η^3 but-2-enyl-dicarbonyl-nitrosyliron was also reported in this paper.

Due to its air sensitivity, derivatives of η^3-allyl-dicarbonyl-nitrosyliron are more easily characterised. The triphenylphosphine derivative, η^3-allyl-carbonyl-triphenylphosphine-nitrosyliron was obtained by warming equimolar quantities of

the reactants in a tetrahydrofuran solution. Cardaci reported the same result using toluene.[60] This study also showed that the reactions with phosphines can proceed via a monohapto η^1-allyl intermediate depending on the conditions employed. In certain cases insertion of the phosphine ligand was reported without loss of CO or any other ligand resulting in the monohapto complex. Using the general synthetic method reported, a series of substituted η^3-allyl dicarbonyl nitrosyl complexes shown in Fig. 1.6 were prepared.[60]

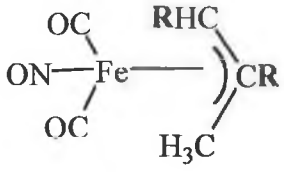

R = H, Me, Cl, CN, Ph, MeCl

Figure 1.6 Series of substituted η^3-allyl iron complexes synthesised by Cardaci.

In reacting these compounds with phosphorus ligands such as PPh_2Et, PPh_3, and $P(OMe)_3$, formation of the η^1 allyl species was identified using IR and ^1H NMR spectroscopy. η^3-2-Chloroallyl-dicarbonyl-nitrosyliron reacted with PPh_3, in benzene at 25°C, to form η^1-2-chloroallyl-dicarbonyl-nitrosyl-triphenylphosphine-iron (yield 40%), with no evolution of CO observed (Reaction 1.8). However when the same reaction took place in toluene at 50°C, the η^3-2-chloroallyl carbonyl-triphenylphosphine-nitrosyliron species is formed (yield 75%). Reactions of (η^3-R-C_3H_4) $Fe(CO)_2NO$ (where R = H, 1-Me, or 2-Me) with PPh_3 only ever yielded the η^3 species, and the η^1 intermediate was not detected.

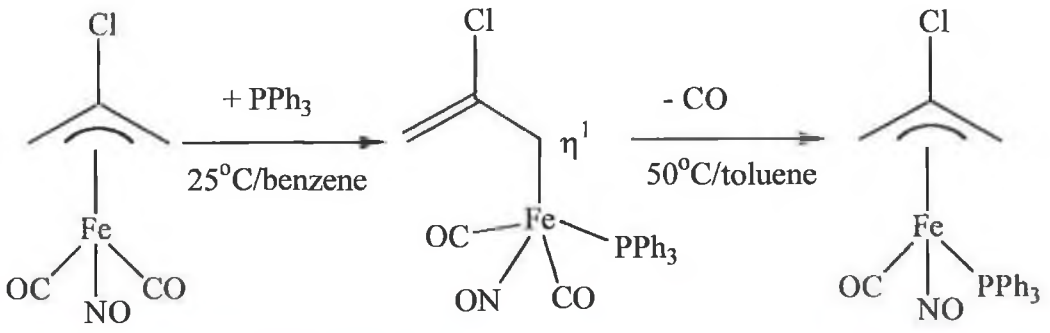

Reaction 1.8 Addition of PPh_3 to η^3-2-chloroallyl-dicarbonyl-nitrosyliron resulting in formation of η^3-2-chloroallyl-carbonyl-nitrosyl triphenylphosphinoiron. The reaction proceeds via the η^1-allyl species.

A CO insertion reaction occurred, if the 1-chloroallyl or 2-chloroallyl complexes reacted with 1,2-bis (diphenylphosphino) ethane (DPPE) at 25°C for 24 hours.[60] This yielded a β,γ-unsaturated complex, either 4- or 3-chlorobut-3-enoyl Fe(CO)DPPE(NO), depending on the initial substitution. β,γ-Unsaturated acyliron complexes such as these may be converted to the corresponding carboxylic acid esters by treatment with an alcohol in the presence of iodine.[61]

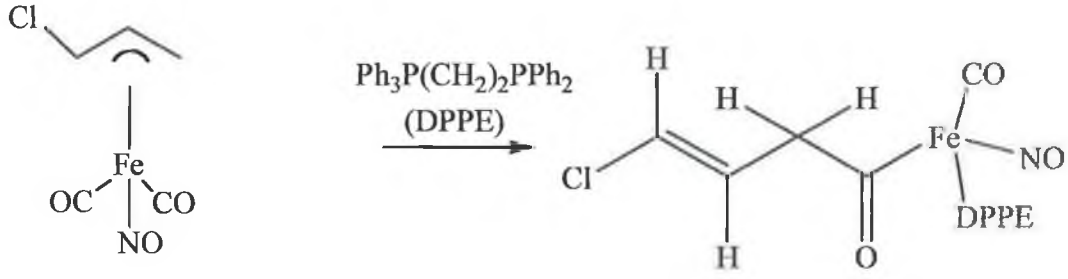

Reaction 1.9 Formation of 1,2-DPPE-carbonyl 4-chlorobut-3-enoyl-nitrosyliron.

In monosubstituted allyl ligands, CO insertion occurs regioselectively at the terminal carbon of the allyl group.[62] A subsequent study investigated the effect of

1,3-disubstitution on the allyl ligands.[63] Further evidence of CO insertion occurring at the terminal carbon was reported. It was also reported that if a methyl group and phenyl group were the substituents, CO insertion occurs at the methyl carbon (Reactions 1.9 and 1.10).

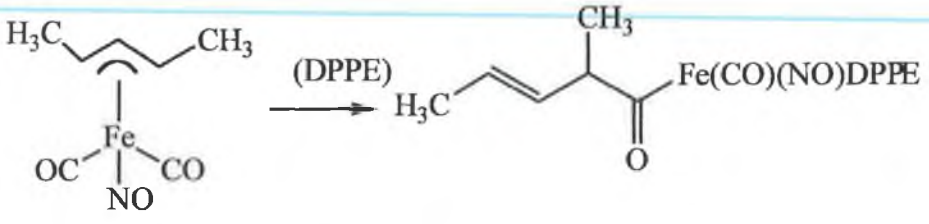

Reaction 1.9 CO insertion reaction of 1,3-disubstituted allyl iron complex occurs at the terminal carbon, resulting in β,γ-unsaturated complex.

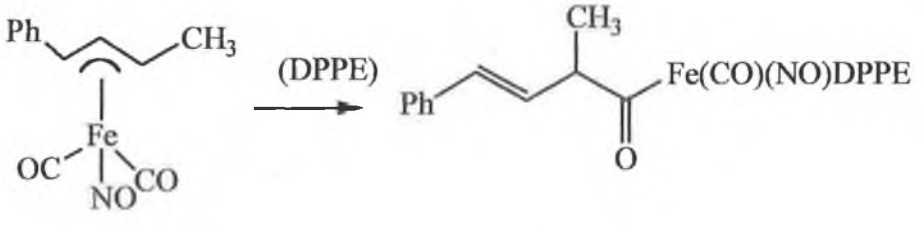

Reaction 1.10 CO insertion reaction occurs at methyl carbon of 1,3-disubstituted allyl iron complex with methyl and phenyl substituents, yielding a β,γ-unsaturated complex.

The rate of reaction was found to increase slightly using alkyl groups as substituents, and increase greatly if there was a phenyl group on the terminal carbon. This can be rationalised in terms of the resonance structures of the η^3-allyl ligand shown in Figure 1.7. The iron atom co-ordinates to the allyl through both π- and σ-bonds. CO insertion occurs on the σ-bond, therefore, the larger the contribution from resonance structure I, the faster the reaction.

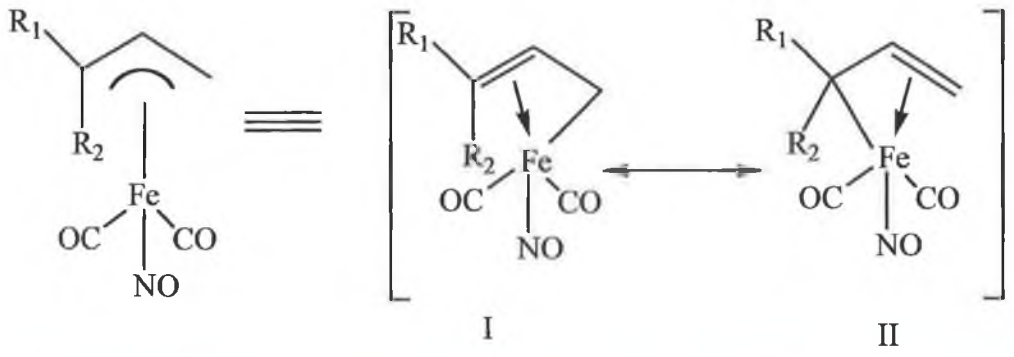

Figure 1.7 Resonance structures of η^3-allyl-dicarbonyl-nitrosyliron.

In contrast to the analogous nickel[64] and palladium[65] η^3-allyl complexes, 1-methoxycarbonyl-allyl iron $(CO)_2NO$ does not undergo CO insertion, when reacted with DPPE. It appears that if the substituent is electron withdrawing, the rate is either greatly decreased (R= Cl) or the reaction does not occur (R= CN, COOMe) at all.

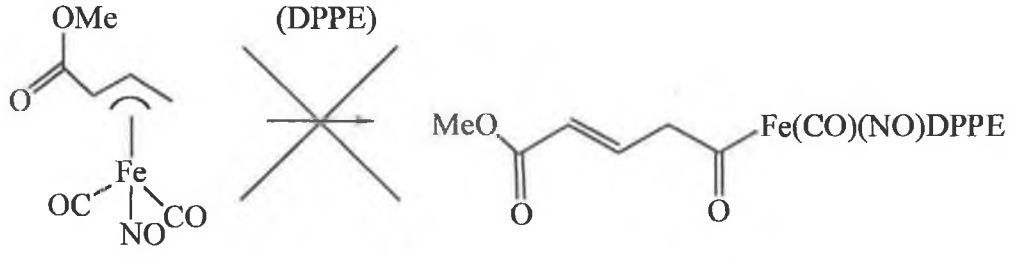

Reaction 1.11 For R = COOMe, CO insertion reaction does not occur for addition of DPPE to π-R C_3H_4 $Fe(CO)_2NO$.

Another, more recent study reports the synthesis of planar chiral η^3-allyl-dicarbonyl-nitrosyliron complexes,[66] which can be used in asymmetric organic reactions. Using chiral η^3-allyl-dicarbonyl-nitrosyliron complexes as intermediates of organic reactions, it is possible to synthesise natural products with great selectivity. One possible reaction of these compounds would be asymmetric amination to yield optically active γ-amino-α,β-unsaturated carboxylic acid

derivatives.[66] The complexes themselves were synthesised by reaction of optically active (S)-allyl tosylate and (R)- allyl bromide, with tetrabutylammonium tricarbonylnitrosylferrate ($Bu_4N^+[Fe(CO)_3NO]^-$). The reaction scheme shown below in Reaction 1.12 shows the two enantiomers that resulted from the reaction with allyl tosylate. Similar products were observed when the reaction was carried out using optically active allyl bromide.

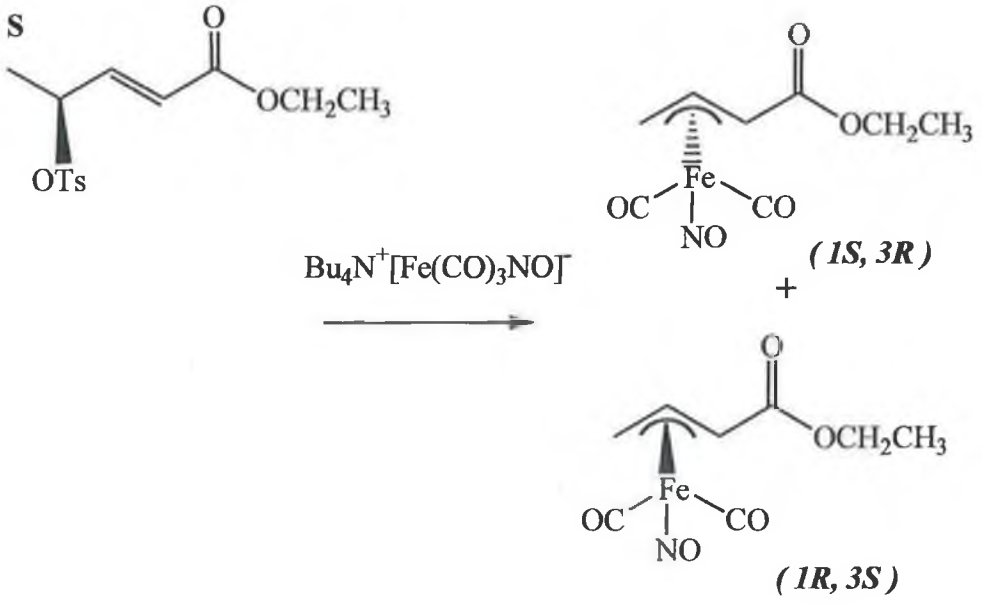

Reaction 1.12 Synthesis of chiral η^3-allyl-dicarbonyl-nitrosyliron complexes.[66]

It was found that the solvent used was particularly important in determining which enantiomer was formed. For the tosylate reaction, it was found that the inversion (1S, 3R) product predominated in dichloromethane, tetrahydrofuran, acetone and toluene, while the retention (1R, 3S) product was the major product in acetonitrile. Stereoselectivities of up to 94% e.e. were attained for the inversion product. The retention product is formed as a result of the co-ordination of acetonitrile to $Bu_4N^+[Fe(CO)_3NO]^-$ with loss of CO. This then reacts with the allyl tosylate via oxidative addition to form the (1R, 3S) product. The reaction of allyl bromide with

$Bu_4N^+[Fe(CO)_3NO]^-$ yielded the same products as before. Again the inversion product was favoured, in all solvents, however the stereoselectivity or yields weren't as efficient as for the allyl tosylate reactions.[66]

Derivatives of η^3-allyl-dicarbonyl-nitrosyliron, from $Bu_4N^+[Fe(CO)_3NO]^-$, had previously been used in reactions to yield alkylated products.[67] This is of importance in organic synthesis as a potential β-acylcarbanion equivalent. The basic reaction is shown in Scheme 1.3.

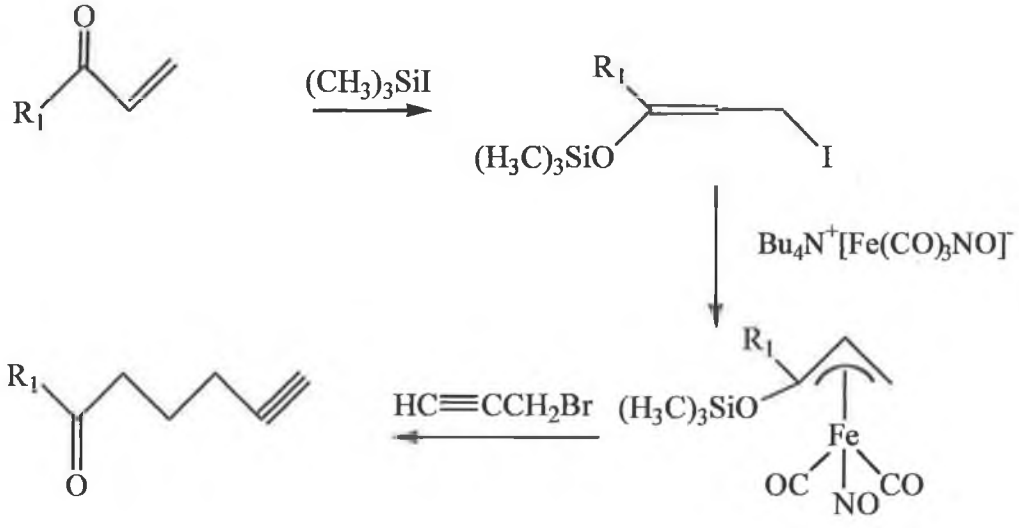

$\mathbf{R_1}$ = C_6H_5, p-$CH_3C_6H_4$, p-ClC_6H_4, C_2H_5,-$(CH_2)_3$-, C_6H_5O

Scheme 1.3 Use of $Bu_4N^+[Fe(CO)_3NO]^-$ to generate η^3-allyl iron complex as an intermediate in an organic alkylation reaction.

An α,β-unsaturated ketone such as phenyl vinyl ketone was treated with iodotrimethylsilane. The complex formed was reacted with $Bu_4N^+[Fe(CO)_3NO]^-$, and 2-propynyl bromide was added as the alkylating agent resulting in formation of 4-pentynyl phenyl ketone. η^3-1-Trimethylsiloxoallylic dicarbonyl nitrosyl iron is the

key intermediate in this reaction. The reaction was carried out using a series of different substituent R-groups. Cycloaddition reactions occur if the 2-alkyl allyl iron intermediate is formed from the precursor, 2-alkyl-3-iodo-1-trimethylsiloxypropene, resulting in a pyran derivative.[68]

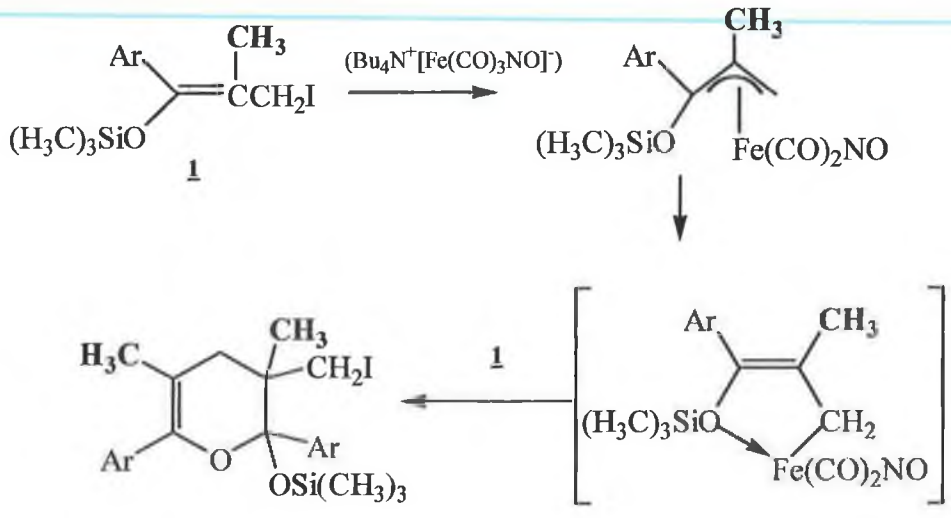

Reaction 1.13 Use of η^3-allyl iron complex as intermediate in the reaction to form a dihydropyran derivative.

Another related study has involved generation of η^3-1-azaallyl-dicarbonyl-nitrosyliron complexes.[69] The η^3-azaallyl iron complexes were generated as intermediates in the dimerisation of α-bromoimines with tetrabutylammonium tricarbonylnitrosylferrate ($Bu_4N^+[Fe(CO)_3NO]^-$) to yield 1,4-diketones. (Reaction 1.14)

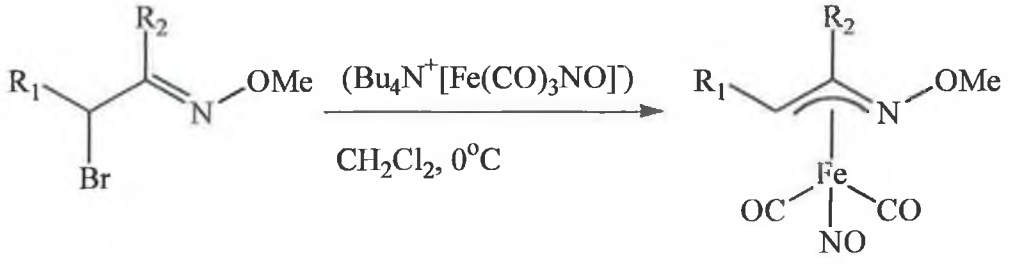

Reaction 1.14 Generation of η^3-1-azaallyl-dicarbonyl-nitrosyliron complex.

$Bu_4N^+[Fe(CO)_3NO]^-$ has also been used to catalyse reactions involving the alkylation of allylic carbonates with malonate anions, resulting in formation of an analogous allylic iron intermediate.[70] On the basis that retention of configuration is observed in these reaction, and that for π-allyl palladium mediated alkylation reactions inversion of configuration is observed, it was concluded that the allylic intermediate is an η^1 σ-allyl complex.[70] This obviously contradicts the previously reported reactions of Pauson's group,[59] and others.[58] Specifically, Roustan reported the reaction of substituted η^3-allyl-dicarbonyl-nitrosyliron complexes with malonate anions to form alkylated organic products.[71] The reactions reported above (Reaction 1.12) prove that this interpretation was incorrect. They indicate that both inversion and retention products may result, depending on the co-ordination ability of the solvent involved, and the nature of substitution on the allyl group.

The effects of substituents on η^3-allyl-dicarbonyl-nitrosyliron have also been investigated using IR and Mössbauer spectroscopy.[72] It has been proposed that both the carbonyl groups and the nitrosyl groups absorb the electronic effect of the substituent. This leads to a decrease in ν_{CO} and ν_{NO} if the substituent is electron donating, such as a methyl group, the CO (or NO) bond is weakened through electron donation to the antibonding π* orbitals. If the substituent is electron withdrawing, then the opposite effect is seen and ν_{CO} increases.

Polarographic studies carried out on η^3-allyl-dicarbonyl-nitrosyliron and some derivatives, have reported that the electron change is not localised about the NO π* orbital,[73] as has been previously reported for other carbonyl nitrosyl transition metal complexes. Cardaci's group found evidence that the Fe-π-ligand bond was cleaved

during the reduction. Infrared monitored chemical reduction of the compound using $NaBH_4$ gave evidence for formation of $Na^+[Fe(CO)_3NO]^-$. Based upon other reductions carried out using the 1-CH_3, 1-Cl, and 2-Cl π-allylic derivatives, the reaction was proposed to progress via the reaction intermediate $[Fe(CO)_2NO]^-$, and not via $[C_3H_5Fe(CO)_2]$, the expected intermediate if the π-allyl iron bond was uninvolved in the reduction process. The proposed reaction mechanism is shown below in Reaction 1.15 – 1.17.

$$\pi\text{–}C_3H_5Fe(CO)_2NO \xrightarrow{+\,2e^-} [Fe(CO)_2NO]^- + C_3H_5^- \xrightarrow{\text{solvent}} CH_3CH{=}CH_2$$

Reaction 1.15 Cleavage of the Fe-allyl bond occurs resulting in the reaction intermediate $[Fe(CO)_2NO]^-$.[73]

$$[Fe(CO)_2NO]^- + \pi\text{–}C_3H_5Fe(CO)_2NO \longrightarrow [Fe(CO)_3NO]^- + CH_3CH{=}CH_2 + \text{unstable products}$$

Reaction 1.16 Reaction intermediate $[Fe(CO)_2NO]^-$ reacts with parent species, η^3-allyl $Fe(CO)_2NO$ forming $[Fe(CO)_3NO]^-$.[73]

$$2\,[Fe(CO)_2NO]^- \longrightarrow [Fe(CO)_3NO]^- + \text{unstable products} \longrightarrow CO + Fe^+ + NOH^-$$

Reaction 1.17 Decomposition of reaction intermediate $[Fe(CO)_2NO]^-$ to $[Fe(CO)_3NO]^-$ and subsequently to its elements.[73]

The proposed mechanism involves cleavage of the iron- allyl π-bond. This contradicts conclusions previously reported on related systems such as η^3-allyl $Fe(CO)_3X$ (X = Cl, Br, I).[74] It was reported that the π-allyl iron bonds remain

unaffected by the reduction process, and only the Fe-X bond was cleaved. Reactions 1.16 and 1.17 are competitive reactions, though it appears that Reaction 1.16 predominates. Another noteworthy point of the mechanism proposed is that two moles of η^3-allyl-dicarbonyl-nitrosyliron are used in the formation of one mole of $Na^+[Fe(CO)_3NO]^-$.

1.6 Chemistry of Iron-Nitrosyl Complexes

An iron carbonyl nitrosyl complex was first reported by Mond and Wallis in 1922, however the composition they proposed was later proved to be incorrect.[75] The correct formula, $Fe(CO)_2(NO)_2$ was assigned in 1932.[76] Iron dicarbonyl nitrosyl, $Fe(CO)_2(NO)_2$ is isoelectronic with $Ni(CO)_4$, $Co(CO)_3(NO)$, $Mn(CO)(NO)_3$ and $Cr(NO)_4$. The isoelectronic nature of this series led to a number of studies, which attempt to understand the nature of bonding in transition-metal carbonyls and nitrosyls. $Fe(CO)_2(NO)_2$ may be synthesised in a number of ways,[77] probably the most convenient of which is the method described by Reactions 1.18 and 1.19.[78] Iron dicarbonyl nitrosyl has a basically tetrahedral co-ordination with a C_{2v} symmetry. In the past, $Fe(CO)_2(NO)_2$ has been used as a catalyst in the dimerisation of dienes.[79]

$$Fe(CO)_5 + NaNO_2 + 2NaOH \xrightarrow{+H_2O} Na[Fe(CO)_3NO] + CO + Na_2CO_3 + H_2O$$

Reaction 1.18 Generation of $Na^+[Fe(CO)_3NO]^-$ from reaction of $Fe(CO)_5$ and $NaNO_2$.[78]

$$Na[Fe(CO)_3NO] + NaNO_2 + 2CH_3CO_2H \longrightarrow Fe(CO)_2(NO)_2 + CO + 2Na[CH_3CO_2] + H_2O$$

Reaction 1.19 Synthesis of $Fe(CO)_2(NO)_2$ from $Na^+[Fe(CO)_3NO]^-$, CH_3COOH and $NaNO_2$.[78]

1.6.1 Electronic Studies of $Fe(NO)_2L_2$ Type Complexes

Electron diffraction studies on $Fe(CO)_2(NO)_2$ and the other isoelectronic complexes mentioned above, have provided valuable information in gaining an understanding of the nature of the bonding in $Fe(CO)_2(NO)_2$, and also a number of trends with regard to the bonding in this series of compounds was observed.[80] Considerable evidence was produced in these studies to confirm the presence of $d\pi$-π^* back-bonding. Evidence for $d\pi$-π^* back-bonding included shortening of the Fe-N bond-length in relation to a standard Fe-N single bond, and lengthening of the N-O bond when compared to the bond length of nitric oxide. There appears to be a tendency for the bond order of both M-C and M-N to increase as the atomic number of the metal increases, but the back bonding of the M-N links increases as the number of M-C bonds increase across the series. For example, the Mn-C bond of $Mn(NO)_3CO$ is much weaker than the Cr-N bond of $Cr(NO)_4$, which would the next compound in the series. Similarly the Mn-N bond is stronger than the Cr-N bond, indicating that the $d\pi$ bonding that was previously shared between four Cr-N bonds is now predominately distributed between three Mn-N bonds.

The crystal structure of both $Fe(CO)(NO)_2(PPh_3)$ and $Fe(NO)_2(PPh_3)_2$ has also been reported.[81] The N-O bond in $Fe(NO)_2(PPh_3)_2$ was found to be 1.19 Å. For

$Fe(CO)(NO)_2(PPh_3)$ the bond-length is 1.15 Å, indicating the effect of introducing a ligand that is electron-donating. In the original electron diffraction study the Fe-N-O bond angle was assumed to be exactly linear, however a subsequent microwave study from Kukolich and co-workers[82] found that the angle was 176.4°. The N-O bonds are bent in such a way as to bring the O atoms closer together.

1.6.2 Thermal Chemistry of $Fe(NO)_2L_2$ Type Complexes

$Fe(CO)_2(NO)_2$ undergoes CO substitution reactions with a variety of different reagents. The first reported substitution reactions of $Fe(CO)_2(NO)_2$ was the reaction of $Fe(CO)_2(NO)_2$ with acetonitrile to yield $Fe(NO)_2(CNCH_3)_2$.[83] Several years later, the reaction of $Fe(CO)_2(NO)_2$ with aromatic phosphines, arsines and stibines was reported.[84] Malatesta reported triphenylphosphine and triphenylphosphite replacing both CO ligands whereas triphenylarsine, tritolylarsine and triphenylstibine replaced only one of the CO ligands. These reactions were all carried out in toluene at room temperature. These derivatives are all stable in air when completely dry, however if water is present they are easily oxidised. Dinitrosyl bis-triphenylphosphine iron is the most stable of the derivatives

$Fe(CO)_2(NO)_2$ undergoes a series of CO-substitution reactions with reagents such as pyridine, imidazole, pyrrolidine and tetrabutylammonium halides.[85] A kinetic study carried out on the addition of triphenylphosphine found similarities between the rates of CO-substitution reaction for $Co(NO)(CO)_3$, and $Fe(CO)_2(NO)_2$, which conformed to the basic rate law given in Equation 1.1.[85]

$$\text{rate} = k_2 [Fe(NO)_2(CO)_2] [L]$$

Equation 1.1 Rate law for CO substitution of $Fe(CO)_2(NO)_2$ where L is triphenylphosphine, triphenylphosphite or triphenylarsine.

This was not the case with substitution reactions involving reagents such as amines and halides. The rates of reaction between $Fe(CO)_2(NO)_2$ and halides or amines was much faster than for the same reagents with $Co(NO)(CO)_3$. This is most likely due to the NO groups being better π-acceptors than CO, thus stabilising the metal by de-localisation of its extra electron density as a result of attack on the carbonyl. With the iron systems intermediate state having one CO and two NO's, this would be more stabilised than the cobalt system which would have two CO's and only one NO.[85]

Not surprisingly, for phosphine derivatives of the isoelectronic $Co(NO)(CO)_3$, the υ_{CO} and υ_{NO} are shifted to lower frequency.[86] The phosphines are weaker electron acceptors than the nitrosyl or carbonyl groups, resulting in an increase in the electron density on the metal. This electron density is transferred to the remaining nitrosyl and carbonyl groups as previously explained, increasing the back-bonding, resulting in a reduction in the N-O and C-O force constants and subsequent reduction in υ_{CO} and υ_{NO}.

The reaction of $Fe(CO)_2(NO)_2$ and triphenylphosphine using tetrabutylammonium halides as catalysts gave rise to both $Fe(CO)(NO)_2(PPh_3)$ and $Fe(NO)_2(PPh_3)_2$,as shown in Reaction 1.20.[85]

$$2\ Fe(NO)_2(CO)_2 + 3\ (C_6H_5)_3P \xrightarrow{(n\text{-}C_4H_9)_4NCl} Fe(NO)_2(CO)[(C_6H_5)_3P] + Fe(NO)_2[(C_6H_5)_3P]_2 + 3\ CO$$

Reaction 1.20 Catalysed reaction of $Fe(CO)_2(NO)_2$ and PPh_3 yielding mono- and di-substituted products.

Based on these kinetic studies, it was proposed that $Fe(NO)_2(PPh_3)_2$ is not formed from $Fe(CO)(NO)_2(PPh_3)$. Both are formed directly from a separate intermediate species, and that the rates of relative formation are dependent upon the nature and concentration of the catalyst used. The rate law given in Equation 1.2 describes this reaction.[85]

$$\text{rate} = k_2\,[Fe(NO)_2(CO)_2][(C_6H_5)_3P\} + k_y\,[Fe(CO)_2(NO)_2][(n\text{-}C_4H_9)_4NCl]$$

Equation 1.2 Rate law describing reaction of $Fe(CO)_2(NO)_2$ with PPh_3 in the presence of tetrabutylammonium chloride catalyst.[85]

$Fe(NO)_2(PPh_3)_2$ and other related iron nitrosyl complexes such as $Fe(NO)_2(DPPE)$ (DPPE = 1,2 bis (diphenylphosphino)ethane)) have also been synthesised by intermolecular nitrosyl transfer reactions.[87] Nitrosyl transfer from $CoNOD_2$ (D is the monoanion of dimethylglyoxime) is observed, where NO is bent, to $FeCl_2(PPh_3)_2$ and $FeHCl(DPPE)_2$. The overall reaction of $CoNOD_2$ and $FeCl_2(PPh_3)_2$ is shown in Reaction 1.21.

$$FeCl_2PPh_3 + 2CoNOD_2 + 2PPh_3 \longrightarrow Fe(NO)_2PPh_3 + 2CoClD_2PPh_3$$

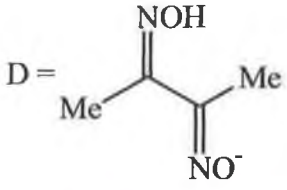

Reaction 1.21 Formation of $Fe(NO)_2(PPh_3)_2$ by nitrosyl transfer using $CoNOD_2$ as the transfer reagent.[87]

The reaction proceeds via two NO/Cl transfer reactions and evidence of a transient nitrosyl stretch was initially observed, however as the reaction proceeded this band disappeared, and the two nitrosyl stretches due to $Fe(NO)_2(PPh_3)_2$ were observed. In this reaction, the transfer reagent $CoNOD_2$ has a bent NO configuration, though this is not a prerequisite for a nitrosyl transfer reaction. Nitrosyl transfer from the linear RuNO group of $Ru(NO)_2(PPh_3)_2$ to $RuCl_2(PPh_3)_3$ has been reported to yield $RuNOCl(PPh_3)_2$.[88]

Another CO substitution reaction which $Fe(CO)_2(NO)_2$ undergoes is the formation of mono- and bis- carbene complexes. Fischer-type mono carbenes were reported in the early 70's,[89] but by using the ligand bi (1,3-dimethylimidazolidin-2-ylidene), mono- and bis- carbene complexes were synthesised as shown in Scheme 1.4.[90]

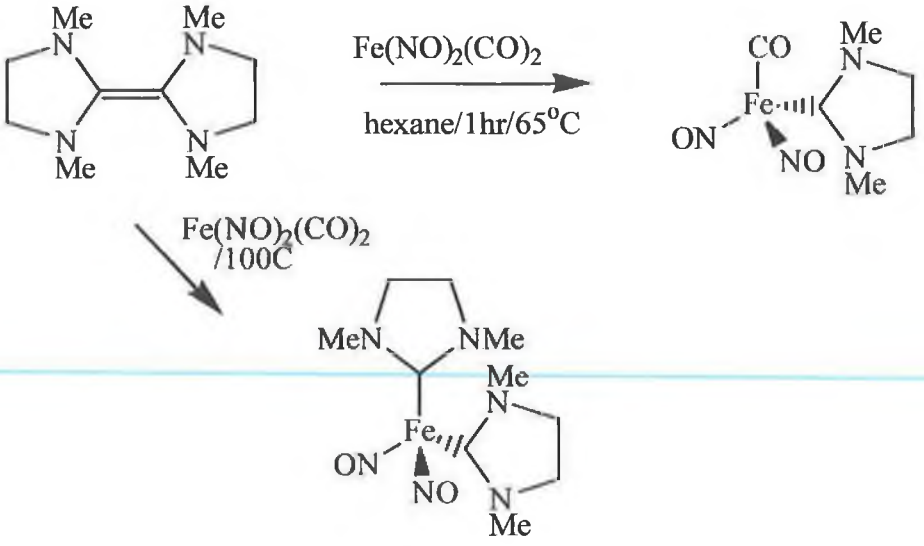

Scheme 1.4 Formation of mono- and bis- carbene complexes by reaction of $Fe(CO)_2(NO)_2$ with the olefin, $[:CN(Me)CH_2CH_2N(Me)]_2$.[90]

$Fe(CO)(NO)_2(PPh_3)$ can be conveniently and very selectively synthesised through the reaction of bis (triphenylphosphino) iminium and $[Fe(CO)_2(PPh_3)_2(NO)](PF_6)$.[91] This reaction takes place without the formation of $Fe(NO)_2(PPh_3)_2$, which was the predominant product from Malatesta's reaction where $Fe(CO)(NO)_2(PPh_3)$ was previously reported.[84] It was also found that bis (triphenylphosphino) iminium nitrite ($PPNNO_2$) reacted with $Fe(CO)_5$ to form $PPN[Fe(CO)_3NO]$, with the reaction being complete in ten minutes.[91] This is in contrast to the original reaction to form $[Fe(CO)_3NO]$,[78] which can require approximately two days to reach completion with an overall yield of only 50 %, in contrast to a reported yield of 95 %.

$Fe(CO)_2(NO)_2$ undergoes reaction with bis (triflouromethyl) phosphine to form the dimeric complex $Fe_2(NO)_4[P(CF_3)_2]_2$.[92] The Fe_2P_2 ring structure (see Figure 1.7) proposed is planar, with the geometry about the Fe molecules tetrahedral. The structure of $Fe_2(NO)_4[P(CF_3)_2]_2$ is shown in Figure 1.7. Several years earlier, the arsenic derivative, $Fe_2(NO)_4[As(CF_3)_2]_2$ had also been reported.[93]

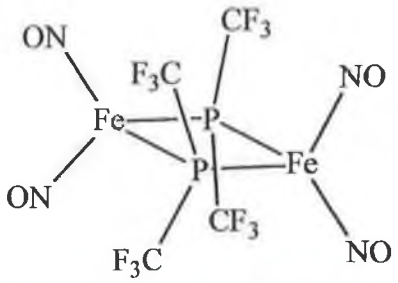

Figure 1.7 Planar structure of $Fe_2(NO)_4[P(CF_3)_2]_2$ as proposed by Dobbie and co-workers.[92]

$Fe_2(NO)_4[P(CF_3)_2]_2$ was found to be diamagnetic, which was rationalised by the metal-metal bond. The infrared spectrum of $Fe_2(NO)_4[P(CF_3)_2]_2$ showed υ_{NO} bands appearing at 1822 and 1798 cm^{-1}. This can be contrasted with the observed υ_{NO} of $Fe_2(NO)_4(PMe_2)_2$ at 1753 and 1733 cm^{-1}, indicating more Fe-P bonding in the perfluoroalkyl complex, and consequently less Fe-NO back-bonding.[92]

1.6.3 Matrix Isolation Studies of $Fe(NO)_2L_2$ Type Complexes

A limited number of matrix isolation studies have been reported for $Fe(CO)_2(NO)_2$ and other related complexes. Poliakoff, Turner and co-workers have carried out low temperature studies, the first of specific interest being the photolysis of $Fe(CO)_5$ in a low temperature argon matrix doped with NO to generate $Fe(CO)_2(NO)_2$.[94] The reaction was found to be reversible, as photolysis of $Fe(CO)_2(NO)_2$ carried out in a CO matrix generated $Fe(CO)_5$ with release of NO. This indicates that a steady state exists between $Fe(CO)_5$ and $Fe(CO)_2(NO)_2$ during photolysis. By varying the concentration of the reactants, and matrix constituents it should be possible to

control the position of the steady state, with resultant release or consumption of NO in the photoreaction depending on the conditions.

Studies were also carried out on the isoelectronic $Co(CO)_3NO$. In a CO matrix, IR monitored photolysis showed formation of two new ν_{CO} bands and a band due to free NO. Further investigations using ^{13}C isotopes indicated the product formed to be $[Co(CO)_4]$. In photolysis of organometallic carbonyl nitrosyl complexes, reversible CO loss is favoured above NO loss. The main reasons for this are thought to be, CO loss having a higher quantum yield than NO loss, and NO being involved in a much more efficient reversible process, so that overall NO loss is not observed. It has also been proposed that NO loss requires an incoming ligand to replace it, so NO loss is unlikely to occur in inert matrices, resulting in the preferential loss of CO. The study from Poliakoff and Turner does show that if the conditions are altered or arranged favourably, NO loss can occur.

Poliakoff and Turner also carried out photolysis experiments on $Fe(CO)_2(NO)_2$ and $Co(CO)_3NO$ dissolved in liquid xenon at -104°C, doped with 1-butene.[95] Photolysis resulted in formation of the novel species $Co(CO)_2NO(\eta^2$-1-butene), $Fe(NO)_2(\eta^2$-1-butene$)_2$, and $Fe(CO)(NO)_2(\eta^2$-1-butene). Use of xenon avoided the problem of solvent absorption peaks, thus making the infrared characterisation more straightforward. This group had previously used liquid xenon as the reaction media in the photochemical generation of $Fe(CO)(NO)_2(H_2)$ and $Co(CO)_2(NO)(H_2)$,[96] both of which have potential use in catalytic systems.

1.6.4 Chemistry of Selected Iron Nitrosyl Complexes

As already discussed in Section 1.4.1, the reaction of NO with iron in the body is crucial to some of the most important biological processes, such as activation of guanylate cyclase (leading to key regulatory processes) and inhibition of enzymes. In order to understand these processes better, numerous studies focussing particularly on the metalloporphyrins involved have been carried out. Attention has also been focussed on reactions of NO with Fe-S clusters, which are present in many key enzymes. There is evidence to suggest that this may be the reaction responsible for the cytotoxicity of NO.[97] Other Fe-S nitrosyls such as the Roussin's salts have potential as NO-donor drugs. Iron dithiocarbamate complexes have also received significant attention due to their high reactivity with NO, resulting in stable nitrosyl complexes. These complexes have characteristic electron paramagnetic resonance signals and as a result may be used to detect and quantify biological production of NO.

There has been extensive research into both the nature and structure of nitrosyl metalloporphyrins and their reactions, particularly with regard to dissociation and recombination of NO. Nitrosyl metalloporphyrins can have linear or bent conformation of the NO, depending on the number of metal d-electrons and nitrosyl π^* electrons involved.[98] Fe(TPP)NO (TTP = *meso*-tetraphenylporphyrin) has been oxidised to $Fe(TPP)NO^+$, with resultant shift in the infrared bands, from 1678 cm^{-1} (bent) to 1848 cm^{-1} (linear).[99]

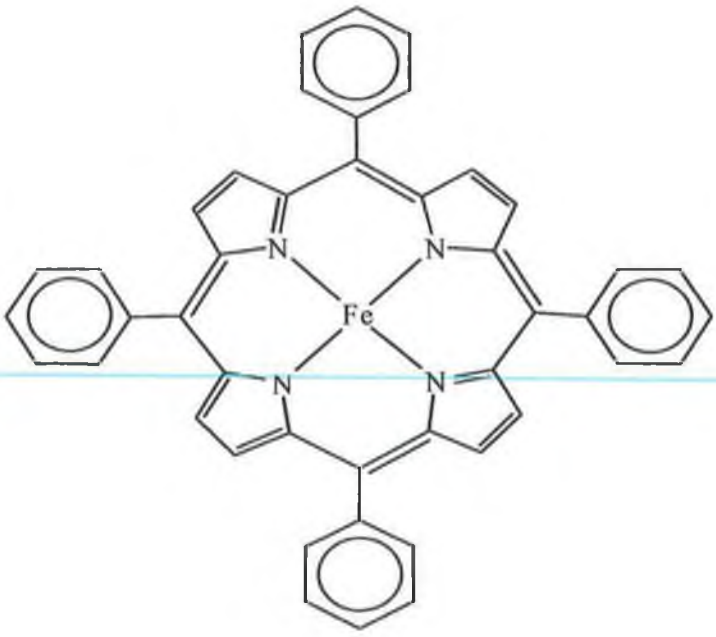

Figure 1.8 Structure of iron tetraphenylporphyrin (Fe(TPP)).

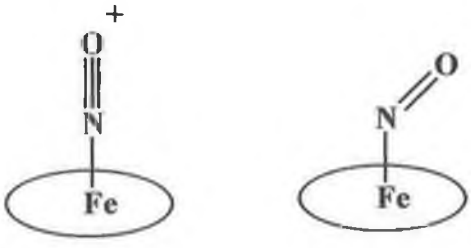

Figure 1.9 Representations of linear and bent configuration of nitrosyl iron tetraphenylporphyrin (Fe(TPP)NO.

Photochemistry of nitrosyl metalloporphyrins had been carried out even before the biological significance of NO was discovered.[100] Photodissociation of NO from myoglobin (Mb) was observed, however the quantum yield was quite small. Dissociation of NO from met-myoglobin ($Fe^{III}Mb$) was a much more efficient process. It is thought that photodissociation of MbNO is hindered by the surrounding protein structure creating a 'pocket' effect. This idea would seem to be

supported by the contrasting ease of dissociation of NO from Fe(TPP)(NO) upon photolysis.[101]

The cubic Fe_4S_4 cluster core is found in a range of biological systems, specifically as an active site in non-heme iron protein structures. $Fe_4S_4(NO)_4$, shown in Figure 1.10, may be synthesised from the reaction of $[Fe(CO)_3NO]^-$ with elemental sulphur in toluene.[102]

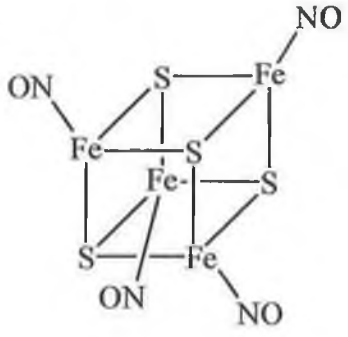

Figure 1.10 Structure of the cubic nitrosyl Fe_4S_4 cluster, $Fe_4S_4(NO)_4$.

There have been a large number of other Fe-S clusters reported. These discoveries date back to the 1850's, when Roussin discovered the nitrosyl Fe-S clusters.[103] $NH_4[Fe_4S_3(NO)_7]$, Roussin's black salt (RBS) and $Na_2[Fe_2S_2(NO)_4]$, Roussin's red salt (RRS).

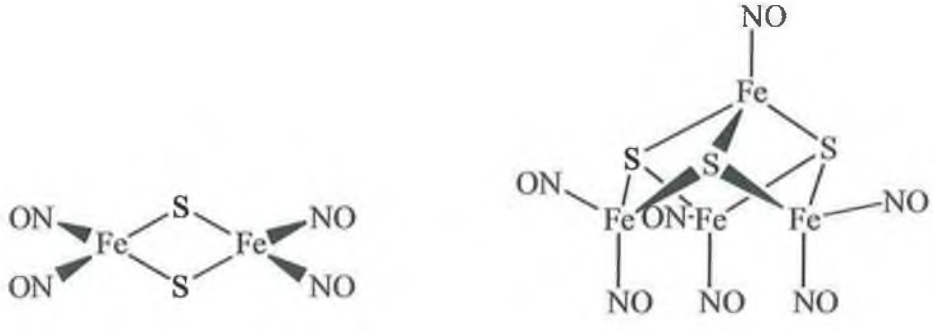

$Fe_2S_2(NO)_4^{2-}$ $Fe_4S_3(NO)_7^-$

Roussin's Red Anion Roussin's Black Anion

Figure 1.11 Structure of the anions of Roussin's red and black salts.

Roussin's salts are quite well suited as a source of NO to biological targets, given the availability of NO, their water solubility, and stability under typical biological conditions. Upon photolysis, these compounds have been shown to release NO.[104] Ford and co-workers reported treatment of hypoxic tumour cell cultures, which are more resistant to radiation therapy than aerobic tumour cells, with RRS.[104] These cell cultures were then simultaneously subjected to γ-radiation and white light irradiation. The proportion of induced cell death was significantly higher than results obtained from similar control experiments carried out in the dark. Similarly, photolysis of RBS also generated NO, though the quantum yields were much lower. Flash photolysis studies of RBS have also been carried out.[105] Both RRS and RBS may be used as precursors in the delivery of NO, to sensitise γ-radiation and induce cell death. While NO loss from RRS is more efficient, RRS is thermally unstable, and left to stand at room temperature over a number of hours is converted to RBS, which is thermally stable. It is therefore likely that further studies in this area will focus more on RBS and perhaps some of its derivatives, in an effort to find a suitable, stable precursor for photochemical generation of NO.

Iron dithiocarbamates (Fe(DTC)) were first reacted by Cambi with NO to form nitrosyl complexes in the early 1930's.[106] Fe(DTC)NO was initially studied as one of the first compounds to exhibit a spin resonance signal. Its electronic structure was also investigated, due to it being regarded as representative of penta co-ordinate transition metal-nitrosyl complexes. Fe(DTC) is once again the subject of interest due to it's high affinity to NO. Fe(DTC) has been used to quantitatively detect NO produced from biological sources.[107] As mentioned above clear, distinctive, easily

interpreted EPR spectra may be recorded. Low frequency EPR spectrometers are already being used to measure in vivo generation of NO.

1.7 Low Temperature Studies of other Nitrosyl Complexes

Reports featuring low temperature studies of NO date back more than forty years, from basic reports of the spectrum of nitric oxide, to more modern spectroscopic studies of NO reactions with metals, to photochemical studies of important biological metal nitrosyls. The first report of low temperature NO species recorded the infrared spectra some of the oxides of nitrogen,[108] such as nitric oxide monomer and dimers, and nitrogen dioxide. In this study NO was deposited at liquid helium temperatures (approximately 4 K) onto a spectrometer cold cell using argon and carbon dioxide as the matrix host gases. The NO monomer was identified as having a υ_{NO} of 1883 cm^{-1} in CO_2 and 1875 cm^{-1} in Ar matrices respectively. The *cis* and *trans* dimers of $(NO)_2$ were also identified from their infrared spectra. The *cis* dimer's symmetric NO stretch appeared at 1862 cm^{-1}, and its asymmetric stretch appeared at 1768 cm^{-1}. The *trans* dimer has an asymmetric stretch at 1740 cm^{-1}, while its symmetric mode is infrared inactive.

N_2 has also been used as the matrix host gas, as was the case for the first report of photolysis of a matrix-isolated oxide of nitrogen.[109] NO/N_2 was deposited slowly (1mm/min) on the CsI window at 4 K to yield a single peak at 1880 cm^{-1}, the isolated NO monomer. Allowing the matrix to warm to 15 K or 20 K and then being cooled to 4K again resulted in formation of four new peaks at 1870, 1785, 1776 and

1764 cm^{-1} respectively. Samples were allowed to warm to temperatures of 25, 30, 35 and 40 K, and were subsequently cooled again to 4 K. ^{15}NO enriched experiments were also carried out. Together with the variable temperature experiments, the growth patterns observed indicated formation of three different dimer species, the most stable being a *cis* O=N–N=O with peaks at 1870 and 1776 cm^{-1}. Perhaps of more relevance to this study was their photolysis of an N_2O film at 77K, using a hydrogen discharge lamp. Photolysis led to formation of peaks at 1867 and 1768 cm^{-1}, identical to those observed when pure NO is deposited at 15 K. Subsequent photolysis of a sample mixture of N_2O and O_3 in an argon matrix at 4 K, using a mercury arc lamp resulted in depletion of the ozone band at 1040 cm^{-1} and formation of two new peaks at 1868 and 1778 cm^{-1}. Both of these photolysis experiments indicated formation of a species corresponding to the most stable *cis* O=N–N=O dimer identified earlier.

Studies of the reaction of NO and metals (transition or otherwise) have been undertaken for a variety of reasons. Tamaru and co-workers reported the interaction of Fe and NO at 77 K,[110] resulting in a peak at 1720 cm^{-1}. This is unlikely to be the FeNO monomer, as the study was carried out 77 K, and as already mentioned, NO dimerised at temperatures as low as 15 K. A more recent study of the reaction of NO with a series of first row transition metals was carried out with a view to better understanding both catalytic processes for reduction of NO_x and corrosion of metal surfaces by NO_x.[111] Another study similarly focussed on the reaction of NO with beryllium and magnesium,[112] again to catalyse the decomposition of NO to N_2 and O_2. Ruschel's studies dealt with the reactions of NO with iron, cobalt, nickel, copper and zinc.[111] Three different iron nitrosyl complexes were identified in this

study, FeNO, Fe_2NO and $Fe(NO)_2$. The FeNO and CoNO complexes identified are found to have a linear NO configuration, whereas NiNO and CuNO were found to have a bent structure. The experimentally observed results were consistent with theoretical studies carried out by the same researchers. The study involving Be and Mg, resulted in formation of the novel species, BeNO being observed.[112] Another species containing Be and NO, BeOBeNO was also observed. The same authors previously reported the reaction of laser ablated Fe atoms with N_2O and NO in N_2 matrices.[113] Again FeNO and $Fe(NO)_2$ were identified, though novel iron nitride oxides were also identified. The complexes formed were found to be NFeO, $NFeO_2$ and N_2FeO.

Haemoglobin and myoglobin, oxygen carrying, iron containing proteins have been shown to undergo recombination with NO at room temperatures.[114] The low temperature photolysis of denatured haemoglobin resulting in recombination with NO has also been reported.[115] Haemoglobin can have different quaternary protein structures depending on the concentration of NO involved. At low NO concentration, nitrosyl haemoglobin (HbNO) is said to be in the low affinity T state. At high NO concentration, HbNO is said to be in the high affinity R state. The haemoglobin was prepared from human blood, and then nitrosylated with NO gas. The HbNO was then denatured. This involves heating the sample in order to break the bond between iron and proximal histidine. Photodissociation and recombination was observed using epr spectroscopy. There were two different processes of recombination observed, the faster recombination process involved the low affinity T state, which was temperature independent. The slower recombination process involved the high affinity R state. It was found that as the temperature was

increased (from 4 K to 10 K) the rate of recombination was also increased. It is thought that as the temperature increases, motion in the polypeptide chains of haemoglobin increases, which allows the rate of the recombination process to increase.

The photochemical reactions of organometallic species are often dependent on temperature and the medium involved. One such example is the cationic complex $[\eta^5\text{-}(C_5H_5)Mn(CO)_2NO]^+$.[116] $[\eta^5\text{-}(C_5R_5)Mn(CO)_2NO]^+$ and some derivatives (R_5 = H_5, H_4Me, Me_5) were photolysed in low temperature glasses, as films and also at room temperatures. The primary photo-process is loss of CO and is independent of the temperature and medium. The secondary process that occurs is dependent on the medium and temperature. In a 1,2-epoxyethylbenzene glass at 77 K, loss of NO^+ is observed, and the resultant species dimerises with CO as a bridging ligand. In the low temperature film, deposited on CaF_2 window, again at 77 K, again loss of NO^+ is observed, however the novel species $[\eta^5\text{-}(C_5H_5)Mn(CO)]$ was proposed, based on the spectroscopic evidence. When the sample was warmed to room temperature and photolysed, loss of CO was initially observed. Subsequent photolysis resulted in loss of NO, and formation of the charged species $[\eta^5\text{-}(C_5H_5)Mn(CO)][PF_6]$. The secondary photoreactions are summarised in Scheme 1.5.

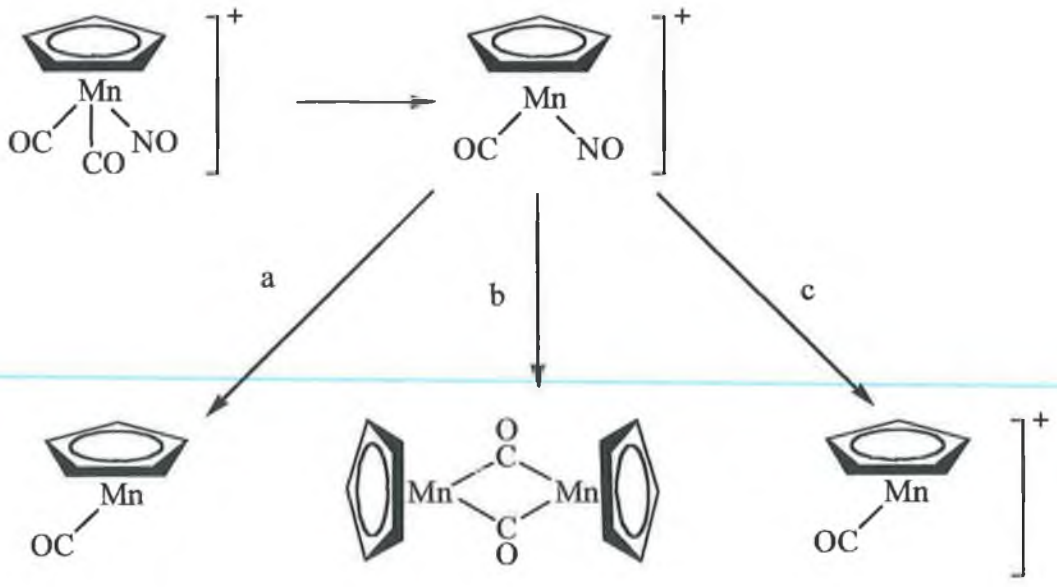

Scheme 1.5 Photolysis of $[\eta^5\text{-}(C_5H_5)Mn(CO)_2NO]^+$. Primary photoreaction is loss of CO. Secondary processes are described in reactions a, b and c. **a)** photolysis in a film at 77 K with loss of NO^+. **b)** photolysis in a glass at 77 K with loss of NO+ and dimerisation. **c)** photolysis in a film at 298 K.

1.8 Conclusions

This chapter introduces and explains the nature of bonding in the various types of organometallic complexes, focussing particularly on bonding in metal-nitrosyl complexes, and metal-allyl complexes. The study of transients and other short lived species are also discussed, with particular emphasis on techniques such as low temperature matrix isolation, solution phase flash photolysis, as these were the methods employed in this study.

Some aspects of the chemistry of NO are described in this chapter. The various roles of NO in biochemical systems are explained. This is particularly relevant in providing a context for the experiments that were carried out. NO is now generally accepted as having a crucial role in the immune system's ability to fight intracellular parasites and infections, with cytotoxicity being the specific biological role of interest in this study. NO has also been acknowledged in a number of other important biological responses, such as enzyme regulation, vasodilation, penile erection and neurotransmission.

The chemistry and photochemistry of the complexes being studied, and similar complexes to those in this study are also highlighted. Allyl iron carbonyl nitrosyl complexes have been known for the past forty years, and various aspects of their chemistry have been reported. For instance, thermal substitution reactions of allyl iron dicarbonyl nitrosyl complexes, loss of CO is reported. The chemistry of complexes of the type $M(NO)_2L_2$ are also reported, due to their similarity to complexes studied, such as $Fe(NO)_2(PPh_3)_2$ and $Fe(NO)_2$DPPE.

1.9 Bibliography

[1] Zeisse W. C. *Pogg. Ann. Phy. Chem.* **1827**, *9*, 623

[2] Mond L.; Langer C.; Quincke. *J. Am. Chem. Soc.* **1890**, 749

[3] Kealy T. J.; Pauson P. L. *Nature* **1951**, *168*, 1039

[4] Wilkinson G.; Rosenblum M.; Whiting M. C.; Woodward R. B. *J. Am. Chem. Soc.* **1952**, *74*, 2125

[5] Fischer E. O.; Pfab W. *Z. Naturforsch. B* **1952**, 7, 372.

[6] Hedberg L.; Hedberg K.; Satija S. K.; Swanson B. I. *Inorg. Chem.* **1985**, *24*, 2766.

[7] Hoffmann R.; Chen M. M. L.; Elian M.; Rossi A. R.; Mingos D. M. P. *Inorg. Chem.* **1974**, *13*, 2666.

[8] Cotton F. A.; Wilkinson G. *Advanced Inorganic Chemistry"*,3rd ed.; Wiley: New York, **1973**.

[9] Whittle E.; Dows D. A.; Pimentel G. C. *J. Chem. Phys.* **1954**, *22*, 1943.

[10] Norrish R. G. W.; Porter G. *Nature* **1949**, *164*, 658.

[11] a) Lefohn A. S.; Pimentel G. C. *J. Chem. Phys.* **1971**, *55*, 1213.

b) Tan L. Y.; Winer A. M.; Pimentel G. C. *J. Chem. Phys.* **1972**, *57*, 4028.

[12] Burdett J. K.; Downs A. J.; Gaskill G. P.; Graham M. A.; Turner J. J.; Turner R. F. *Inorg. Chem.* **1978**, *17*, 523.

[13] Sweany R. L.; Symons M. C. R. *Organometallics* **1982**, *1*, 834.

[14] Barton T. D.; Grinter G.; Thomson A. J.; Davies B.; Poliakoff M. *J. Chem. Soc. Chem. Comm.* **1977**, 841.

[15] Chetwynd-Talbot J.; Grebenik P.; Perutz R. N.; Powell M. A. *Inorg. Chem.* **1983**, *22*, 1675.

[16] Peden C. H. F.; Parker S. F.; Barrett P. H.; Pearson R. G. *J. Phys. Chem.* **1983**, *87*, 2329.

[17] Hepp A. F.; Wrighton M. S. *J. Am. Chem. Soc.* **1983**, *105*, 6249.

[18] Bock C. R.; Hughey IV J. L.; Meyer T. J. *J. Am. Chem. Soc.* **1975**, *97*, 4440.

[19] a)Heiss L. N.; Lancaster J. R. Jr.; Corbett J. A.; Goldman W. E. . *Proc. Natl. Acad. Sci. USA* **1994**, *91*, 267.

b) US Department of Health, **1993**.

[20] Stratmann H.; Buck M. *Air and Water Pollution*, **1966**, *10*, 313

[21] Partington J. R. *"A History of Chemistry"*, Macmillan Press: London, **1962**, 237.

[22] Partington J. R. *"A History of Chemistry"*, Macmillan Press: London, **1962**, 235.

[23] Partington J. R. *"A Short History of Chemistry"*, 3rd ed.; Dover Publications Inc.: New York, **1989**, 110.

[24] a) Hewitt C. N. *Atmospheric Environment*, **2001**, *35*, 1155.

b) Luria M.; Valente R. J.; Tanner R. L.; Gillani N. V.; Imhoff R. E.; Mueller S. F. *Atmospheric Environment*, **1999**, *33*, 3023.

Kenneth J. Olszyna and James F. Meagher

[25] US EPA: *http://www.epa.gov/docs/ozone/science/sc_fact.html*

[26] Ford P. C.; Bourassa J.; Miranda K.; Lee B.; Lorkovic I.; Boggs S.; Kudo S. Laverman L. *Coord. Chem. Rev.*, **1998**, *171*, 185.

[27] Woike T.; Kirchner W.; Schetter G.; Bartel T.; Kim H.; Haussäll S. *Opt. Commun.* **1994**, *106*, 6.

[28] Haussäll S.; Schetter G.; Woike T. *Opt. Commun.*,**1995**, *114*, 219.

[29] Mitchell H. H.; Shonle H. A.; Grindley H. S. *J. Biol. Chem.* **1916**, *24*, 461.

[30] Magee P. N.; Barnes J. M.; *Journal Name* **1956**,

[31] Pivnick H.; Johnston M. A.; Thacker C.; Loynes R. *Can. Inst. Food Sci.Technol. J.* **1970**, *3*, 103.

[32] Reddy D.; Lancaster J. R.; Cornforth D. P. *Science* **1983**, *221*, 769.

[33] Giddings G. G. *J. Food Sci.* **1977**, *42*, 288.

[34] Green L. C.; Tannenbaum S. R.; Goldman P. *Science* **1981**, *212*, 56.

[35]Green L. C.; Ruiz de Luzuriaga K.; Wagner D. A.; Rand W.; Istfan N.; Young V. R.; Tannenbaum S. R. *Proc. Natl. Acad. Sci. USA* **1981**, *78*, 7764.

[36] Hegesh E.; Shiloah J. *Clin. Chim. Acta* **1982**, *125*, 107.

[37] Wagner D. A., Young V. R.; Tannenbaum S. R. *Proc. Natl. Acad. Sci. USA* **1983**, *80*, 4518.

[38] Stuehr D. J.; Marletta M. A. *Proc. Natl. Acad. Sci. USA* **1985**, *82*, 7738.

[39] Stuehr D. J.; Marletta M. A. *J.Immunol.* **1987**, *139*, 518.

[40] Miwa M.; Stuehr D. J.; Marletta M. A.; Wishnok J. S.; Tannenbaum S. R. *Carcinogenesis* **1987**, *8*, 955.

[41] Marletta M. A.; Yoon P. S.; Iyengar R.; Leaf C. D.; Wishnok J. S. *Biochemistry* **1988**, *27*, 8706.

[42] Blough N. V.; Zaffiriou O. *Inorg. Chem.* **1985**, *24*, 3504.

[43] Fukuto J. M.; Ignarro L. J. *Acc. Chem. Res.* **1997**, *30*, 149.

[44] Hibbs Jr. J. B.; Taintor R. R.; Vavrin Z. *Science* **1987**, *235*, 473.

[45] Brunton T. L. *Lancet* **1867**, *ii*, 97.

[46] Murad F.; Mittal C. K.; Arnold W. P.; Katsuki S.; Kimura H. *Adv. Cyclic Nucl. Res.* **1978**, *9*, 145.

[47] Craven P. A.; De Rubertis F. R. *Biochim. Biophys. Acta* **1983**, *745*, 310.

[48] Furchgott R. F.; Zawadzki J. V. *Nature* **1980**, *288*, 373.

[49] Furchgott F. R. *"Vasodilation: Vascular Smooth Muscle, Peptides, Autonomic Nerves, and Endothelium"*, Vanhoutte P. M., Ed.; Raven Press: New York, **1986**; p401.

[50] Ignarro L. J.; Byrns R. E.; Wood K. S. *"Vasodilation: Vascular Smooth Muscle, Peptides, Autonomic Nerves, and Endothelium"*, Vanhoutte P. M., Ed.; Raven Press: New York, **1986**; p427.

[51] Palmer R. M.; Ferrige A. G.; Moncada S. *Nature* **1987**, *327*, 524.

[52] Ignarro L. J.; Buga G. M.; Wood K. S.; Bryns R. E.; Chaudhuri G. *Proc. Natl. Acad. Sci. USA* **1987**, *84*, 9265.

[53] Nava E.; Plamer R. M.; Moncada S. *Lancet* **1991**, *338*, 1555.

[54] Garthwaite J.; Charles S. L.; Chess-Williams S. *Nature* **1988**, *336*, 385.

[55] Bredt D. S.; Snyder S. H. *Proc. Natl. Acad. Sci. USA* **1989**, *86*, 9030.

[56] Bredt D. S.; Snyder S. H. *Proc. Natl. Acad. Sci. USA* **1990**, *87*, 682.

[57] Bruce R.; Chaudhari F. M.; Knox G. R.; Pauson P. L. *Z. Naturforsch. B* **1965**, *20*, 73.

[58] Murdoch H. D. *Z. Naturforsch. B* **1965**, *20*, 179.

[59] Chaudhari F. M.; Knox G. R.; Pauson P. L.; *J. Chem. Soc. (C)* **1967**, 2255.

[60] Cardaci G.; Foffani A. *J. Chem. Soc. Dalton Trans.* **1974**, 1808.

[61] Davies S. G.; Smallridge A. J. *J. Organmet. Chem.* **1990**, *384*, 195.

[62] Nakinishi S.; Yamamoto T.; Furukawa N.; Otsuji Y. *Synthesis* **1994**, 609.

[63] Nakanishi S.; Sawai Y.; Yamamoto T.; Takata T. *Organometallics* **1996**, *15*, 5432.

[64] Casser L.; Chiusoli G. P.; *Tetrahedron Lett.* **1965**, 3295.

[65] Tsuji J.; Imamura S.; Kiji J. *J. Am. Chem. Soc.* **1964**, *86*, 4491.

[66] Yamaguchi H.; Nakanishi S.; Takata T. *J. Organomet. Chem.* **1998**, *554*, 167.

[67] Ito K.; Nakanishi S.; Otsuji Y. *Chem. Lett.* **1987**, 2103.

[68] Ito K.; Nakanishi S.; Otsuji Y. *Chem. Lett.* **1988**, 473.

[69] Nakanishi S.; Masuzaki K.; Takata T. *Inorg. Chem. Comm.* **2000**, *3*, 469.

[70] Xu Y.; Zhou B. *J. Org. Chem.* **1987**, *52*, 974.

[71] Roustan J. L. A.; Houlihan F. *Can. J. Chem.* **1979**, *57*, 2790.

[72] Clarke H. L.; Fitzpatrick N. J. *J. Organomet. Chem.* **1974**, *66*, 119.

[73] Paliani G.; Murgia S. M.; Cardaci G. *J. Organomet. Chem.* **1971**, *30*, 221.

[74] Gubin S. P.; Denisovich L. I. *J. Organomet. Chem.* **1968**, *15*, 471.

[75] Mond R. L.; Wallis A. E. *J. Chem. Soc.* **1922**, *121*, 32.

[76] Anderson J. S.; Hieber W. *Z. Anorg. Allg. Chem.* **1932**, *208* 238.

[77] King R. B. "*Organometallic Syntheses*", Academic Press: London, **1965**, *1*, 167.

[78] Hieber W.; Beuttner H. *Z. Anorg. Allg. Chem.* **1963**, *320*, 101.

[79] Candlin J. P.; James W. H. *J. Chem. Soc. C* **1968**, 1856.

[80] Hedberg L.; Hedberg K.; Satija S. K.; Swanson B. I. *Inorg. Chem.* **1985**, *24*, 2766.

[81] Albano V. G.; Araneo A.; Bellion P. L.; Ciani G.; Manassero M. *J. Organomet. Chem.* **1974**, *67*, 413.

[82] Kukolich S. G.; Wallace D. W.; Wickwire D. M.; Sickafoose S. M.; Roehrig M. A. *J. Phys. Chem.* **1962**, *1*, 368.

[83] Hieber W.; von Pigenot D. *Chem. Ber.* **1956**, *89*, 616.

[84] Malatesta L.; Araneo A. *J. Am. Chem. Soc.* **1957**, *79*, 3803.

[85] Morris D. E.; Basolo F. *J. Am. Chem. Soc.* **1968**, *90*, 2536.

[86] Horrocks W. D.; Taylor R. C. *Inorg. Chem.* **1963**, *2*, 723.

[87] Ungermann C. B.; Caulton K. G. *J. Am. Chem. Soc.* **1975**, *98*, 3862.

[88] Gaughan A. P.; Corden B. J.; Eisenberg R.; Ibers J. A. *Inorg. Chem.* **1974**, *13*, 786.

[89] Fischer E. O.; Kreissel F. R.; Winkler E. *Chem. Ber.* **1972**, *105*, 588.

[90] Lappert M. F.; Pye P. L. *J. Chem. Soc. Dalton Trans.* **1977**, 2173.

[91] Stevens R. E.; Yanta T. J.; Gladfelter W. L. *J. Am. Chem. Soc.* **1981**, *103*, 4981.

[92] Dobbie R. C.; Hopkinson M. J.; Whittaker D. *J. Chem. Soc. Dalton Trans.* **1972**, 1030.

[93] Cullen W. R.; Hayter R. G. *J. Am. Chem. Soc.* **1964**, *86*, 1030.

[94] Crichton O.; Poliakoff M.; Rest A. J.; Turner J. J. *J. Chem. Soc. Dalton Trans.* **1973**, 1321.

[95] Gadd G. E.; Poliakoff M.; Turner J. J. *Inorg. Chem.* **1986,** *25*, 3604.

[96] Gadd G. E.; Upmacis R. K.; Poliakoff M.; Turner J. J. *J. Am. Chem. Soc.* **1986**, *108*, 2547.

[97] Drapier J.-C.; Pellat C.; Henry Y. *J. Biol. Chem.* **1991**, *266*, 10162.

[98] Enemark J. H.; Feltham R. D. *J. Am. Chem. Soc.* **1974**, *96*, 5002.

[99] Mu X. H.; Kadish K. M. *Inorg. Chem.* **1990**, *29*, 1031.

[100] Hoffman B. M.; Gibson Q. H. *Proc. Natl. Acad. Sci. USA* **1978**, *75*, 21.

[101] Hoshino M.; Arai S.; Yamaji M.; Hama Y. *J. Phys. Chem.* **1986**, *90*, 2109.

[102] Chu C. T. W.; Lo F. Y. K.; Dahl L. F. *J. Am. Chem. Soc.* **1982**, *104*, 3409.

[103] Roussin M. L. *Ann. Chim. Phys.* **1858**, *52*, 285.

[104] Bourassa J.; DeGraff W.; Kudo S.; Wink D. A.; Mitchell J. B.; Ford P. C. *J. Am. Chem. Soc.* **1997**, *119*, 2853.

[105] Bourassa J.; Lee B.; Bernard S.; Schoonover J.; Ford P. C. *Inorg. Chem.* **1999**, *38*, 2947.

[106] Cambi L.; Cagnasso A. *Atti. Accad. Naz. Lincei* **1931**, *13*, 809.

[107] Mordvintchev P.; Mulsch A.; Busse R.; Vanin A. *Anal. Biochem.* **1991**, *199*, 142.

[108] Fateley W. G.; Bent H. A.; Crawford Jr. B. *J. Chem. Phys.* **1959**, *31*, 204.

[109] Guillory W. A.; Hunter C. E. *J. Chem. Phys.* **1969**, *50*, 3516.

[110] Bandow H.; Onishi T.; Tamaru K. *Chem. Lett.* **1978**, 83.

[111] Ruschel G. K.; Nemetz T. M.; Ball D. W. *J. Mol. Struct.* **1996**, *384*, 101.

[112] Kushto G. P.; Ding F.; Liang B.; Wang X.; Citra A.; Andrews L. *Chemical Phys.* **2000**, *257*, 223.

[113] Andrews L.; Chertihin G. V.; Citra A.; Neurock M. *J. Phys. Chem.* **1996**, *100*, 11235.

[114] Cornelius P. A.; Hochstrasser R. M.; Steele A. W. *J. Mol. Biol.* **1983**, *163*, 962.

[115] Cambraia-Alves O.; Wajnberg E. *Int. J. Biol. Macromol.* **1998**, *23*, 157.

[116] Palmer B. J.; Becalska A.; Hill R. H. *J. Photochem. Photobiol. A: Chem.* **1991**, *57*, 457.

2 Introduction

The various biological responses of NO have been outlined in the previous chapter. The cytotoxicity of NO is of specific interest to this study. When generated in the body, NO diffuses freely from its point of synthesis. Therefore, if the synthesis of NO could be controlled, and more specifically the location of the synthesis controlled, then the effect that NO has could also be controlled. One possibility would be to deliver a photochemically active NO donor molecule to the site of interest. This part of the body would then be irradiated with light of an appropriate wavelength. If NO could be photochemically generated in this way, in an area of the body which was affected by tumour cells, this would enhance the body's ability to kill the tumour cells.

This project set out to investigate the possibility of photochemically generating NO. Iron complexes were chosen as there are many nitrosyl complexes in the body bound to iron, e.g. haemoglobin, myoglobin, and met-myoglobin. If the study was successful, this would hopefully enable faster and more favourable transfer to clinical experiments. (η^3-Allyl)$Fe(CO)_2NO$ was chosen as the first complex to be investigated, due to its relative ease of synthesis, range of previously reported chemistry and potential substitution of the allyl group. The substituents of the allyl group can be altered to change the solubility, the nature of M-CO and M-NO bonding and the stereochemistry of the complexes being studied. As the experiments proceeded it was observed that loss of CO was the primary photoreaction of (η^3-allyl)$Fe(CO)_2NO$ and its derivatives, it was then decided that

nitrosyl complexes without CO ligands may provide a better option, thus $Fe(NO)_2(PPh_3)_2$ was studied.

2.1 The Photochemistry of Nitric Oxide containing Organometallic Compounds of Iron

In recent years, NO has been shown to play a role in a number of important biological functions. This has led to a great increase in the area of chemical and biochemical research of NO. Controlling the chemical generation and detection of NO has been the focus of a number of research groups. There have been a number of transition metal photochemical studies, reporting the photo-generation of NO.[1,2] NO loss has been observed in $Co(CO)_3NO$ in a CO matrix at 20 K,[3] as well as at room temperature in the gas-phase.[4] The photochemistry of $Co(CO)_3NO$ should be of relevance, as it is isoelectronic with $Fe(CO)_2(NO)_2$, a precursor to one of the complexes investigated in this study. Poliakoff et al.[3] reported CO dissociation in Ar and CH_4 matrices at 20 K to form the unsaturated species $Co(CO)_2NO$, whereas in a CO matrix, NO loss occurs and $Co(CO)_4$ is formed. They proposed an equilibrium existing between $Co(CO)_3NO$, NO, and CO. By varying conditions such as concentration of NO or CO in the matrix, they could selectively generate either CO or NO.

(η^3-Allyl)$Fe(CO)_2NO$ has been reported to undergo CO substitution reactions, though in some of the reports carried out at room temperature there is a possibility that the mechanism was photochemical and not thermal, as was originally thought.[5]

In the original reports of aryl phosphine and phosphite substitution of CO in (η^3-allyl)$Fe(CO)_2NO$ only the η^3-allyl species was observed during the reaction, however subsequent reports of CO substitution of other substituted η^3-allyl species, such as (η^3-2-chloroallyl)$Fe(CO)_2NO$, have reported evidence for formation of the η^1-allyl species in infrared and ^1H NMR spectra.[6] The basic reaction is shown below in Reaction 2.1.

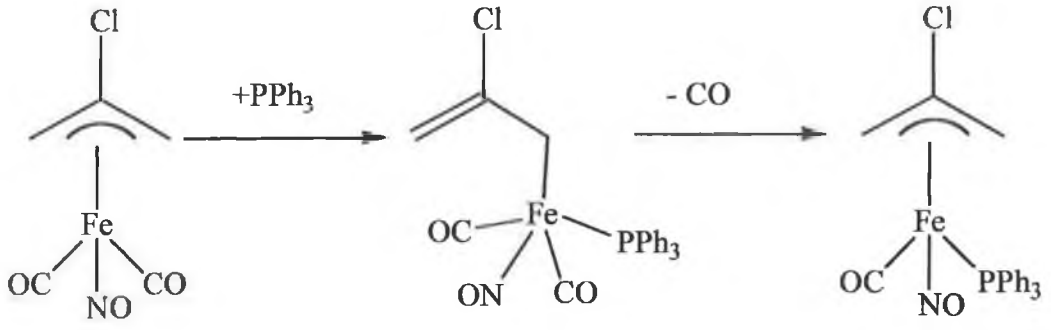

Reaction 2.1 (η^3-2-Chloroallyl)$Fe(CO)_2NO$ reacts with PPh_3, via the η^1-allyl intermediate, to yield (η^3-2-chloroallyl)$Fe(CO)NO(PPh_3)$.

2.2 Photochemistry of (η^3-allyl)$Fe(CO)_2NO$

The IR and UV spectra of (η^3-allyl)$Fe(CO)_2NO$, recorded in degassed spectroscopy grade cyclohexane, are shown below. The IR and ^1H NMR spectra recorded corresponded to the spectra of an authentic pure sample.[5,7,8,9] The infrared spectrum of (η^3-allyl)$Fe(CO)_2NO$ contains two strong carbonyl stretching bands and one strong nitrosyl stretching band. The ^1H NMR spectrum of (η^3-allyl)$Fe(CO)_2NO$ recorded, was consistent with reported values, with doublets at 3.14 (2H) and 3.97

ppm (2H), and a multiplet at 4.30 ppm (1H). The electronic absorption spectrum in cyclohexane solvent is shown in Figure 2.2. The spectrum consists of weak absorption bands centred at $\lambda = 378$ nm and at $\lambda = 480$ nm, which extend into the visible region of the spectrum.

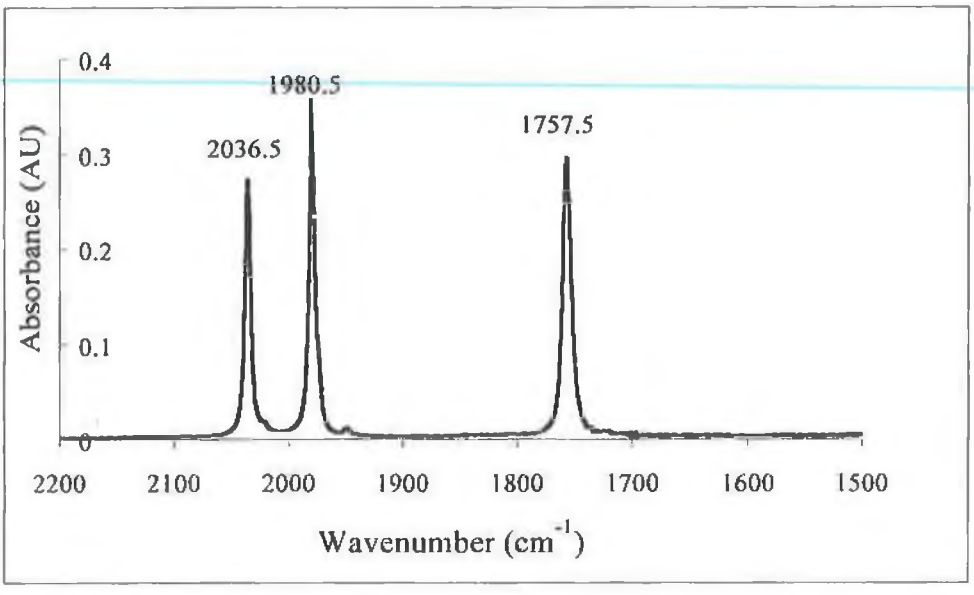

Figure 2.1 Infrared spectrum of (η^3-allyl)$Fe(CO)_2NO$ in cyclohexane solvent.

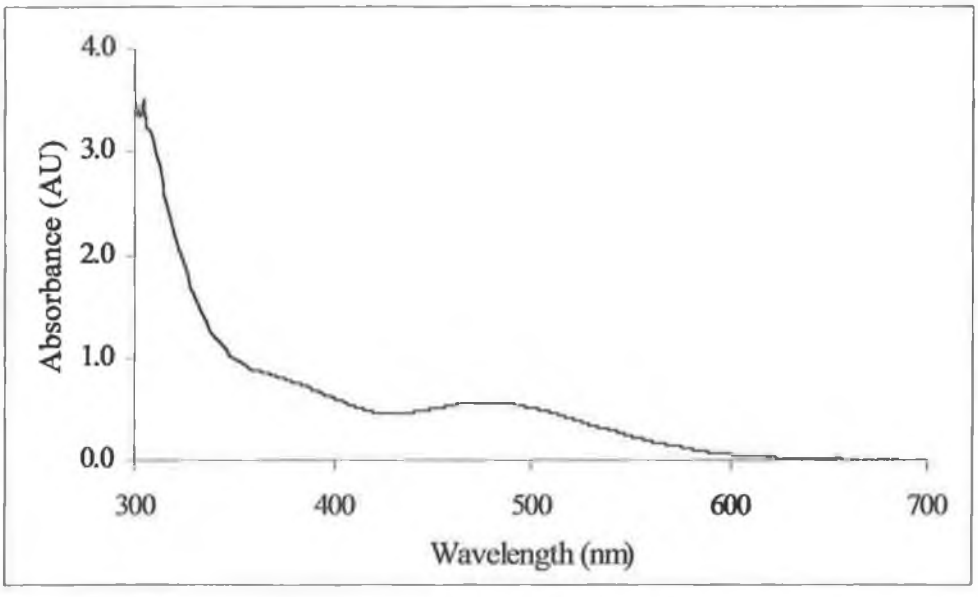

Figure 2.2 UV/vis absorption spectrum of (η^3-allyl)$Fe(CO)_2NO$ (2.2×10^{-3} M) in cyclohexane.

2.2.1 Steady state photolysis of (η^3-allyl)$Fe(CO)_2NO$

A series of steady state photolysis experiments were conducted on (η^3-allyl)$Fe(CO)_2NO$ in the presence of various trapping ligands and solvents. These reactions were monitored using primarily infrared (IR) and ultraviolet/visible (UV/vis) spectroscopy. Laser flash photolysis and matrix isolation experiments were also carried out. IR monitored steady state photolysis experiments were carried out, because both the carbonyl and nitrosyl ligands have strong absorbances in the IR spectrum, consequently chemical changes induced can be conveniently monitored.

2.2.1.1 IR monitored photolysis of (η^3-allyl)$Fe(CO)_2NO$ with excess PPh_3

(η^3-Allyl)$Fe(CO)_2NO$ was photolysed ($\lambda_{exc.} > 340$ nm) in degassed cyclohexane in the presence of a 10-fold excess of triphenylphosphine in a sealed IR cell. As can be seen from the difference spectrum (Figure 2.3), upon photolysis, the parent bands were depleted, with concomitant formation of new peaks, with CO stretching bands at 2037 and 1981 cm^{-1}, in addition the NO stretching band at 1758 cm^{-1} decreased in intensity. The product formed, exhibited ν_{CO} and ν_{NO} bands at 1945 and 1710 cm^{-1} respectively, indicating substitution of one CO by PPh_3.

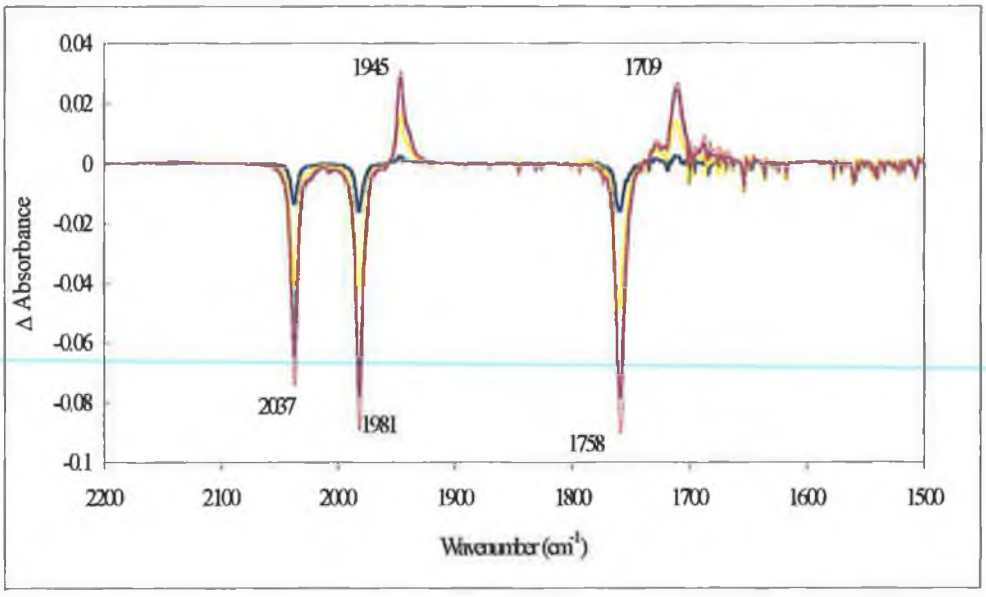

Figure 2.3 Difference spectrum showing photolysis ($\lambda_{exc.} > 340$ nm) of (η^3-allyl)$Fe(CO)_2NO$ with excess triphenylphosphine.

This species was subsequently isolated and the spectrum (Figure 2.29) was compared with that of an authentic pure sample of (η^3-allyl)carbonyltriphenylphosphinenitrosyliron. The ν_{CO} and ν_{NO} peaks also were within experimental error of those reported in the literature.[6] This shift of the bands of the NO and CO absorptions to lower frequency compared to those of (η^3-allyl)$Fe(CO)_2NO$ is expected because of the electron donating effect of the triphenylphosphine ligand. The addition of the triphenylphosphine ligand increases electron density on the metal centre. The extra electron density is then transferred from the metal centre to the π^* orbitals of the remaining CO and NO ligands. This increases the strength of the M-C and M-N bond, and also increases the length of the C=O and N=O bond. The frequency of the CO and NO stretching modes would be shifted even lower if the substituents on the allyl group were more electron donating substituents than merely hydrogen.[10] The (η^1 allyl) derivative has been reported as a reaction intermediate in the thermal reactions of substituted (η^3-

allyl)Fe(CO)$_2$NO derivatives with aromatic and alkyl phosphines in co-ordinating solvents,[10] similar to that described above in Reaction 2.1, though in this study no evidence of formation for the (η^1 allyl) intermediate was found.

2.2.1.2 UV/vis monitored photolysis of (η^3-allyl)Fe(CO)$_2$NO with excess PPh_3

(η^3-Allyl)Fe(CO)$_2$NO was photolysed ($\lambda_{exc.}$ > 340 nm) for 20 minutes in degassed cyclohexane in the presence of a 10-fold excess of triphenylphosphine. There was an increase in absorption across the entire spectral region, although the greatest increase was observed in the region from 350 nm to 500 nm. No isosbestic point was observed in this process.

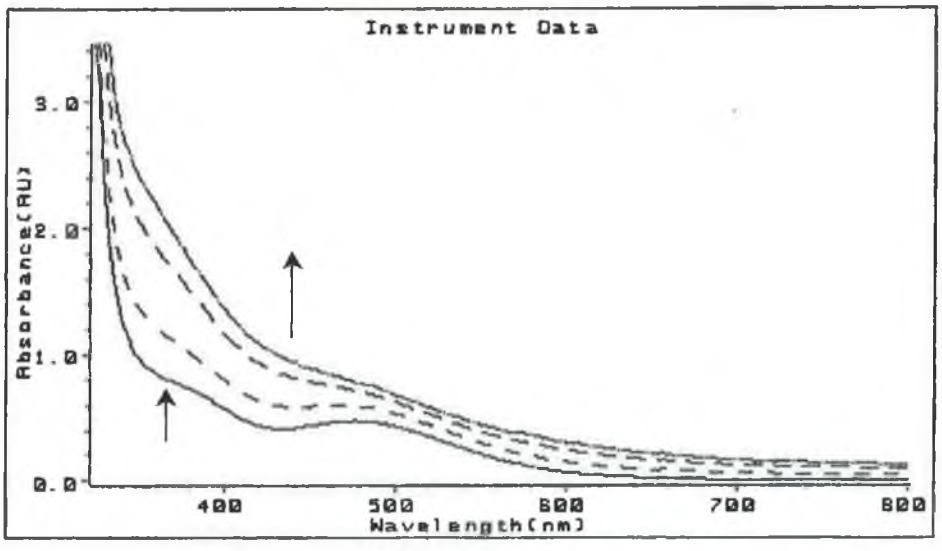

Figure 2.4 UV/vis spectra showing changes upon photolysis of (η^3-allyl)Fe(CO)$_2$NO in cyclohexane in the presence of excess PPh_3.

The absorption increase across the spectrum, especially in the visible region may have been caused in part by a precipitate, which formed as the experiment

proceeded, however the growth in absorption, especially between 350 and 500 nm indicates that a new species was being formed. To confirm the changes, an infrared spectrum of the solution was recorded before and after the experiment, and the changes that occurred are shown in Figure 2.5 below.

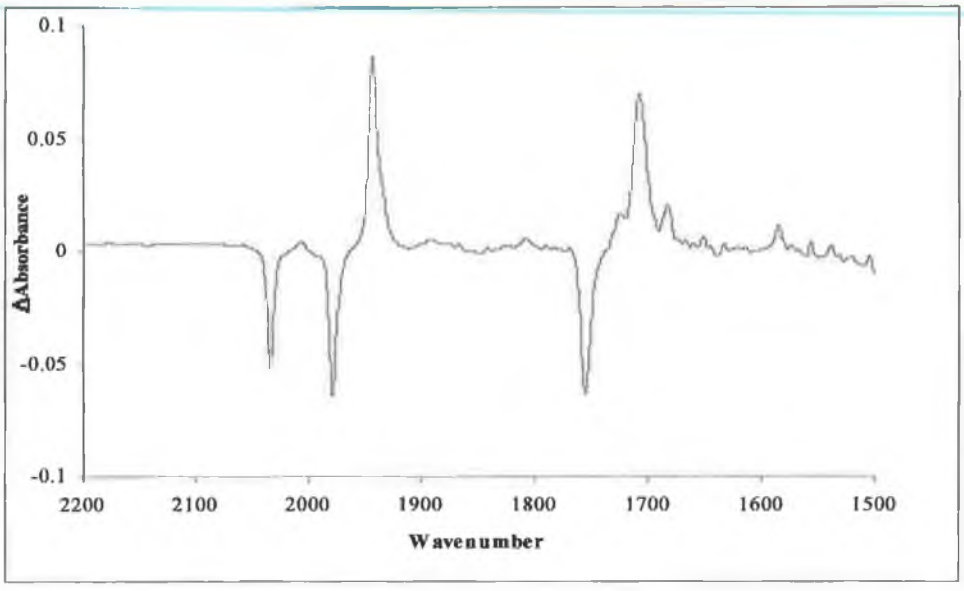

Figure 2.5 Difference spectrum showing changes due to photolysis of (η^3-allyl)$Fe(CO)_2NO$ in cyclohexane in the presence of excess PPh_3.

This would appear to confirm that the changes in the UV/vis spectrum were a result of the formation of (η^3-allyl)$Fe(CO)NO(PPh_3)$, as the peaks are consistent with results from the infrared monitored experiments and with the reported literature values. There is also a peak at approximately 1685 cm^{-1}, which can't be assigned to either (η^3-allyl)$Fe(CO)_2NO$ or (η^3-allyl)$Fe(CO)NO(PPh_3)$. One possible explanation of this feature would be the nitrosyl stretching band of (η^3-allyl)$Fe(PPh_3)_2NO$. The shifting of the υ_{NO} band to even lower frequency would be expected because of the electron donating effect of the second triphenylphosphine ligand. Also with the

removal of both CO's from the metal, the nitrosyl ligand receives a greater electron density. This proposed reaction will be discussed later.

2.2.1.3 IR monitored photolysis of (η^3-allyl)Fe(CO)$_2$NO with excess pyridine

(η^3-Allyl)Fe(CO)$_2$NO was photolysed ($\lambda_{exc.} > 340$ nm) in degassed cyclohexane in the presence of a 10-fold excess of pyridine, in a sealed IR cell. Figure 2.6 shows the difference spectra, illustrating the changes that occurred during photolysis. Again, depletion of the parent bands was observed, and new peaks formed at 2003 cm^{-1} and 1715 cm^{-1} which were assigned to a ν_{CO} band at 2003 cm^{-1} and ν_{NO} band at 1715 cm^{-1}. It is proposed that upon photodissociation of CO, pyridine co-ordinates to the metal, as a two electron donor, as shown in Reaction 2.2.

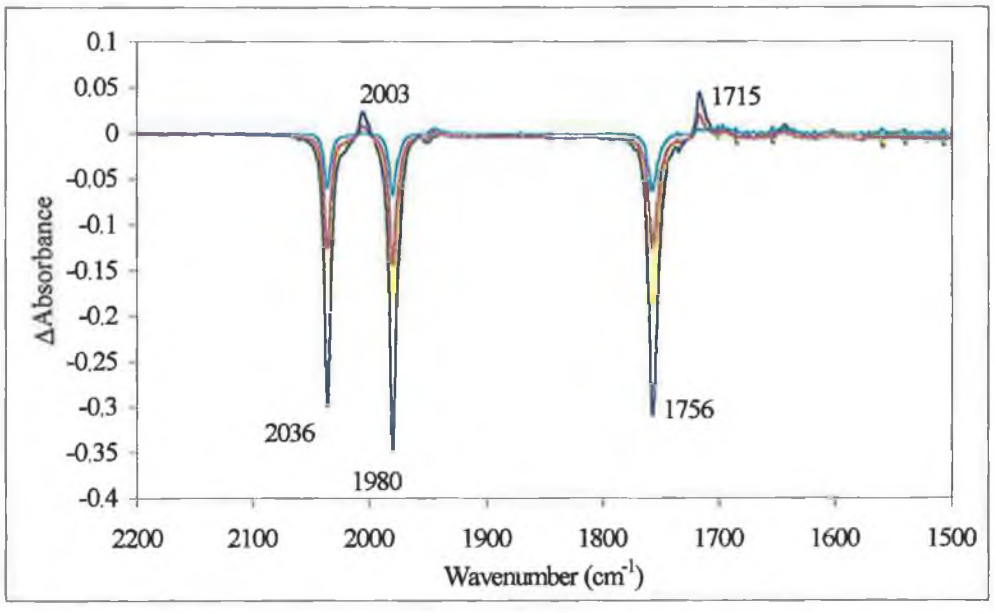

Figure 2.6 Difference spectrum showing photolysis ($\lambda_{exc.} > 340$ nm) of (η^3-allyl)Fe(CO)$_2$NO in the presence of excess pyridine in cyclohexane solution.

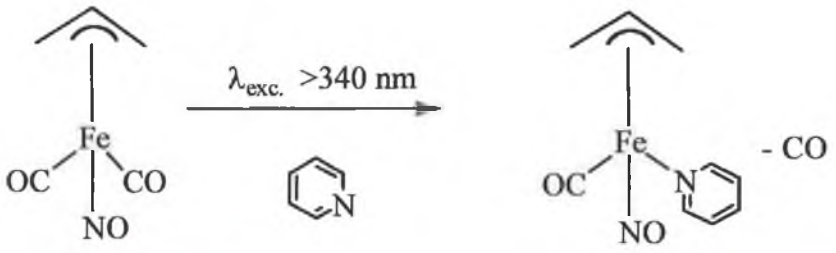

Reaction 2.2 Suggested reaction upon photolysis of $(\eta^3\text{-allyl})Fe(CO)_2NO$ with excess pyridine.

The proposal is consistent with the frequencies observed, given the larger shifts induced in ν_{CO} and ν_{NO} by substitution of CO with the more electron donating triphenylphosphine. A much larger shift in ν_{CO} was observed upon reaction with triphenylphosphine than with pyridine. The products could not be isolated however, to perform further analysis.

2.2.1.4 UV/vis monitored photolysis of $(\eta^3$-allyl)$Fe(CO)_2NO$ with excess pyridine

As in the IR monitored experiment described in the previous section, $(\eta^3$-allyl)$Fe(CO)_2NO$ was photolysed ($\lambda_{exc.}$ > 400 nm) in degassed cyclohexane in the presence of a 10-fold excess of pyridine for a total of sixty minutes. The changes in the UV/vis spectrum were recorded and are presented below in Figure 2.7. A broad increase in absorption across the range of the spectrum was observed, but again the changes are most pronounced in the region between 350 and 500 nm.

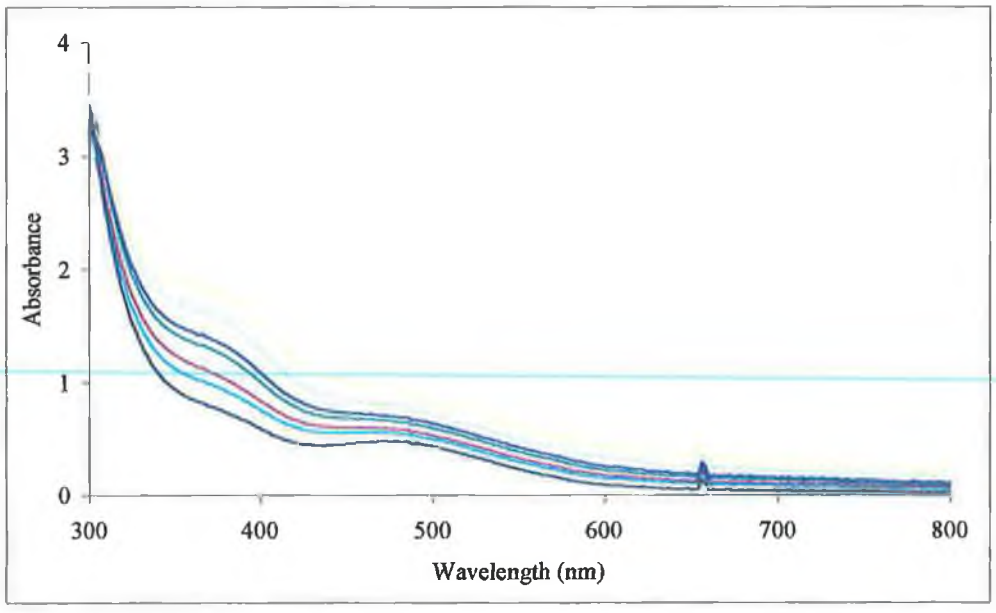

Figure 2.7 UV/vis spectra of changes following photolysis ($\lambda_{exc.} > 400$ nm) of (η^3-allyl)$Fe(CO)_2NO$ in cyclohexane in the presence of excess pyridine.

This is due to the substitution of CO by the pyridine group. Again infrared spectra at the beginning and end of the experiment were used to monitor prodcut formation. The parent bands at 2035, 1979, and 1756 cm^{-1} had decreased in intensity and new bands at 2010 and 1712 cm^{-1} were formed. The changes were identical to those observed previously, and confirmed the substitution of one CO by pyridine.

2.2.1.5 IR monitored steady state photolysis of (η^3-allyl)$Fe(CO)_2NO$ in THF

(η^3-Allyl)$Fe(CO)_2NO$ was photolysed ($\lambda_{exc.} > 340$ nm) in degassed, dry tetrahydrofuran (THF). These experiments were undertaken to determine whether THF would act as a donor ligand in a manner similar to pyridine. Photolysis was carried out for 60 minutes, with spectra being recorded at regular time intervals.

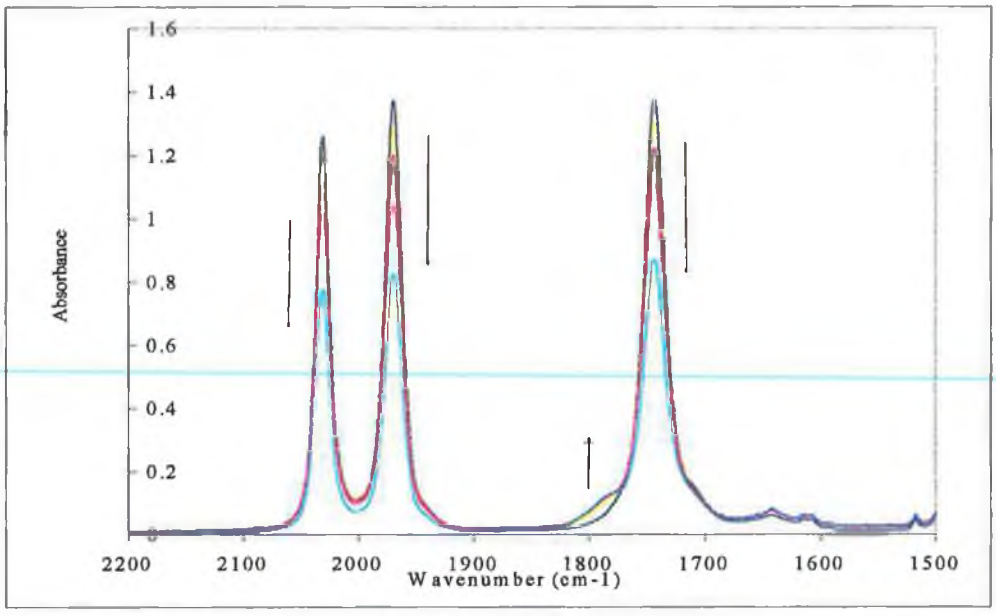

Figure 2.8 IR spectra of photolysis ($\lambda_{exc.} > 340$ nm) of (η^3-allyl)Fe(CO)$_2$NO in THF.

Figure 2.8 shows the spectra recorded during the experiment. As before, a depletion in the parent bands was observed. Though no new bands formed clearly, there was formation of a shoulder band close to the parent nitrosyl band between 1800 and 1775 cm^{-1}, and formation of a weak band centred around 1635 cm^{-1}. This may be an indication of formation of a THF bound CO substitution product, such as (η^3-allyl)Fe(CO)NO(THF) but the intensity of the peaks are weak, and the shifting of the ν_{CO} band in particular is very large in comparison to the previous experiments. This may be the result of a low extinction coefficient of the product formed or the compound formed may be decomposing. As with the pyridine experiment, it was not possible to isolate the product formed and no further analysis was possible.

2.2.1.6 *UV/vis monitored steady state photolysis of (η^3-allyl)Fe(CO)$_2$NO in THF*

(η^3-Allyl)Fe(CO)$_2$NO was photolysed ($\lambda_{exc.} > 340$ nm) in degassed, dry THF for a total of thirty minutes, and the changes in the UV/vis region were recorded. As can be seen from Figure 2.9 below, an increase in absorption in the region between 350 and 500 nm was observed. This may indicate the formation of a new species, most probably the result of substitution of one CO by THF, resulting in (η^3-allyl)Fe(CO)NO(THF).

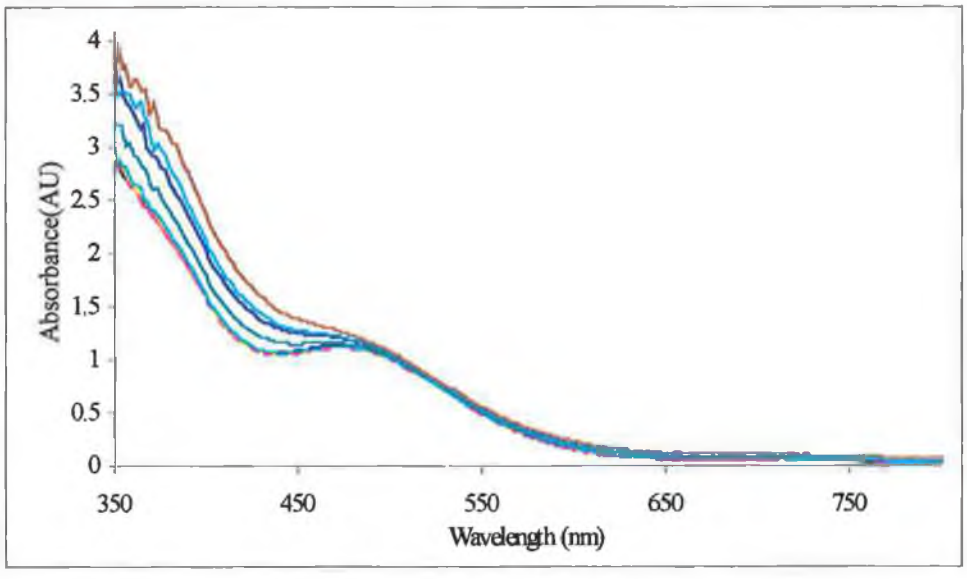

Figure 2.9 UV/vis spectra showing photolysis ($\lambda_{exc.} > 340$ nm) of (η^3-allyl)Fe(CO)$_2$NO in THF.

Unlike the previous UV/vis monitored experiments, the absorption in the visible region remains roughly constant throughout the course of the experiment. This may be accounted for by THF being more polar than the solvents used in previous experiments, with the product formed being soluble in THF. Cyclohexane, a non-

polar solvent was used previously. It was subsequently found when (η^3-allyl)Fe(CO)NO(PPh_3) was synthesised and isolated, it was only sparingly soluble in non-polar solvents, such as pentane and cyclohexane. This would account for the formation of precipitate in the photolysis of (η^3-allyl)$Fe(CO)_2NO$ and PPh_3 in cyclohexane.

2.2.2 Laser flash photolysis of (η^3-allyl)$Fe(CO)_2NO$

Laser flash photolysis experiments were carried out with λ_{exc} of 355 nm or 532 nm. No transient signals were detected for λ_{exc} = 532 nm. At λ_{exc} = 355 nm, flash photolysis studies were carried out in cyclohexane under either an atmosphere of CO or Ar.

2.2.2.1 Laser flash photolysis of (η^3-allyl)$Fe(CO)_2NO$ under 1 atm. of CO

Following flash photolysis (λ_{exc} = 355 nm) under an atmosphere of CO, weak transient signals were observed at 340 nm and 400 nm. A typical transient absorption decay recorded at 340nm is shown below in Figure 2.10. The transient signal observed at 340 nm was recorded at a 50μs time base, and the observed rate constant, k_{obs} was measured to be 4.8×10^4 s^{-1}. The transient recovers to the pre-irradiated baseline indicating that the parent species was fully reformed.

The UV/vis spectrum was monitored continuously throughout the experiment with no significant changes observed. An IR spectrum recorded after the experiment also

indicated no further bands in the spectrum, other than those assigned to (η^3-allyl)$Fe(CO)_2NO$.

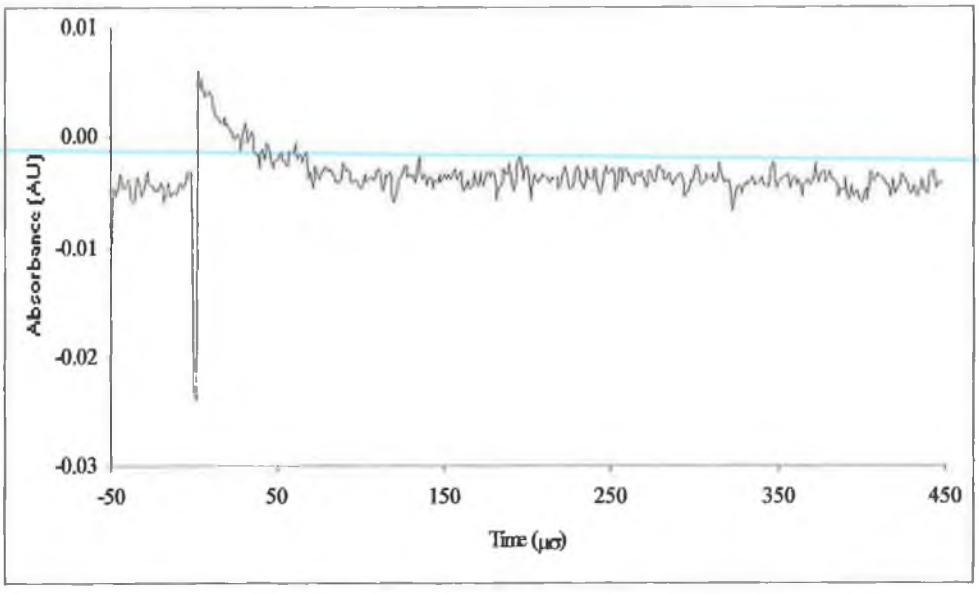

Figure 2.10 A typical transient signal for the decay of (η^3-allyl)$Fe(CO)_2NO$ ($\lambda_{exc.}$ = 355 nm) monitored at 340 nm in cyclohexane under 1atm. of CO.

2.2.2.2 Laser flash photolysis of (η^3-allyl)$Fe(CO)_2NO$ under 1 atm of Ar

Following flash photolysis ($\lambda_{exc.}$ = 355 nm) under an atmosphere of Ar, weak transient signals were observed at 360 nm. A typical transient absorption decay is shown below in Figure 2.11. The transient signal observed was recorded using a 50μs time base, and k_{obs} was measured to be 5 x 10^4 s^{-1}. The transient doesn't recover to the pre-irradiated baseline, indicating formation of a new species. The UV/vis spectrum was monitored throughout the experiment with small changes observed in the region from 350 to 450 nm as shown in Figure 2.13. The transient signal was also monitored at longer time bases such as 500 and 1000 μs, as shown in Figure 2.12 to investigate whether the transient signal would recover to the pre-

irradiated baseline, which it did not. An IR spectrum recorded the following day showed no further bands other than those assigned to (η^3-allyl)$Fe(CO)_2NO$.

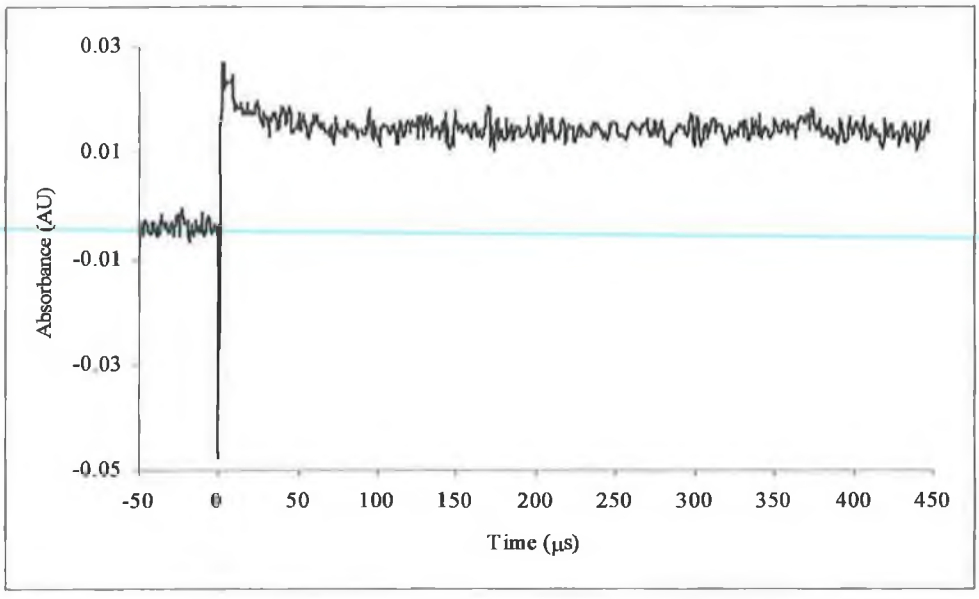

Figure 2.11 A typical transient signal for the decay of (η^3-allyl)$Fe(CO)_2NO$ (λ_{exc} = 355 nm) monitored at 360 nm in cyclohexane under 1atm. of Ar at 50μs time base.

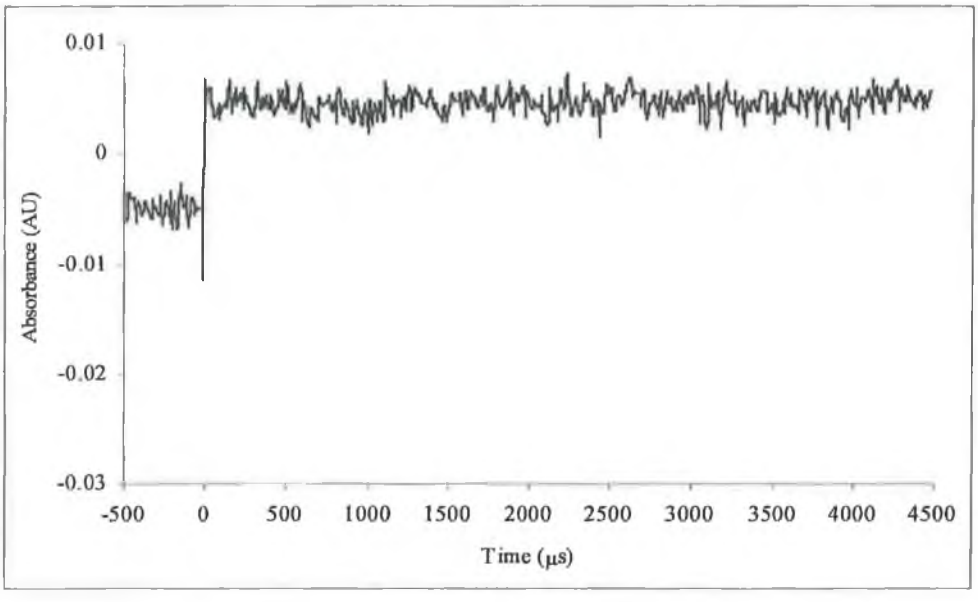

Figure 2.12 A typical transient signal for the decay of (η^3-allyl)$Fe(CO)_2NO$ (λ_{exc} = 355 nm) monitored at 360 nm in cyclohexane under 1atm. of Ar at 500μs time base.

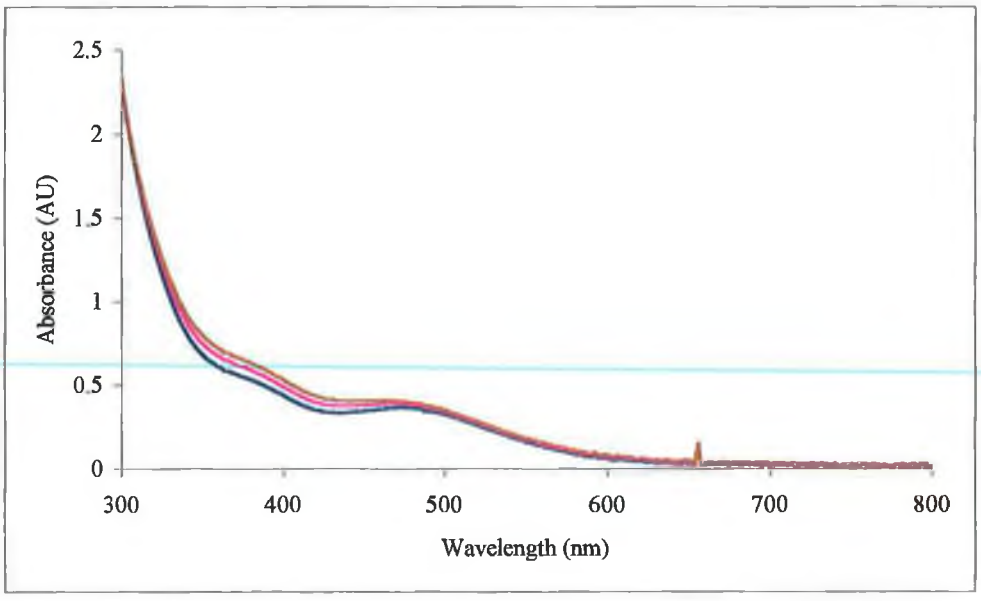

Figure 2.13 Uv/vis spectra of the changes observed during flash photolysis ($\lambda_{exc.}$= 355 nm) of (η^3-allyl)$Fe(CO)_2NO$ in cyclohexane under 1atm. of Ar.

2.2.3 Matrix isolation studies of (η^3-allyl)$Fe(CO)_2NO$

Matrix isolation studies were carried out on (η^3-allyl)$Fe(CO)_2NO$ in an Ar matrix at 20K. IR spectroscopy was used to monitor the progress of the experiment. The CO stretching bands of (η^3-allyl)$Fe(CO)_2NO$ occur at 2040 and 1985 cm^{-1} and the NO stretching band is observed at 1764 cm^{-1}. As expected, these bands are at slightly higher frequency (wavenumber) than those measured in solution. Initial photolysis of the sample ($\lambda_{exc.}$> 500 nm) led to a small decrease in intensity of ν_{CO} and ν_{NO} of (η^3-allyl)$Fe(CO)_2NO$, however no new bands were formed, indicating decomposition of (η^3-allyl)$Fe(CO)_2NO$. Subsequent photolysis ($\lambda_{exc.}$> 400 nm) led to a further decrease in absorbance of ν_{CO} and ν_{NO}. There was also formation of a weak band at 2139 cm^{-1}. This indicates the formation of "free" CO. The further decrease in absorbance of 2040, 1985 and 1764 cm^{-1} indicates further decomposition of (η^3-allyl)$Fe(CO)_2NO$, while the appearance of the band at 2139

cm^{-1} indicates that CO is being released. If decomposition is occurring, then free NO would also be expected to be observed at 1875 cm^{-1} in an Ar matrix.[11] No such peak is observed however.

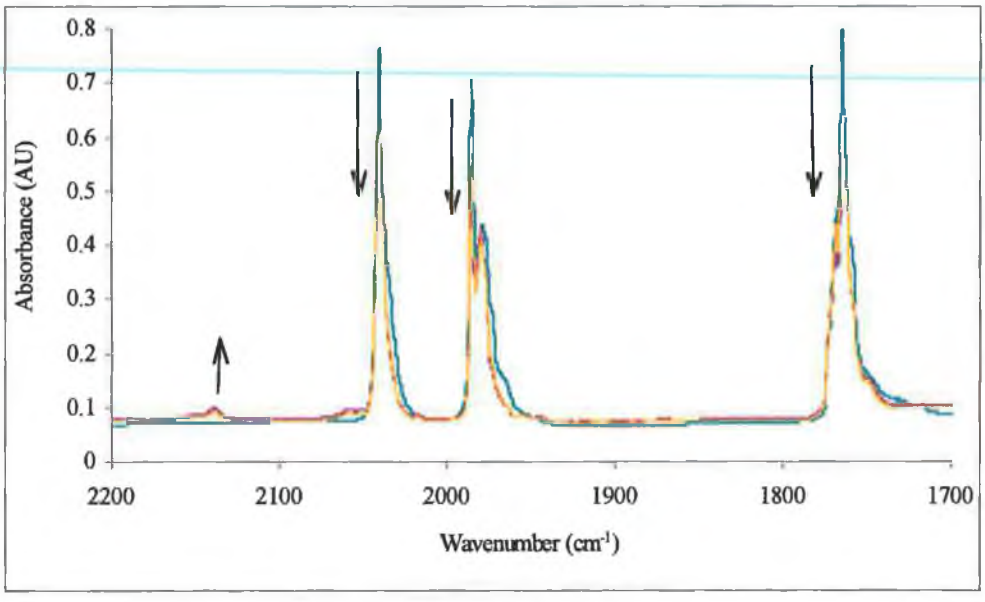

Figure 2.14 Spectral changes observed upon photolysis of (η^3-allyl)$Fe(CO)_2NO$ in an Ar matrix at 20K. The parent bands are seen to decrease in absorbance, with increase in the concentration of free CO

2.2.4 Discussion of photochemistry of (η^3-allyl)$Fe(CO)_2NO$

It is clear from the results of the experiments described in sections 2.2.1.1 to 2.2.1.6, that (η^3-allyl)$Fe(CO)_2NO$ undergoes photochemical substitution of one CO in the presence of a two electron donor. The second CO ligand is also substituted by a triphenylphosphine ligand upon prolonged photolysis. A summary of the reactions is shown in Reaction 2.3.

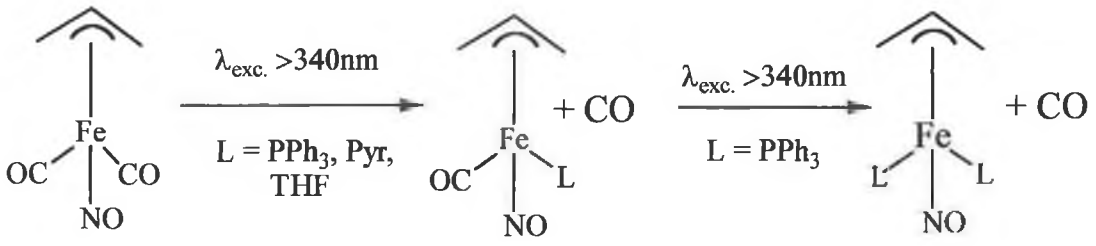

Reaction 2.3 Photochemical reaction ($\lambda_{exc.}$> 340 nm) of (η^3-allyl)Fe(CO)$_2$NO in the presence of two electron donors.

Upon laser flash photolysis ($\lambda_{exc.}$= 355 nm) under an atmosphere of CO, (η^3-allyl)Fe(CO)$_2$NO undergoes reversible solvent mediated loss and recovery of CO. Under an atmosphere of Ar, the transient signal is long-lived and does not recover to the pre-irradiated baseline. It is proposed that a dimeric species of (η^3-allyl)Fe(CO)$_2$NO is formed. This process is described in Scheme 2.1, and will be discussed later.

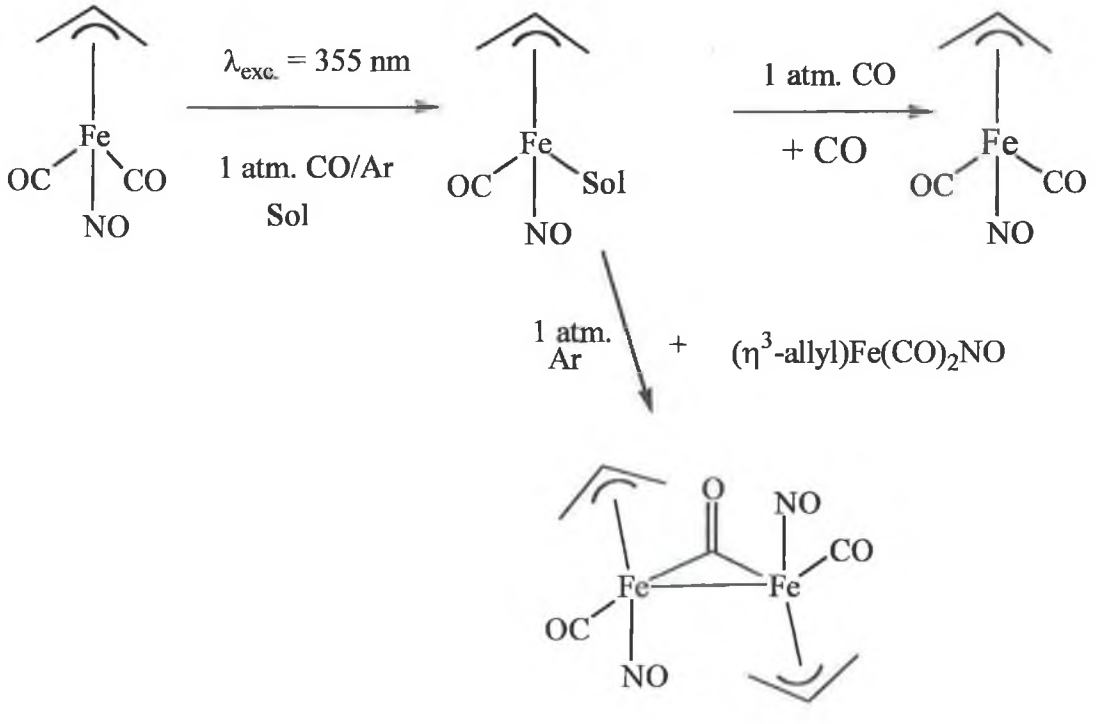

Scheme 2.1 Proposed reactions of (η^3-allyl)Fe(CO)$_2$NO after laser flash photolysis under atmospheres of CO and Ar respectively. Under Ar atmosphere a dimeric species is formed. Sol = Solvent.

2.3 Photochemistry of $(\eta^3$-2-chloroallyl)$Fe(CO)_2NO$

The IR and UV/vis spectra of $(\eta^3$-2-chloroallyl)$Fe(CO)_2NO$, recorded in degassed spectroscopy grade cyclohexane, are shown in Figures 2.15 and 2.16. These bands are within the experimental error of those of an authentic pure sample.[6] The infrared spectrum of $(\eta^3$-2-chloroallyl)$Fe(CO)_2NO$ is similar to that of $(\eta^3$-allyl)$Fe(CO)_2NO$, containing two strong carbonyl stretching bands and one strong nitrosyl stretching bands. The bands observed for $(\eta^3$-2-chloroallyl)$Fe(CO)_2NO$ are shifted to slightly higher wavenumber than the corresponding bands for $(\eta^3$-allyl)$Fe(CO)_2NO$. The shift can be attributed to the electron-withdrawing effect of the chlorine substituent on the allyl ligand, thus reducing the electron density on the metal centre. This has the effect of reducing the amount of back-bonding between the M-CO and M-NO ligands.

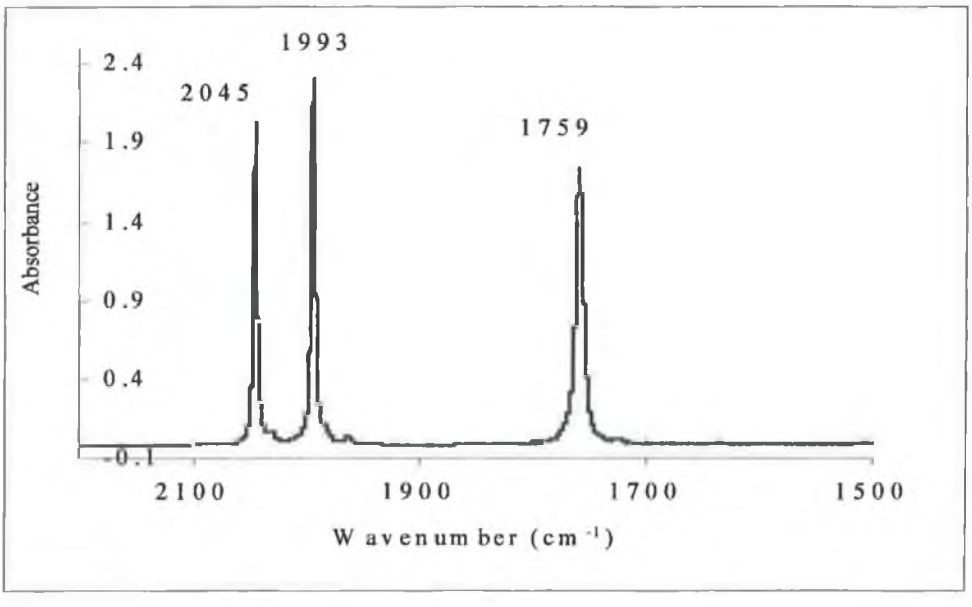

Figure 2.15 IR spectrum of $(\eta^3$-2-chloroallyl)$Fe(CO)_2NO$ recorded in spectroscopy grade cyclohexane.

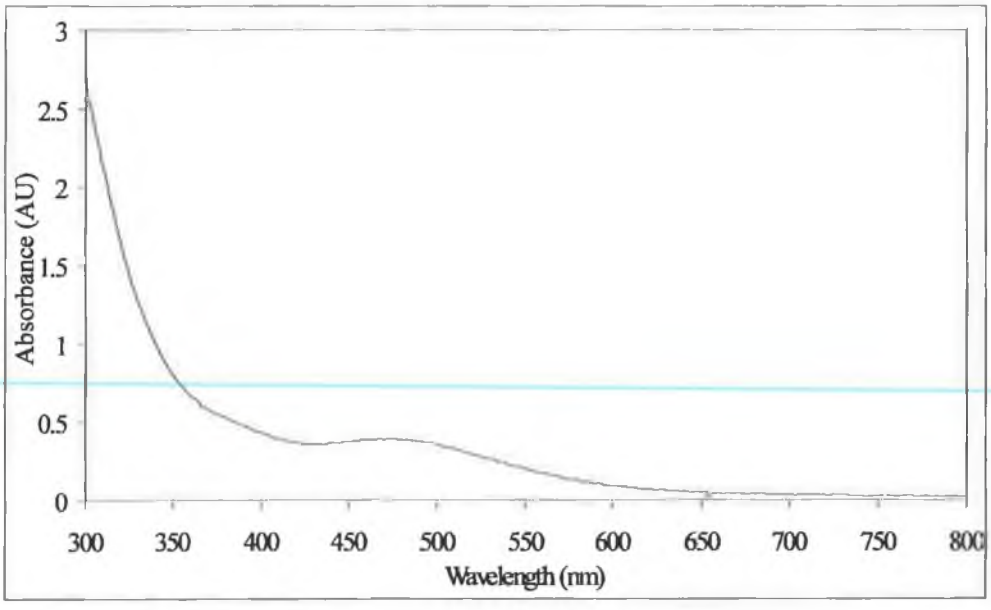

Figure 2.14 UV/vis spectrum of (η^3-2-chloroallyl)$Fe(CO)_2NO$ recorded in spectroscopy grade cyclohexane.

The electronic absorption spectrum in cyclohexane solvent is shown in Figure 2.14. Again the absorption spectrum broadly resembles that of (η^3-allyl)$Fe(CO)_2NO$. There is a broad, low energy absorption band centred about 480 nm. This absorption tails off into the visible region of the spectrum. The ^1H NMR spectrum of (η^3-2-chloroallyl)$Fe(CO)_2NO$ recorded was within the experimental error of those of an authentic pure sample,[6] with singlets appearing at 3.80 (2H) and 4.36 (2H) ppm. The values are shifted downfield due to the de-shielding effect of the chlorine on the allyl ligand. The coupling pattern is greatly simplified due to the substitution of the hydrogen molecule on the central carbon by the chlorine, the multiplet observed for (η^3-allyl)$Fe(CO)_2NO$ at 4.30 ppm, disappeared.

2.3.1 Steady state photolysis of (η^3-2-chloroallyl)$Fe(CO)_2NO$

2.3.1.1 IR monitored photolysis of (η^3-2-chloroallyl)$Fe(CO)_2NO$

(η^3-2-Chloroallyl)$Fe(CO)_2NO$ was photolysed ($\lambda_{exc.} > 340$ nm) in degassed cyclohexane in the presence of a 10-fold excess of triphenylphosphine in a sealed IR cell. As is evident from the difference spectra in Fig. 2.15, upon photolysis, there was a depletion of the parent bands, with concomitant formation of new peaks, indicating formation of a new product.

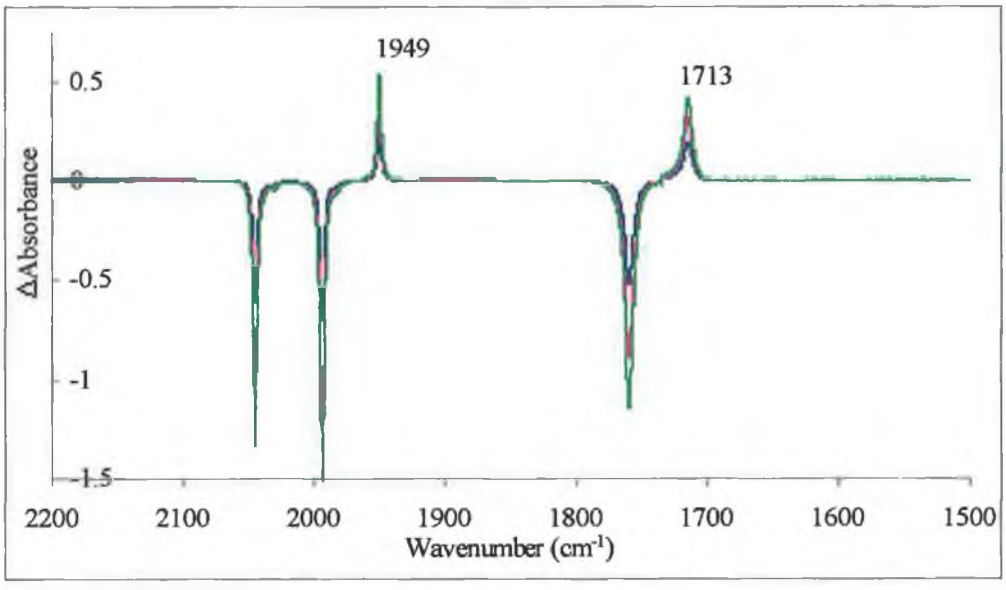

Figure 2.15 Difference spectra showing photolysis ($\lambda_{exc.}$ >340 nm) of (η^3-2-chloroallyl)$Fe(CO)_2NO$ with excess PPh_3 in cyclohexane.

CO stretching bands at 2044 and 1993 cm^{-1} and a single NO stretching band at 1759 cm^{-1} decreased in intensity, a new ν_{CO} at 1949 cm^{-1} and ν_{NO} at 1713 cm^{-1} were formed, indicating substitution of CO by PPh_3, and the formation of (η^3-2-

chloroallyl)Fe(CO)NO(PPh_3). These bands appear at slightly higher frequency than the corresponding bands for (η^3-allyl)Fe(CO)NO(PPh_3) as would be expected due to the greater electron withdrawing effect of the chlorine substituent on the allyl ligand.

2.3.1.2 UV/vis monitored photolysis of (η^3-2-chloroallyl)Fe(CO)$_2$NO

(η^3-2-Chloroallyl)Fe(CO)$_2$NO was photolysed ($\lambda_{exc.} > 340$ nm) for a period of 20 minutes in degassed cyclohexane in the presence of a 10-fold excess of triphenylphosphine. The UV/vis spectra were recorded at regular intervals. There was a general increase in absorption across the entire spectral region, although the increase observed in the region from 350 nm to 500 nm is particularly strong.

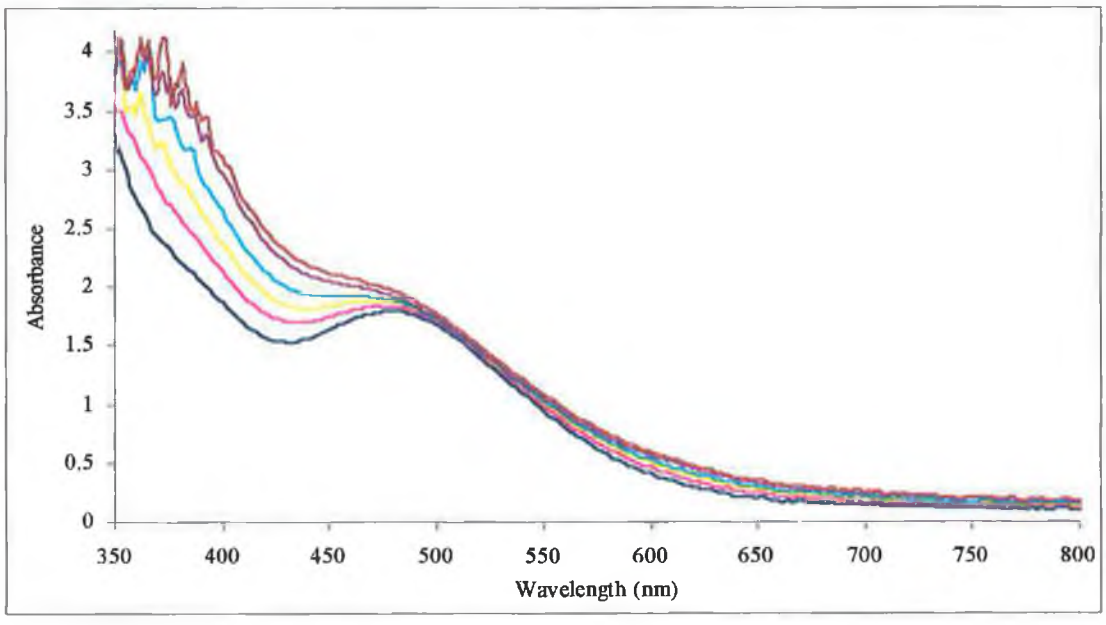

Figure 2.16 UV/vis monitored photolysis of (η^3-2-chloroallyl)Fe(CO)$_2$NO with 10-fold excess PPh_3 in cyclohexane.

The changes that occurred become more obvious when the initial spectrum is subtracted from the other spectra recorded in the course of the experiment to produce a difference spectrum (Figure 2.17). Also the formation of the precipitate as the reaction proceeded indicated formation of an insoluble product.

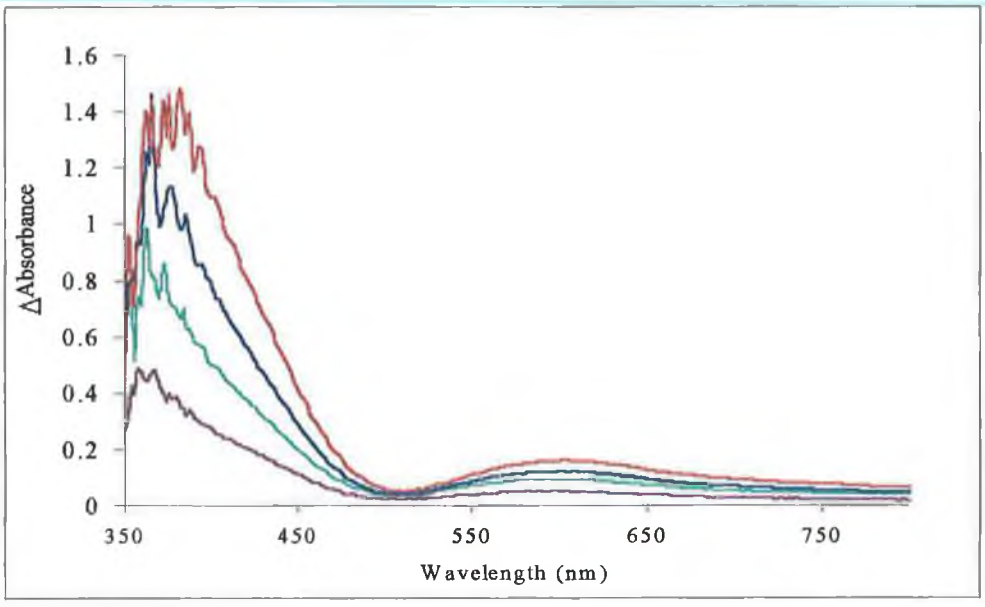

Figure 2.17 UV/vis monitored difference spectrum of photolysis of (η^3-2-chloroallyl)$Fe(CO)_2NO$ with 10-fold excess PPh_3 in cyclohexane.

In order to identify the chemical changes that were observed in the UV/vis spectra, IR spectra of the solution were recorded before and after the experiment, with the spectral changes shown in the difference spectrum, Figure 2.18. The depletion of parent bands and frequency of new bands formed, are consistent with the formation of (η^3-2-chloroallyl)$Fe(CO)NO(PPh_3)$.

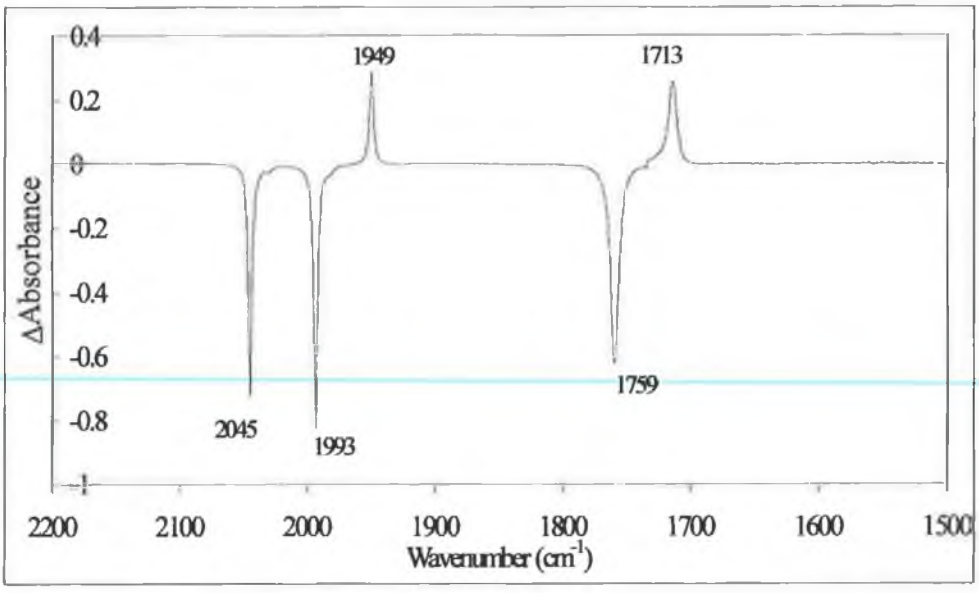

Figure 2.18 IR difference spectrum showing changes that occurred upon photolysis ($\lambda_{exc.} > 340$ nm) of (η^3-2-chloroallyl)Fe(CO)$_2$NO with 10-fold excess PPh_3 in cyclohexane.

Together with the evidence from the IR and UV/vis monitored photolysis experiments of (η^3-allyl)Fe(CO)$_2$NO, and the ^{1}H NMR data from the isolated pure sample of (η^3-allyl)Fe(CO)NO(PPh_3), the results obtained confirmed the photochemical formation of (η^3-2-chloroallyl)Fe(CO)NO(PPh_3).

2.3.2 Laser flash photolysis of (η^3-2-chloroallyl)Fe(CO)$_2$NO

Laser flash photolysis experiments were carried out at $\lambda_{exc.}$ of 355 nm and 532 nm. As with (η^3-allyl)Fe(CO)$_2$NO, no transients of (η^3-2-chloroallyl)Fe(CO)$_2$NO were detected for $\lambda_{exc.}$= 532 nm. At $\lambda_{exc.}$= 355 nm, flash photolysis studies were carried out in cyclohexane under both CO and Ar atmospheres.

2.3.2.1 *Laser flash photolysis of (η^3-2-chloroallyl)Fe(CO)$_2$NO under CO*

Laser flash photolysis was initially carried out under an atmosphere of CO to investigate the reversibility of the system. By keeping the time base constant, and varying the monitoring wavelength, it is possible to build up a point-by-point spectrum of the transient produced at a specific time delay after the laser fired. The spectrum recorded (Figure 2.19), shows a broad featureless absorption of a transient species.

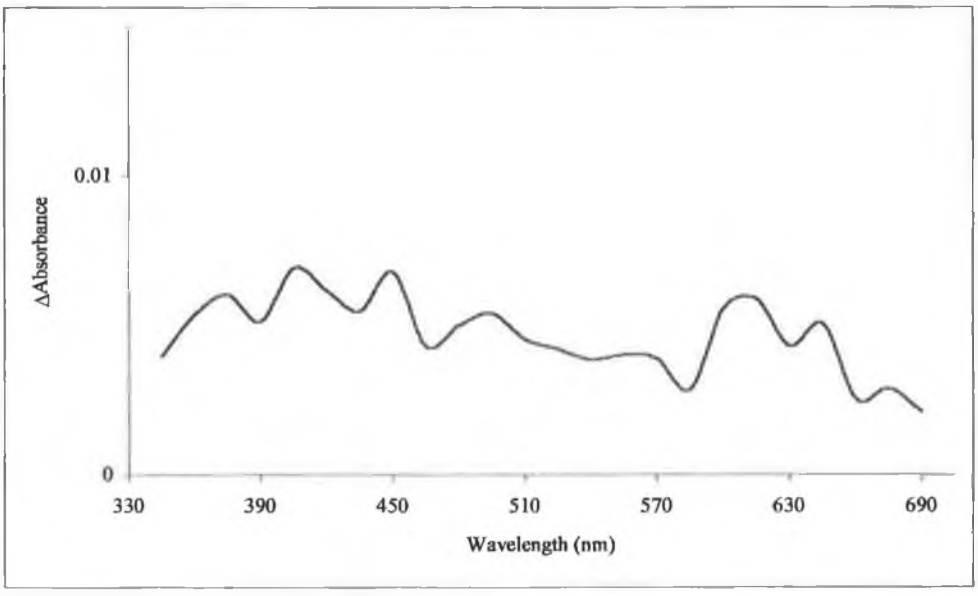

Figure 2.19 Transient absorption difference spectrum of (η^3-2-chloroallyl)Fe(CO)$_2$NO in cyclohexane under 1 atm. CO recorded 10 μs after the laser flash.

At 600nm under an atmosphere of CO, a weak decay process was observed. A typical transient signal recorded at 600 nm is shown below in Figure 2.21. The first order rate of the decay was measured to be 7.5 x 10^4 s^{-1}.

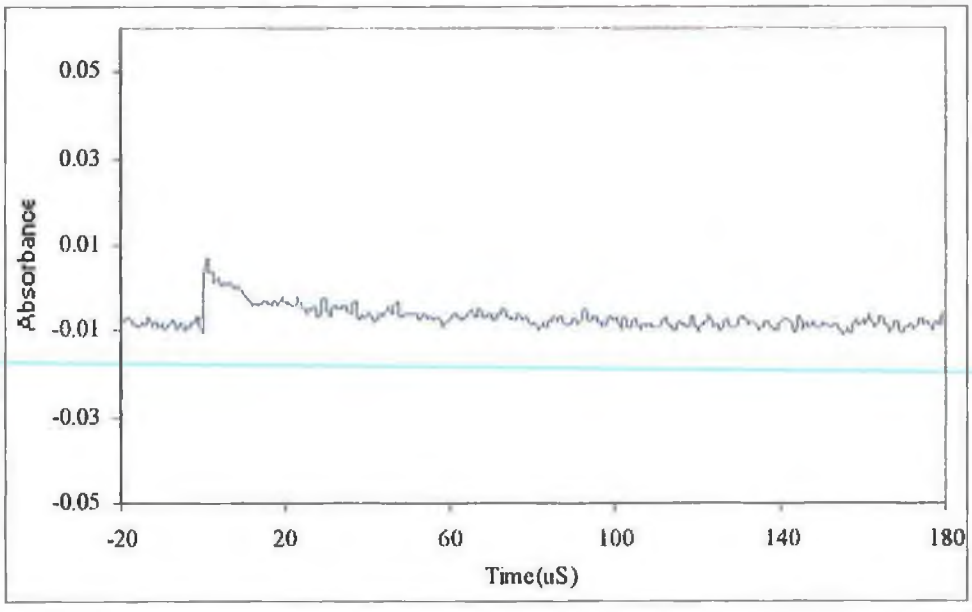

Figure 2.21 Transient signal of (η^3-2-chloroallyl)$Fe(CO)_2NO$ under 1atm. CO for $\lambda_{exc.}$= 355 nm, observed at 600 nm which returns to the pre-irradiated baseline.

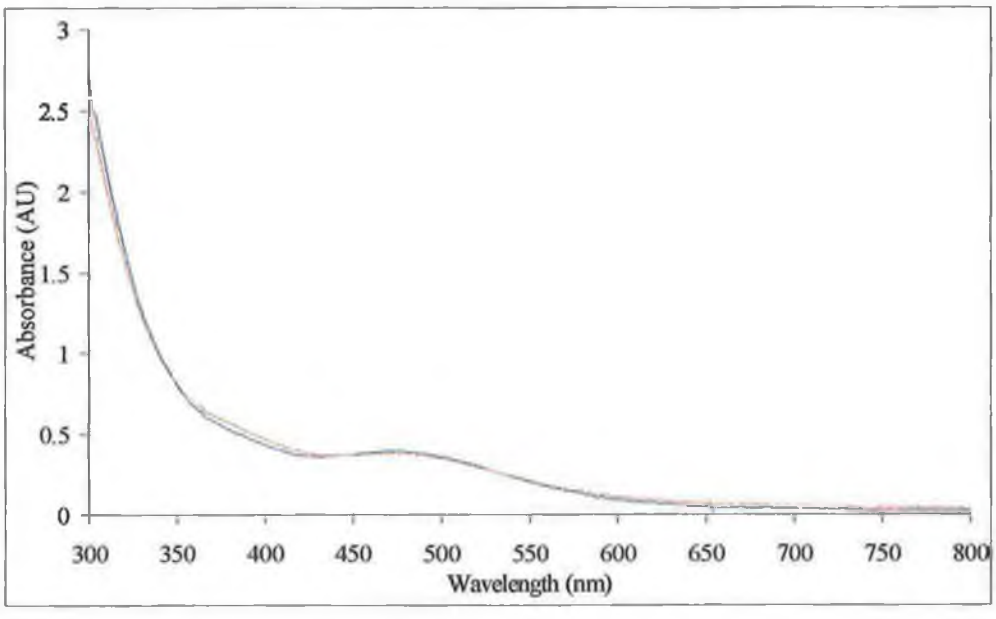

Figure 2.22 UV/vis spectra of sample of (η^3-2-chloroallyl)$Fe(CO)_2NO$ under 1 atm. of CO, taken before and after laser flash photolysis experiment.

2.3.2.2 Laser flash photolysis of (η^3-2-chloroallyl)Fe(CO)$_2$NO under Ar.

As previously carried out with the (η^3-2-chloroallyl)Fe(CO)$_2$NO sample dissolved in cyclohexane under an atmosphere of CO, a similar transient absorption difference spectrum was constructed under an atmosphere of Ar. The resultant spectrum, Figure 2.23 shows a broad featureless absorption throughout the spectral range.

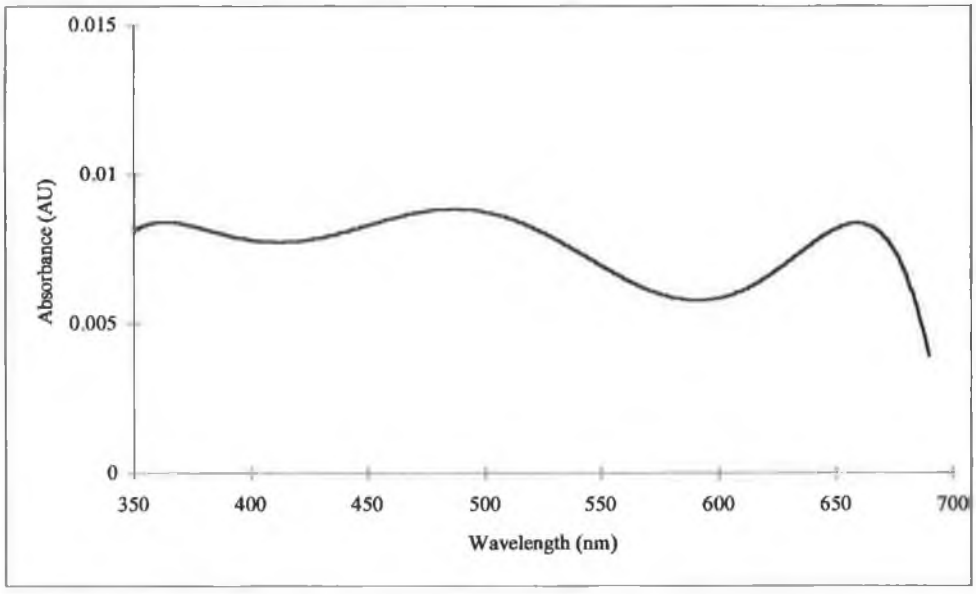

Figure 2.23 Transient absorption spectrum of (η^3-2-chloroallyl)Fe(CO)$_2$NO in cyclohexane under 1atm. of argon recorded 10 μs after the laser has flashed.

In the laser flash photolysis of (η^3-2-chloroallyl)Fe(CO)$_2$NO under 1 atm. of Ar, a transient absorption was observed at 420 nm. This transient signal did decay, however it did not return to the pre-irradiated baseline. Figure 2.24 shows a typical transient signal recorded on a 20 μs time-base.

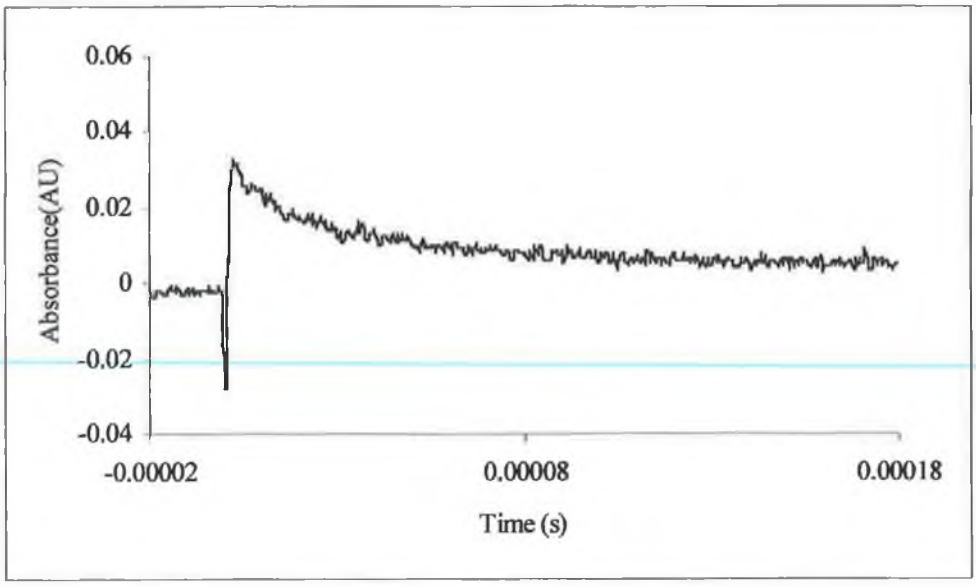

Figure 2.24 Typical transient signal for the decay of (η^3-2-chloroallyl)$Fe(CO)_2NO$ monitored at 420 nm in cyclohexane under 1 atm. of Ar with a 20 μs time-base. The transient does not return to the pre-irradiated baseline, even at much longer time-bases.

Longer time-bases, up to 500 μs were also recorded, as shown in Figure 2.25, but the transient signal remained above the pre-irradiated baseline.

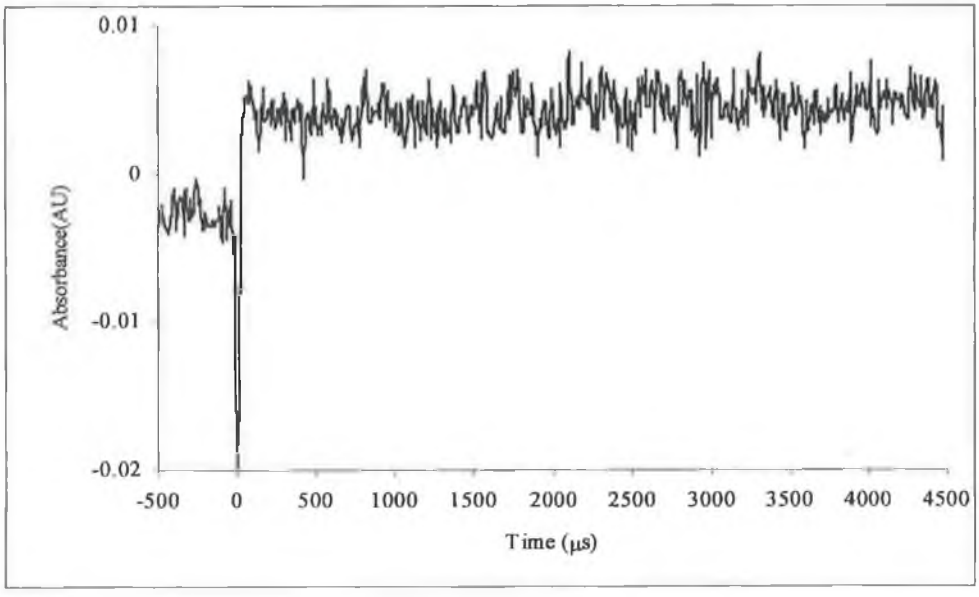

Figure 2.25 Transient signal for the decay of (η^3-2-chloroallyl)$Fe(CO)_2NO$ monitored at 420 nm in cyclohexane under 1 atm. of Ar with a 500 μs time-base

Figure 2.26 also shows the difference between the UV/vis spectra at the beginning and end of the experiment

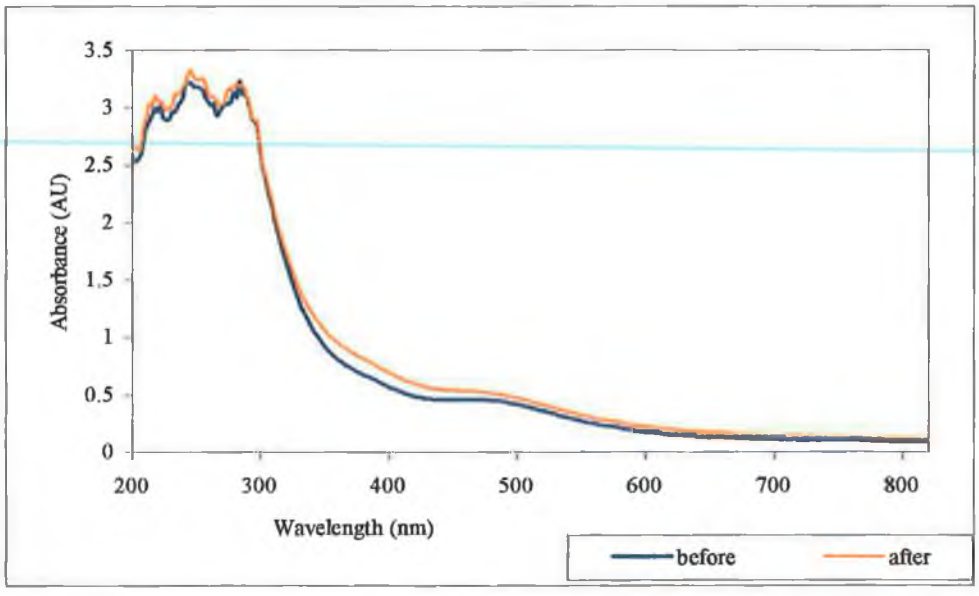

Figure 2.26 UV/vis spectra of sample of (η^3-2-chloroallyl)$Fe(CO)_2NO$ under 1 atm. of Ar, taken before and after laser flash photolysis experiment. Absorbance increases generally from 350 to 800 nm, but changes are most pronounced around 400 nm.

As can be seen from the UV/vis spectra shown in Figure 2.26, there is an increase in absorption from approximately 350 nm right out into the visible region of the spectrum. These changes are due to formation of a stable species, mostly likely a dimer of (η^3-2-chloroallyl)$Fe(CO)_2NO$, similar to that proposed in the flash photolysis studies of (η^3-allyl)$Fe(CO)_2NO$ in Section 2.2.4, and the structure is represented in Figure 2.27. Another potential outcome was the NO ligand going from linear to bent configuration (3 e^- donor $\rightarrow$ 1 e^- donor), with formation of a dimer. An IR spectrum was recorded at the end of the experiment in order to identify the product formed. The IR spectrum, shown in Figure 2.28, exhibited bands at 2045, 1993, 1965, 1759 and 1703 cm^{-1}.

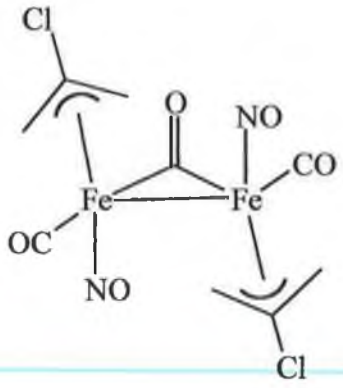

Figure 2.27 Proposed dimer structure of product from laser flash photolysis ($\lambda_{exc.}$ = 355 nm) of (η^3-2-chloroallyl)Fe(CO)$_2$NO under 1 atm. Ar

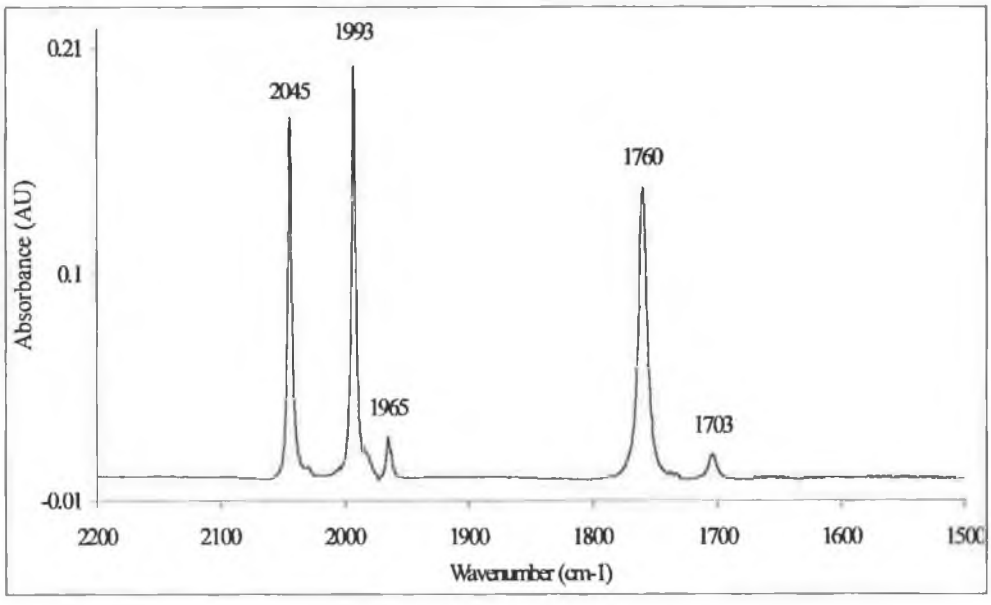

Figure 2.28 IR spectrum of (η^3-2-chloroallyl)Fe(CO)$_2$NO under 1 atm. of Ar, recorded directly after laser flash photolysis experiment. An IR spectrum recorded the following day showed no evidence of the bands at 1965 and 1703 cm^{-1}.

The (η^3-2-chloroallyl)Fe(CO)$_2$NO bands at 2045, 1993, and 1759 cm^{-1} are still the dominant feature of the spectrum, with the new bands attributed to formation of the dimer species. The new bands are consistent with the structure of the proposed dimer, giving rise to strong ν_{CO} and ν_{NO} bands at 1965 and 1703 cm^{-1} respectively. A bridging carbonyl would also be expected to absorb at approximately 1700 cm^{-1}.

However as the absorption of the terminal CO at 1965 cm^{-1} is quite weak, it is unlikely that the bridging carbonyl would be observed, and also it may be obscured by ν_{NO} 1760 or 1703 cm^{-1}. Any process involving the NO ligand changing from a three to a one electron donor must be ruled out as the ν_{NO} would be shifted to a higher frequency, which is not what was observed in the spectrum. The sample was stored overnight under argon, and an IR spectrum recorded the following day showed no evidence of the peaks observed at 1963 and 1701 cm^{-1}.

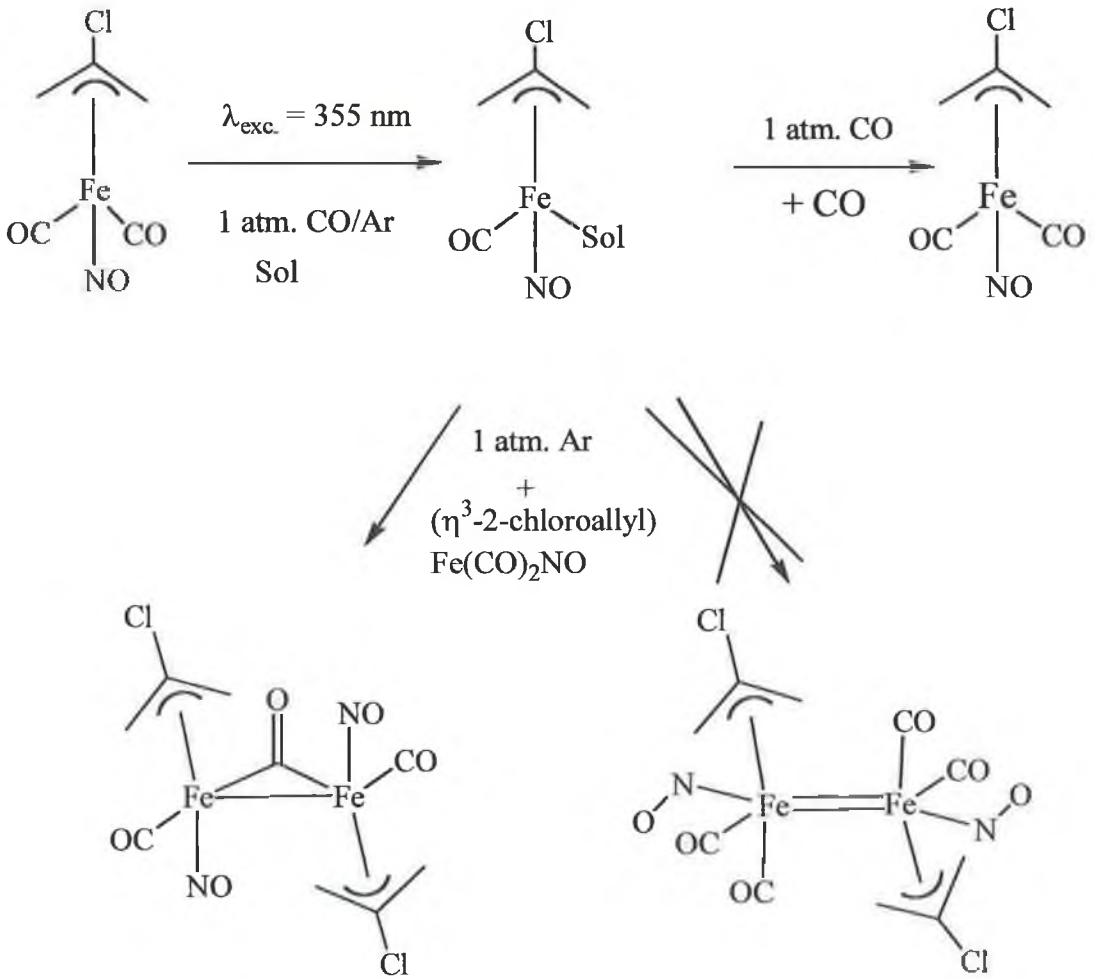

Scheme 2.2 Summary of the proposed reactions upon flash photolysis ($\lambda_{exc.}$ = 355 nm) of (η^3-2-chloroallyl)$Fe(CO)_2NO$ under atmospheres of CO and Ar. Sol = Solvent

When the laser is fired, CO is lost from (η^3-2-chloroallyl)Fe(CO)$_2$NO and a solvated product (η^3-2-chloroallyl)Fe(CO)NO(Sol) is formed. In an atmosphere of CO, recombination is rapid, and the transient observed returns to the pre-irradiated baseline. Under an atmosphere of Ar, the transient does not recover to the pre-irradiated baseline. The solvated species, (η^3-2-chloroallyl)Fe(CO)NO(Sol) reacts with a molecule of (η^3-2-chloroallyl)Fe(CO)$_2$NO to form the dimer described in Figure 2.26. This is a stable species and was observed in the IR spectrum recorded directly after the flash photolysis experiment. The dimer is not as stable as (η^3-2-chloroallyl)Fe(CO)$_2$NO, and after a day there is no longer evidence for the dimer in the IR region, with (η^3-2-chloroallyl)Fe(CO)$_2$NO being reformed.

2.4 Photochemistry of (η^3-allyl)Fe(CO)NO(PPh$_3$)

The IR spectrum of (η^3-allyl)Fe(CO)NO(PPh$_3$) is shown in Figure 2.29, recorded in cyclohexane. The position of the bands are within experimental error of those reported in the literature.[6] The ^{1}H NMR peaks recorded were also within error of the reported values.[6] (η^3-Allyl)Fe(CO)NO(PPh$_3$) was synthesised both photochemically and thermally.

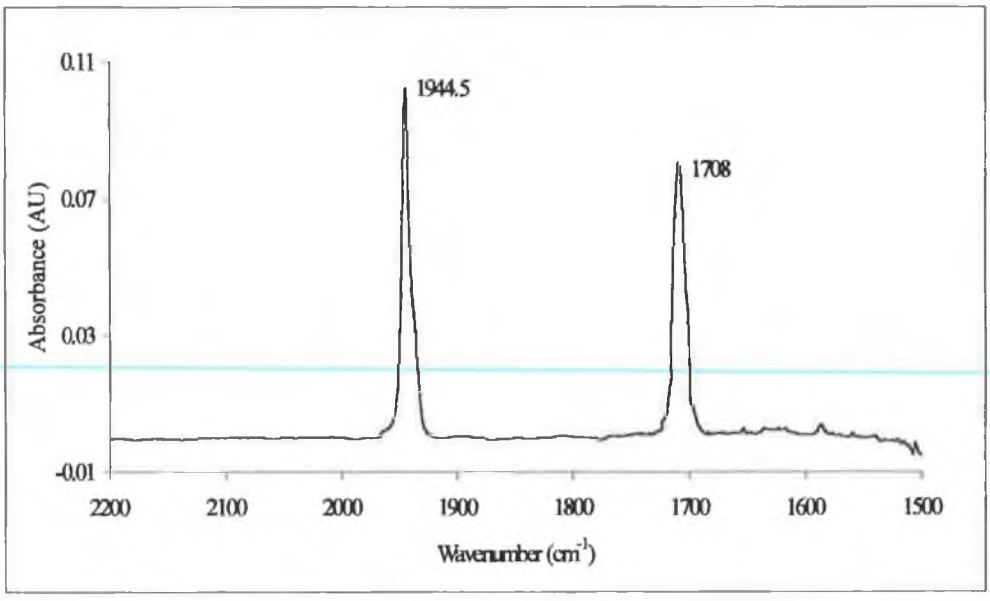

Figure 2.29 IR absorption spectrum of (η^3-allyl)Fe(CO)NO(PPh_3) recorded in cyclohexane solvent

2.4.1 Steady State Photolysis of (η^3-allyl)Fe(CO)NO(PPh_3)

2.4.1.1 IR monitored photolysis of (η^3-allyl)Fe(CO)NO(PPh_3) ($\lambda_{exc.} > 410$ nm) with excess triphenylphosphine

(η^3-Allyl)Fe(CO)NO(PPh_3) was photolysed ($\lambda_{exc.} > 410$ nm) in degassed cyclohexane in the presence of a 10-fold excess of triphenylphosphine in a sealed IR cell for a total of 10 minutes. The spectral changes observed are shown in Figure 2.30. The ν_{CO} and ν_{NO} bands due to (η^3-allyl)Fe(CO)NO(PPh_3) decrease upon photolysis and a new band is formed at 1667 cm^{-1}. The spectral changes are consistent with replacement of CO with PPh_3 with formation of (η^3-allyl)FeNO(PPh_3)$_2$. Substitution of a CO by PPh_3 increases the electron density on

the metal centre. PPh_3 is significantly more electron donating when compared to CO. The excess electron density on the metal is transferred to the anti-bonding orbital of NO, increasing the strength of the M-NO back bonding, and resulting in a lowering of ν_{NO}.

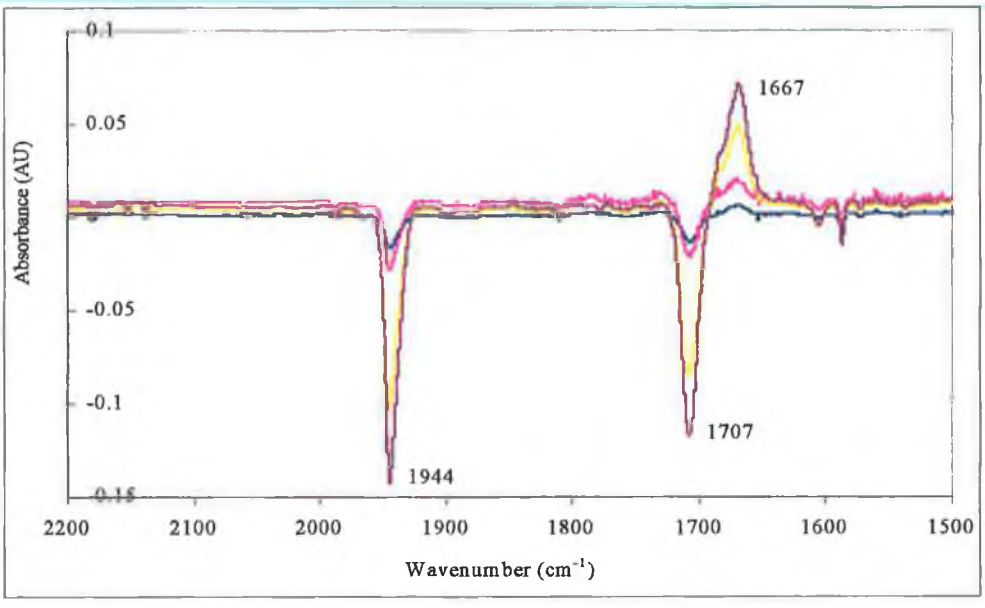

Figure 2.30 IR difference spectrum of photolysis ($\lambda_{exc.} > 410$ nm) of (η^3-allyl)Fe(CO)NO(PPh_3) in cyclohexane solvent.

2.4.1.2 IR monitored photolysis of (η^3-allyl)Fe(CO)NO(PPh_3) ($\lambda_{exc.} > 300$ nm) with excess triphenylphosphine

(η^3-Allyl)Fe(CO)NO(PPh_3) was photolysed ($\lambda_{exc.} > 300$ nm) in degassed cyclohexane in the presence of a 10-fold excess of triphenylphosphine in a sealed IR cell for a total of 60 minutes. The spectral changes observed are shown in Figure 2.31. Initially the ν_{CO} and ν_{NO} bands of (η^3-allyl)Fe(CO)NO(PPh_3) decrease, and as in the experiment above (Section 2.4.1.1), a new band is formed at 1667 cm^{-1}

indicating production of (η^3-allyl)FeNO(PPh_3)$_2$. However upon prolonged photolysis further changes are observed.

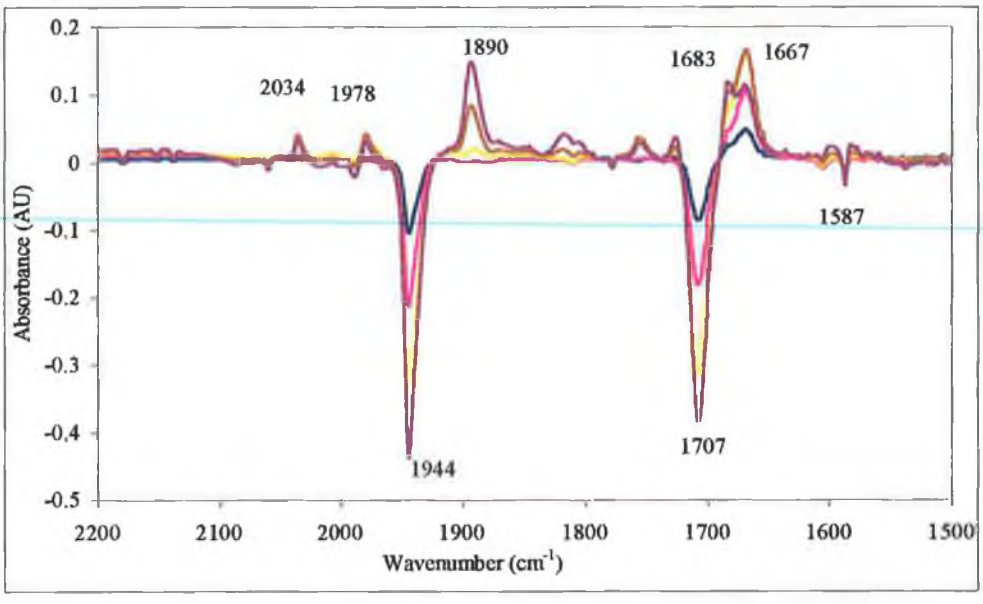

Figure 2.31 Difference spectrum of photolysis ($\lambda_{exc.}$ > 300 nm) of (η^3-Allyl)Fe(CO)NO(PPh_3) with excess triphenylphosphine in cyclohexane solution.

The ν_{NO} stretch at 1667 cm^{-1} assigned to (η^3-allyl)FeNO(PPh_3)$_2$ reaches a maximum absorbance after 15 minutes photolysis (Figure 2.32), and further bands now begin to appear at 2034, 1978 and 1756 cm^{-1}, which correspond to the ν_{CO} and ν_{NO} bands of (η^3-allyl)Fe(CO)$_2$NO in cyclohexane. The band at 1587 cm^{-1} is PPh_3. The absorbance of the bands of (η^3-allyl)Fe(CO)$_2$NO show no major changes upon prolonged photolysis.

Upon further photolysis (t = 30 mins.), the absorbance at 1667 cm^{-1} assigned to (η^3-allyl)FeNO(PPh_3)$_2$ remains unchanged. However a weak band appears at 1683 cm^{-1}, seen as a shoulder in Figures 2.33. There is also a weak band at 1889 cm^{-1}, which corresponds to the reported stretching frequency of free NO gas.[12] This would indicate that the band at 1683 cm^{-1} results from decomposition products with release

of NO. The shoulder at 1683 cm^{-1} may be part of a larger band obscured by the decreasing absorbances of $(\eta^3$-allyl)Fe(CO)NO(PPh_3) at 1707 cm^{-1}.

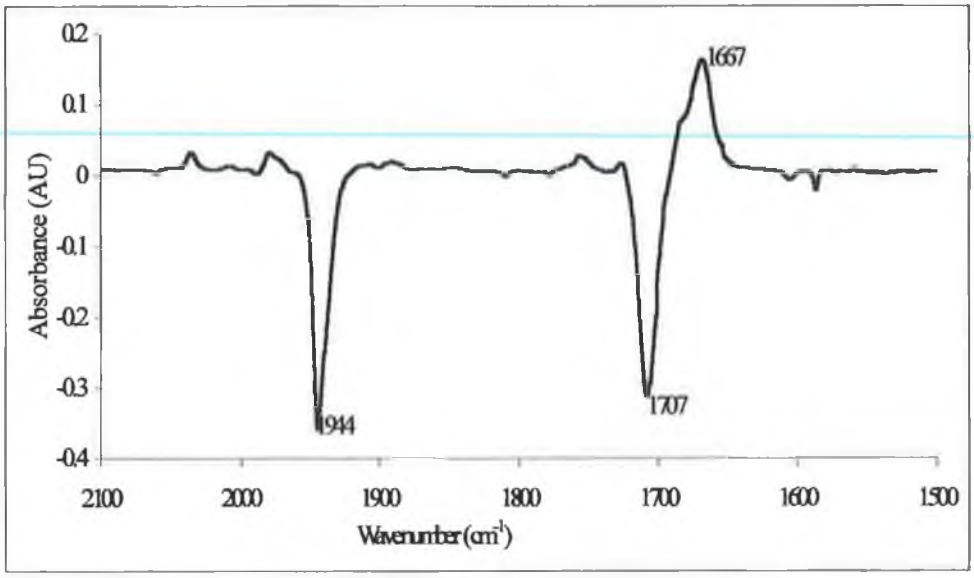

Figure 2.32 Spectral changes observed after 15 mins. photolysis ($\lambda_{exc.}$ > 300 nm) of (η^3-allyl)Fe(CO)NO(PPh_3) with excess triphenylphosphine in cyclohexane.

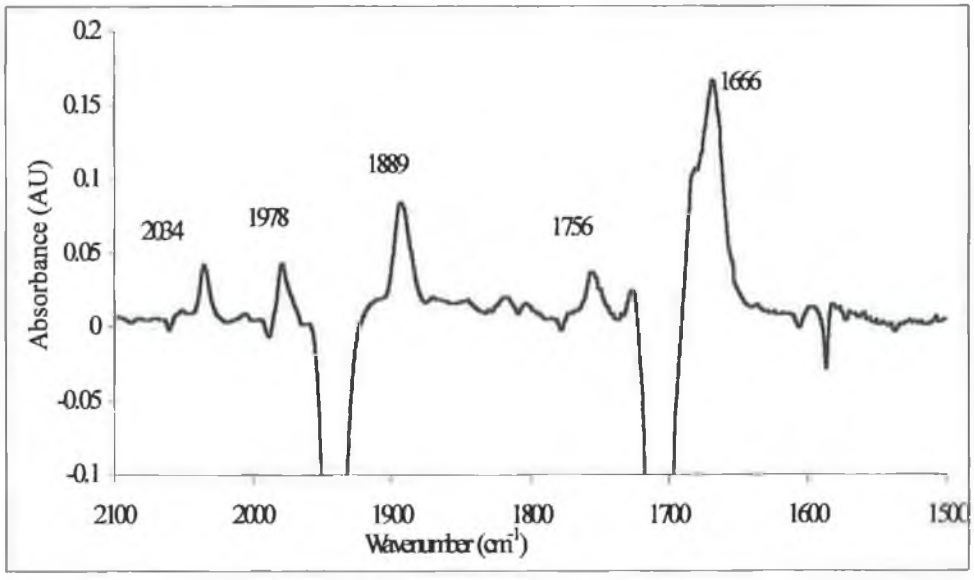

Figure 2.33 Spectral changes observed after 30 mins. photolysis ($\lambda_{exc.}$ > 300 nm) of (η^3-allyl)Fe(CO)NO(PPh_3) with triphenylphosphine in cyclohexane.

Upon further photolysis (t = 60 mins.), (η^3-allyl)FeNO(PPh_3)$_2$ reaches a steady state concentration. The bands of (η^3-allyl)Fe(CO)$_2$NO (2034, 1978 and 1756 cm^{-1}) do not change significantly. The bands at 1890, 1814 and 1683 cm^{-1} increase in intensity, as shown in Figure 2.34.

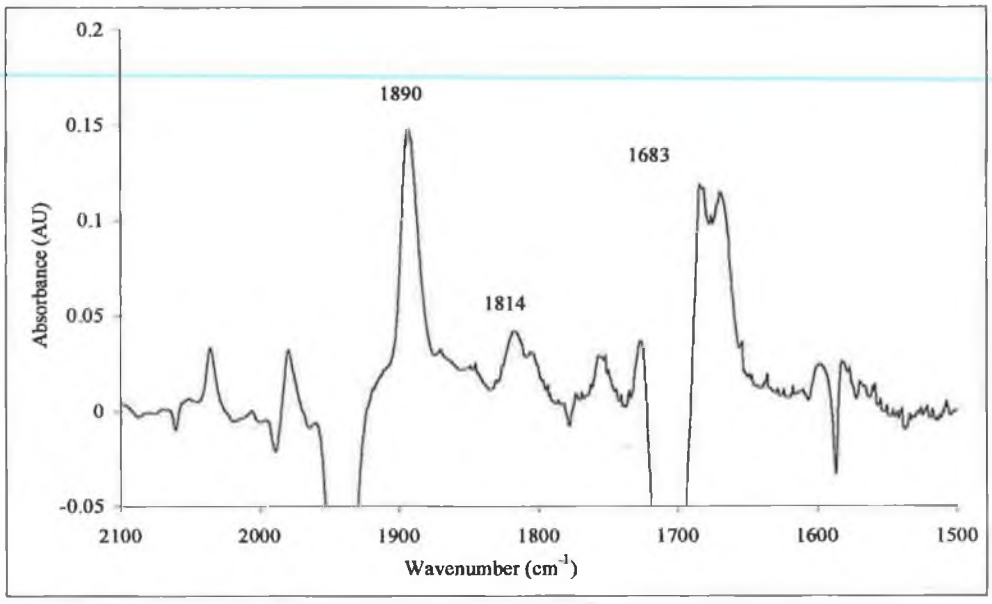

Figure 2.34 Spectral changes observed after 60mins. photolysis ($\lambda_{exc.} > 300$ nm) of (η^3-allyl)Fe(CO)NO(PPh_3) with triphenylphosphine in cyclohexane.

It is therefore proposed that upon steady-state photolysis, under an atmosphere of Ar, with excess PPh_3, (η^3-allyl)Fe(CO)NO(PPh_3) initially loses CO and reacts with PPh_3 to form (η^3-allyl)FeNO(PPh_3)$_2$. After 30 mins. of photolysis, the peaks of (η^3-allyl)Fe(CO)NO(PPh_3) at 1944 and 1707 cm^{-1} are no longer observed. Consequently, subsequent species observed are secondary photoproducts. The peaks at 2034, 1978 and 1756 cm^{-1} suggest the formation of (η^3-allyl)Fe(CO)$_2$NO. Formation of (η^3-allyl)Fe(CO)$_2$NO must be facilitated from the liberated CO of (η^3-allyl)Fe(CO)NO(PPh_3) which remains in the sealed cell. This means the maximum concentration of (η^3-allyl)Fe(CO)$_2$NO is half that of (η^3-allyl)Fe(CO)NO(PPh_3). A dimer of [(η^3-allyl)FeNO(PPh_3)]$_2$CO is also formed with a bridging carbonyl,

similar to the dimer described in Section 2.4.2.2. This dimer then decomposes to release "free" NO and other products. A summary of the proposed photolysis reactions, based upon the IR spectral changes that occur are shown in Scheme 2.3.

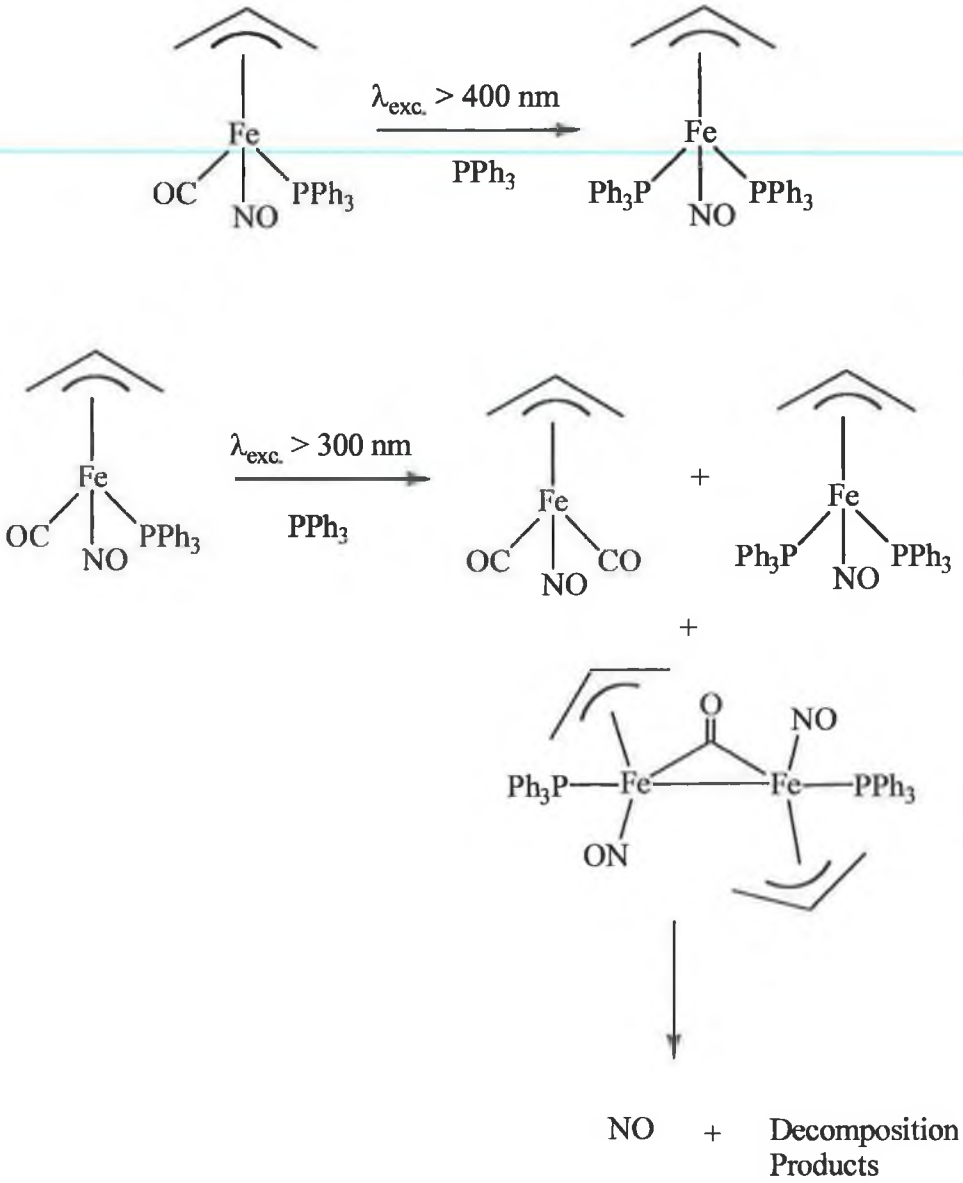

Scheme 2.3 Proposed photoreactions of (η^3-allyl)Fe(CO)NO(PPh_3) when photolysed in the presence of excess PPh_3 in cyclohexane solvent, 1 atm. Ar. Reactions for $\lambda_{exc.}$ > 400 nm and 300 nm are shown.

2.4.1.3 *UV/vis monitored photolysis of (η^3-allyl)Fe(CO)NO(PPh_3)*

Steady state photolysis of (η^3-allyl)Fe(CO)NO(PPh_3) was carried out in toluene under CO or Ar atmospheres using monochromatic light sources. Changes observed are shown in Figures 2.35 and 2.36 respectively. Under an atmosphere of CO, an increase in absorbance was observed as the experiment progressed, between 260 and 290 nm. A decrease in absorption is observed between 290 and 370 nm with an isosbestic point at 290 nm.

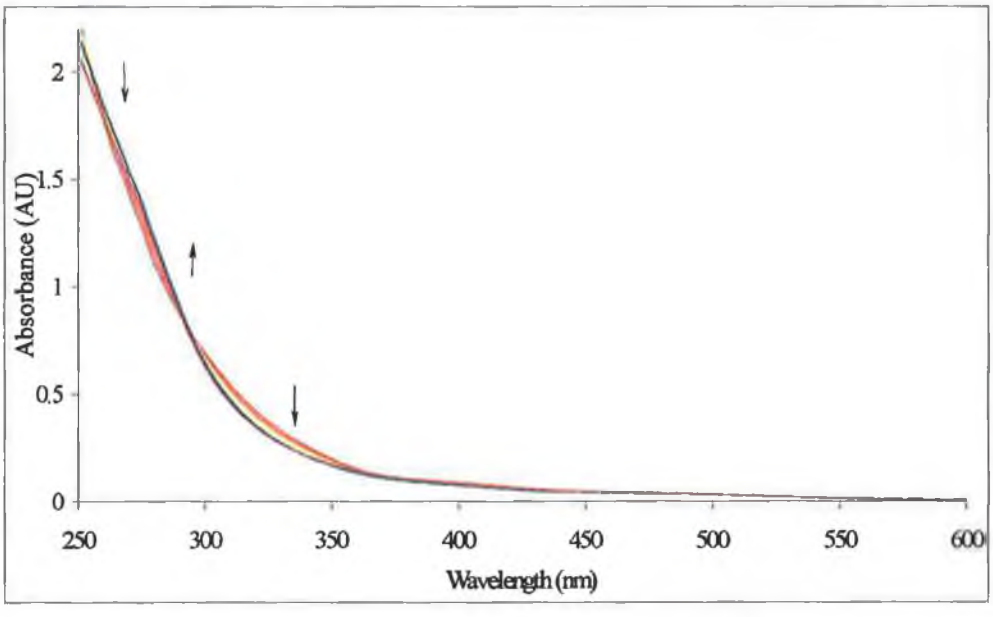

Figure 2.35 Spectral changes observed upon monochromatic ($\lambda_{exc.}$= 266 nm) steady state photolysis of (η^3-allyl)Fe(CO)NO(PPh_3) in toluene under 1 atm. CO.

Under an atmosphere of Ar, absorption decreased across a range from 230 to 350 nm. The changes are most dramatic between 230 and 280 nm. From 350 to 450 nm a small increase in absorption is observed. Again an isosbestic point is observed at 330 nm.

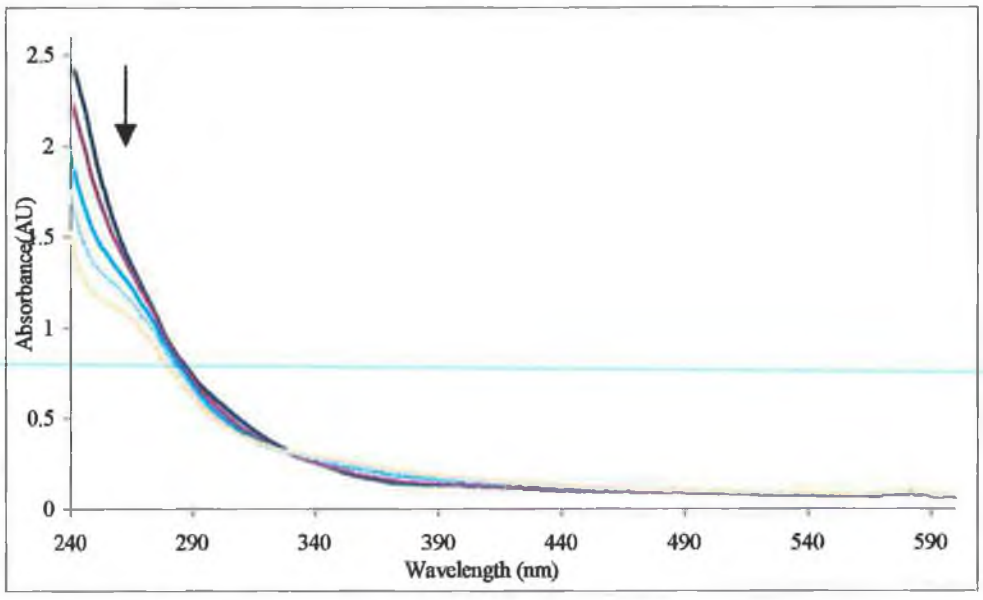

Figure 2.36 Spectral changes observed upon monochromatic (λ_{exc} = 266 nm) steady state photolysis of (η^3-allyl)Fe(CO)NO(PPh_3) in toluene under 1 atm. Ar.

2.4.2 Laser flash photolysis of (η^3-allyl)Fe(CO)NO(PPh_3)

Laser flash photolysis experiments on (η^3-allyl)Fe(CO)NO(PPh_3) were conducted using λ_{exc} = 355 nm. These studies were carried out under an atmosphere of either CO or Ar in toluene. Cyclohexane was not used as (η^3-allyl)Fe(CO)NO(PPh_3) was only sparingly soluble in the solvent. As before a transient absorption difference spectrum was measured and is presented in Figure 2.37. The spectra were recorded at 5, 20, 50 and 100 μs following laser flash photolysis. Photolysis studies were subsequently monitored at 420 nm.

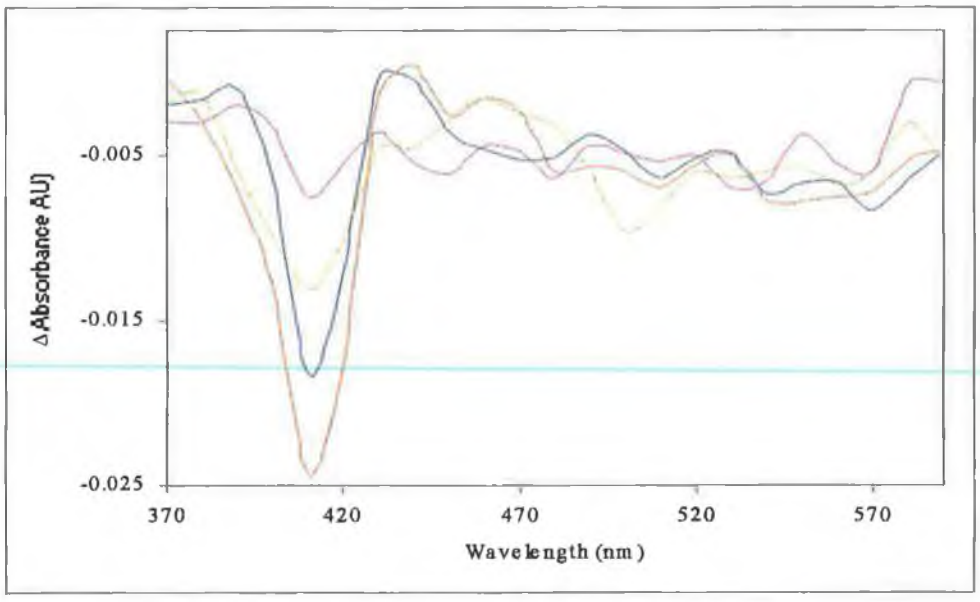

Figure 2.37 Transient absorption difference spectrum of (η^3-allyl)Fe(CO)NO(PPh_3) in toluene under 1 atm. CO recorded at 5, 20, 50 and 100 μs respectively, after the laser flash.

A typical transient depletion and recovery process recorded at 420 nm under 1 atm. of CO is shown in Figure 2.38. Steady-state UV/vis spectra recorded during the experiment showed no changes, indicating the system was reversible. The first order rate of the transient for the recovery was 4.3×10^4 s^{-1}

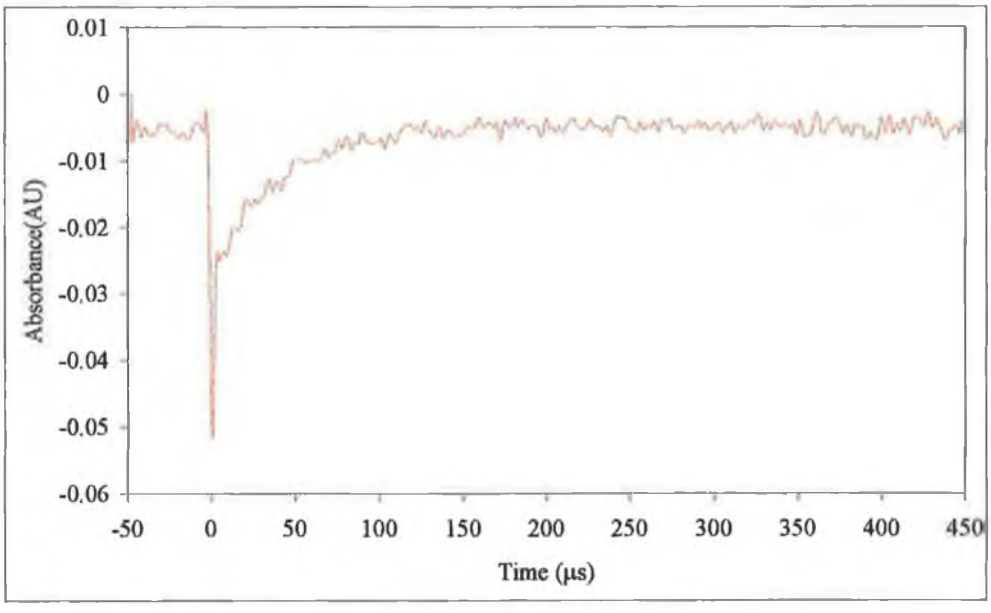

Figure 2.38 Typical transient depletion and recovery of (η^3-allyl)Fe(CO)NO(PPh_3) in toluene under 1 atm. CO monitored at 420 nm, using a 50 μs timebase.

Photolysis studies were also carried out on (η^3-allyl)Fe(CO)NO(PPh_3) in toluene under 1 atm. of Ar, again monitored at 420 nm. A depletion and recovery process was again observed, however the transient species did not recover to the pre-irradiated baseline. A typical depletion and recovery process recorded on a 50 μs time base is shown in Figure 2.39. When recorded on a longer time base such as 500 μs, shown in Figure 2.40, the transient appears as a step, again without returning to the pre-irradiated baseline. The UV/vis spectra recorded throughout the experiment show some small changes in absorption between 350 and 400 nm. IR spectra recorded after the experiment show the bands due to (η^3-allyl)Fe(CO)NO(PPh_3) decreased marginally in absorbance. Again as previously discussed in Sections 2.3.4 and 2.4.2.2, the long-lived species observed upon flash photolysis under an Ar atmosphere is most likely a dimer of the particular species being studied.

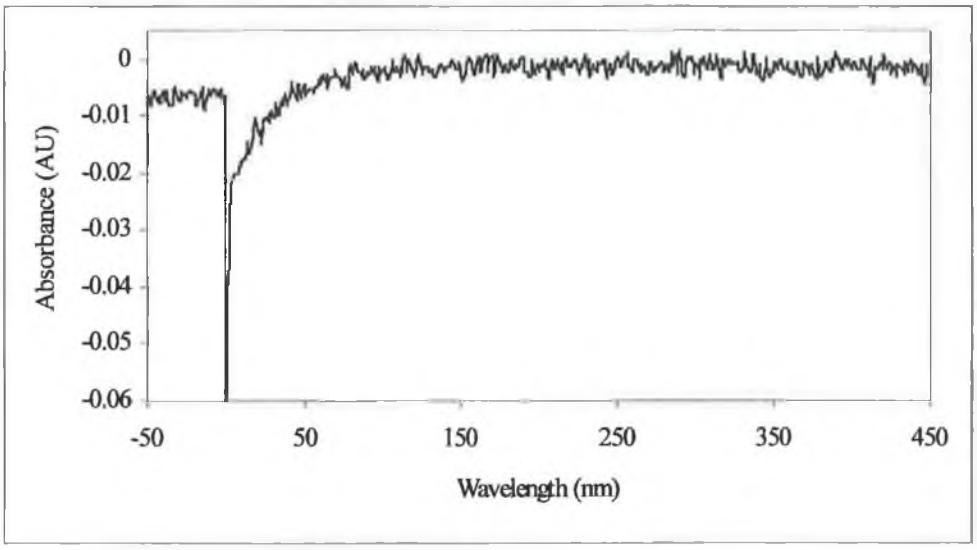

Figure 2.39 Typical transient depletion and recovery of (η^3-allyl)Fe(CO)NO(PPh_3) in toluene under 1 atm. Ar monitored at 420 nm, using a 50 μs timebase. Transient does not return to the pre-irradiated baseline

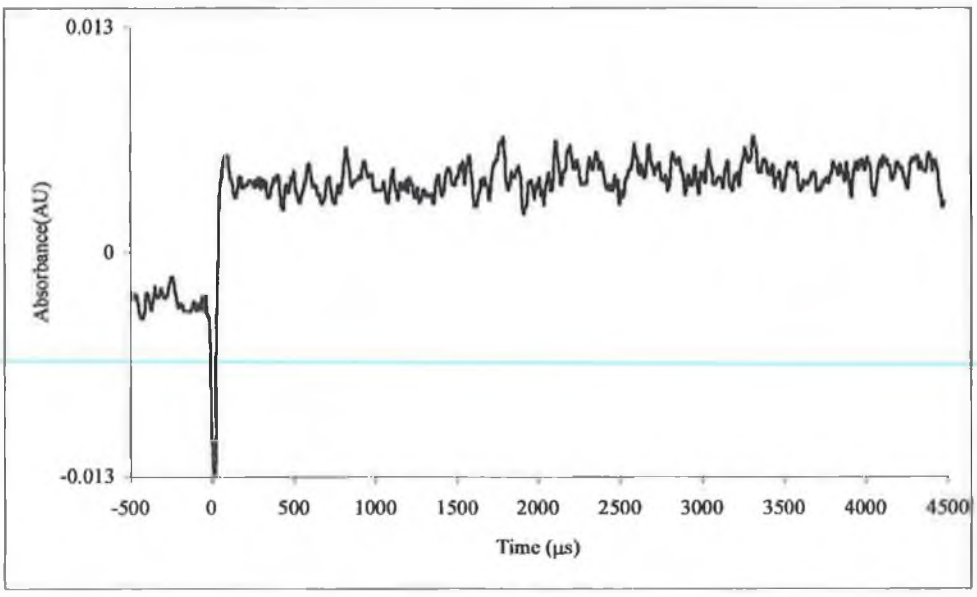

Figure 2.40 Typical transient signal of (η^3-allyl)Fe(CO)NO(PPh_3) in toluene under 1 atm. Ar monitored at 420 nm, using a 500 μs timebase.

2.4.3 Discussion of photochemistry of (η^3-allyl)Fe(CO)NO(PPh_3)

(η^3-Allyl)Fe(CO)NO(PPh_3) undergoes photochemical substitution of CO in the presence of a two electron donor, such as triphenylphosphine. Formation of (η^3-allyl)Fe$(CO)_2$NO is also observed, indicating substitution of the PPh_3 ligand by CO. Upon prolonged photolysis, ($\lambda_{exc} > 300$ nm) the photoproducts, including the dimer described in Section 2.4.1.2, decomposed to release "free" NO and other products.

Under laser flash photolysis ($\lambda_{exc} = 355$ nm), (η^3-allyl)Fe(CO)NO(PPh_3) undergoes solvent mediated loss and recovery of CO, under an atmosphere of CO. Flash photolysis under an atmosphere of Ar also involves initial CO loss, however (η^3-

allyl)Fe(CO)NO(PPh_3) is not reformed efficiently, as occurs with a CO atmosphere, and a dimer species as represented in Scheme 2.4 was observed.

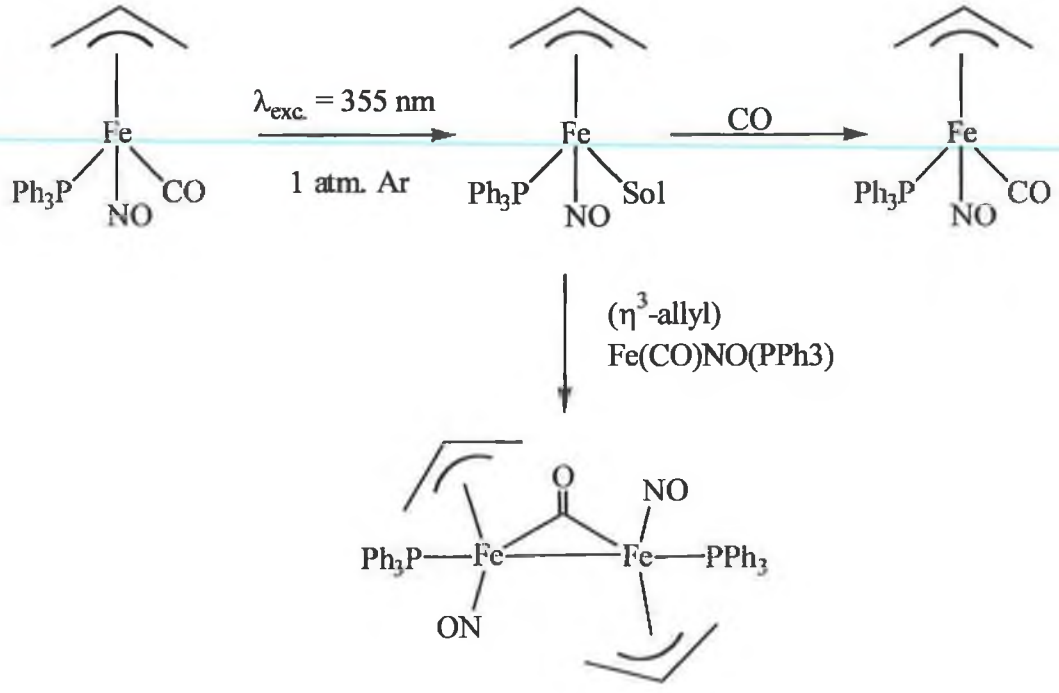

Scheme 2.4 Proposed reaction of (η^3-allyl)Fe(CO)NO(PPh_3) upon flash photolysis (λ_{exc}= 355 nm) under 1 atm. Ar. The dimer species is analogous to those observed with the previous compounds discussed.

2.5 Photochemistry of $Fe(NO)_2(PPh_3)_2$

The primary photoreaction from the previous compounds studied involved loss of CO, which was favoured over loss of NO. To favour loss of NO, a compound without carbonyl ligands, $Fe(NO)_2(PPh_3)_2$ was chosen to be studied. The $Fe(NO)_2(PPh_3)_2$ starting material was characterised from its IR and ^{1}H NMR spectra, the peaks observed being within experimental error of those reported in the literature.[13] $Fe(NO)_2(PPh_3)_2$ has two strong ν_{NO}'s consistent with linear NO

configuration. These bands are observed at 1727 and 1685 cm^{-1} in cyclohexane solvent. $Fe(NO)_2(PPh_3)_2$ is more soluble in dichloromethane and the ν_{NO}'s are shifted to 1714 and 1668 cm^{-1}.

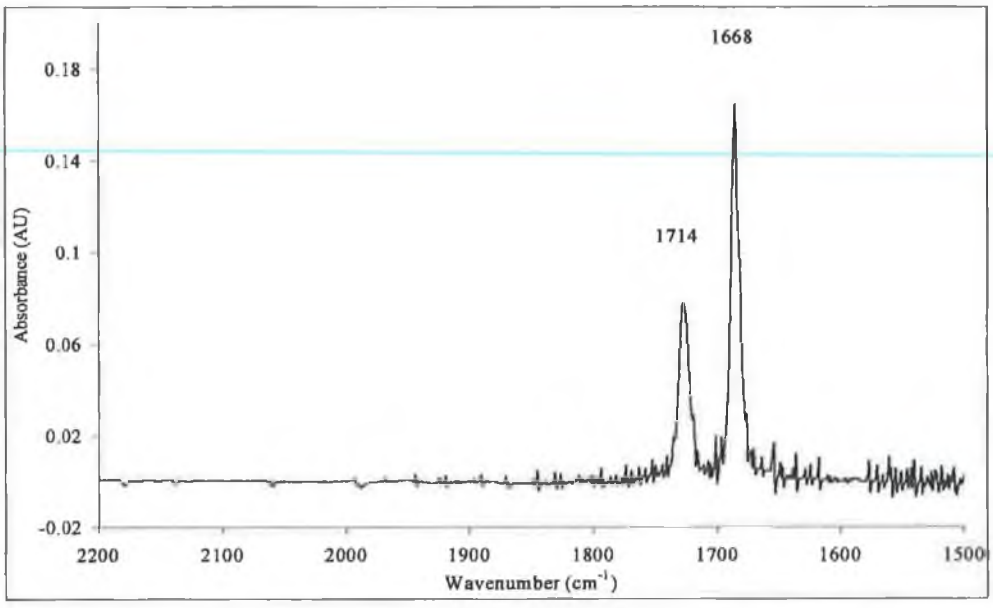

Figure 2.41 IR spectrum of $Fe(NO)_2(PPh_3)_2$ dissolved in dichloromethane solvent.

2.5.1 Steady state photolysis of $Fe(NO)_2(PPh_3)_2$

2.5.1.1 IR monitored photolysis of $Fe(NO)_2(PPh_3)_2$ with excess PPh_3

$Fe(NO)_2(PPh_3)_2$ was photolysed ($\lambda_{exc.} > 340$ nm) in degassed dichloromethane in the presence of a 10-fold excess of triphenylphosphine in a sealed IR cell for a total of 90 minutes. $Fe(NO)_2(PPh_3)_2$ was only sparingly soluble in cyclohexane solvent, and the peaks were weak. Spectra recorded are shown in Figure 2.42. As the reaction proceeds, the parent bands (1714 and 1668 cm^{-1}) decrease and new bands are observed at higher energy (1791 and 1734 cm^{-1}). An isosbestic point is observed at 1723 cm^{-1}.

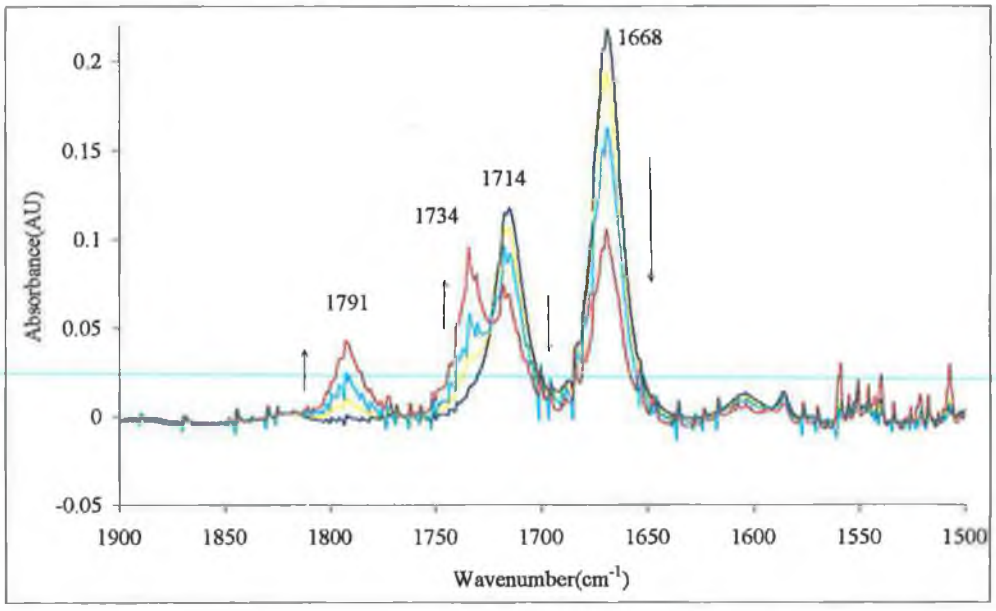

Figure 2.42 IR monitored steady state photolysis of $Fe(NO)_2(PPh_3)_2$ ($\lambda_{exc.} > 340$ nm) in dichloromethane in the presence of excess PPh_3. A decrease in parent bands and formation of new bands was observed

$Fe(NO)_2(PPh_3)_2$ has a pseudo-tetrahedral arrangement, with an N-Fe-N angle of 124° and a P-Fe-P angle of 112°.[14] As with previous compounds studied, NO is a formal three electron donor, resulting in Fe-N-O ligands being almost linear, at 178°. The freqencies of the two new bands indicate formation of a different dinitrosyl species, with less back-bonding from the metal centre than was present in $Fe(NO)_2(PPh_3)_2$. One possibility resulting from photolysis is a rearrangement resulting in an approximately cis-square planar type configuration, with the N-Fe-N angle pushed much closer to 90°, as represented in Figure 2.43. This would result in the Fe-N-O angle also being reduced, with a subsequent increase in absorption frequency.

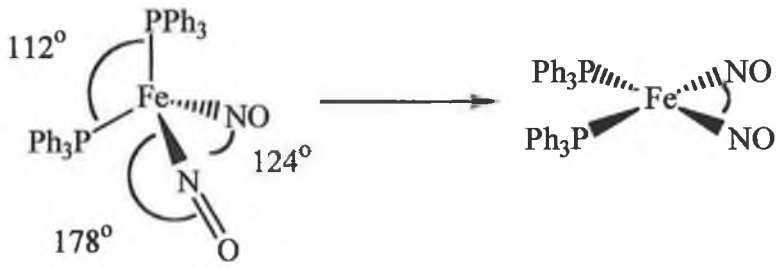

Figure 2.43 Possible photochemical ($\lambda_{exc.} > 340$ nm) rearrangement of $Fe(NO)_2(PPh_3)_2$ from pseudo-tetrahedral arrangement to cis-square planar type configuration with increase in NO absorption frequency.

2.5.1.2 UV/vis monitored photolysis of $Fe(NO)_2(PPh_3)_2$

$Fe(NO)_2(PPh_3)_2$ was photolysed ($\lambda_{exc.} > 340$ nm) in degassed dichloromethane under an atmosphere of CO and Ar respectively. Changes observed in the spectra recorded for the CO experiment are shown in Figure 2.40. The absorbance between 270 and 300 nm increases with photolysis duration, whereas a decrease is observed between 310 and 380 nm. There is an isosbestic point observed at 302 nm. The changes in the spectra occurred irrespective of which gas was present.

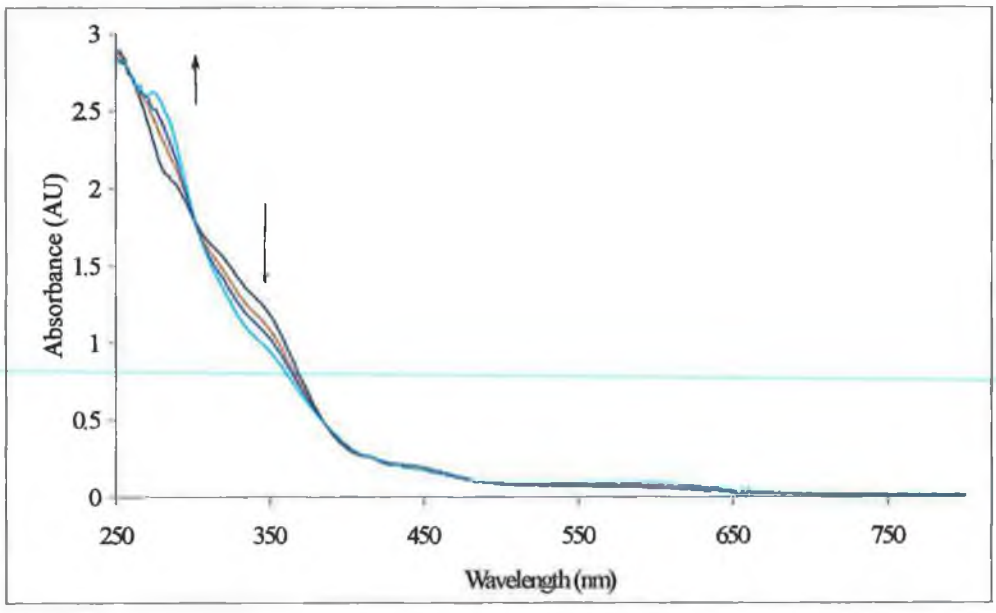

Figure 2.44 UV/vis monitored steady state photolysis of $Fe(NO)_2(PPh_3)_2$ (λ >340 nm) in dichloromethane under 1 atm. CO.

2.5.2 Laser flash photolysis of $Fe(NO)_2(PPh_3)_2$

Laser flash photolysis studies ($\lambda_{exc.}$ = 355 nm) of $Fe(NO)_2(PPh_3)_2$ were attempted under both CO and Ar atmospheres, dissolved in toluene and dichloromethane. No transients were observed however, and the UV/vis spectra taken in the course of the experiments remained unchanged.

2.6 Conclusions

The results in this chapter reported the photochemistry of a series of (η^3-allyl)$Fe(L)_2NO$ type complexes. All of the complexes studied undergo CO

substitution when photolysed in the presence of a suitable two electron donor, such as triphenylphosphine. Upon laser flash photolysis ($\lambda_{exc.}$= 355 nm), under an atmosphere of CO, the complexes undergo reversible loss of CO, with complete reformation of the starting material. All of the compounds studied exhibited weak transients. Under an atmosphere of Ar, the photochemistry resulting from flash photolysis ($\lambda_{exc.}$= 355 nm), is more complex. CO loss is again observed, however the process is not completely reversible. A stable species is also formed. From the evidence available, this species is most likely a dimer formed from the transient species reacting with the parent complex, with a bridging carbonyl ligand. This general reaction is presented in Reaction 2.4

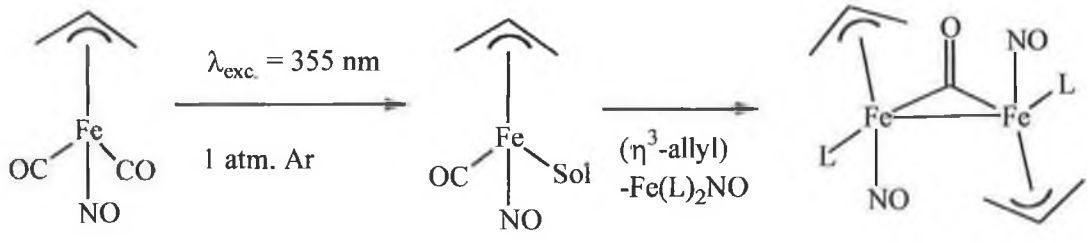

Reaction 2.4 Formation of dimer, observed upon flash photolysis ($\lambda_{exc.}$= 355 nm), of (η^3-allyl)Fe(L)$_2$NO type complex under 1 atm. Ar.

The photolysis ($\lambda_{exc.}$ > 300 nm) of (η^3-allyl)Fe(CO)NO(PPh_3) with excess PPh_3 , described in Section 2.4.1, resulted in CO substitution with formation of both (η^3-allyl)FeNO(PPh_3)$_2$ and (η^3-allyl)Fe(CO)NO. As previously described in Section 2.4.1 , evidence for a dimer of (η^3-allyl)Fe(CO)NO(PPh_3) was also proposed. This dimer was itself photolysed, decomposing to release "free" NO and other decomposition products as shown in Scheme 2.3. It would be useful to isolate the (η^3-allyl)FeNO(PPh_3)$_2$ generated in this reaction, in order to investigate its photochemistry more thoroughly.

The photochemistry of $Fe(NO)_2(PPh_3)_2$ was also investigated. The photochemical rearrangement of $Fe(NO)_2(PPh_3)_2$ from its tetrahedral form to a square-planar arrangement was observed. Matrix isolation studies of this compound may be useful in gaining a fuller understanding its photochemistry.

2.6 Bibliography

[1] Kunkely H.; Vogler A. *J. Photochem. Photobiol. A: Chem.* **1998**, 114, 197

[2] Coppens P.; Formitchev D. V.; Carducci M. D.; Culp K. *J. Chem. Soc. Dalton Trans.* **1998**, 865

[3] Crichton O.; Poliakoff M.; Rest A. J.; Turner J. J. *J. Chem. Soc. Dalton Trans.* **1973**, 1321

[4] Wang W.; Chen F.; Lin J.; She Y. *J. Chem. Soc. Faraday Trans.* **1995**, *91*, 847

[5] Chaudhari F. M.; Knox G. R.; Pauson P. L.; *J. Chem. Soc. (C)* **1967**, 2255.

[6] Cardaci G.; Foffani A. *J. Chem. Soc. Dalton Trans.* **1974**, 1808

[7] Bruce R.; Chaudhari F. M.; Knox G. R.; Pauson P. L. *Z. Naturforsch, B* **1965**, *20*, 73

[8] Murdoch H. D. *Z. Naturforsch, B* **1965**, *20*, 179

[9] Clarke H. L.; Fitzpatrick N. J. *J. Organomet. Chem.* **1974**, *66*, 119

[10] Horrocks W. D.; Taylor R. C. *Inorg. Chem.* **1963**, *2*, 273

[11] Fateley W. G.; Bent H. A.; Crawford Jr. B. *J. Chem. Phys.* **1959**, *31*, 204.

[12] Johnson B. F. G.; McCleverty J. A. *Progr. Inorg. Chem.* **1966**, *7*, 277.

[13] Malatesta L.; Araneo A. *J. Am. Chem. Soc.* **1957**, *79*, 3803.

[14] Albano V. G.; Araneo A.; Bellon B. L.; Ciani G.; Manassero M. *J. Organomet. Chem.* **1974**, *67*, 413

3 Experimental

3.1 Reagents

All reactions were carried out, using conventional glassware, in an anaerobic atmosphere using standard schlenk techniques. Purging with dry pure argon for 10-15 minutes, deoxygenated all solvents used. The following spectroscopic grade solvents were used without further purification: cyclohexane, dichloromethane, heptane, pentane, toluene, methanol and anhydrous diethyl ether (Aldrich Chemicals Co.). *p*-Xylene was distilled over CaF_2 from mixed xylenes, and used immediately. THF was distilled over sodium metal and benzophenone and used immediately. Argon and carbon monoxide were supplied by Air Products. $Fe(CO)_5$ (Aldrich Chemicals Co.) was used without further purification, and stored under argon at low temperature (0-4°C). Allyl bromide, 2, 3-dichloropropene, triphenylphosphine, and *bis*-diphenylphosphino ethane (all Aldrich Chemicals Co.) were used without further purification and stored under nitrogen. Silica gel used for chromatography was neutral silica gel, pH 6.5-7.5 (B. F. Merck)

3.2 Instrumentation

Infrared spectra were recorded on a Perkin Elmer 2000 FT-IR spectrometer using a 0.1mm sodium chloride solution cell. Infrared spectra were generally recorded in spectroscopic grade solvents such as cyclohexane, pentane, and chloroform. NMR (^1H

and ^{13}C) spectra were measured on a Bruker model AC400Hz spectrometer in appropriate deuterated solvents at room temperature. The peaks were calibrated according to the external tetra methyl silane (TMS) standard. UV/vis spectra were recorded on a Hewlett Packard 8452A photodiode array spectrometer using quartz cells of 1cm path length.

3.3 Synthesis of (η^3-allyl)$Fe(CO)_2NO$ type complexes

3.3.1 Synthesis of $[Fe(CO)_2NO]^-Na^+$

The synthesis of $[Fe(CO)_3NO]^-Na^+$ was carried out according to the method of Hieber.[1] Typically $Fe(CO)_5$ (2.5 ml, 18.6 mmol) and an equimolar quantity of finely ground $NaNO_2$ (1.3 g, 18.8 mmol) were added to a solution of sodium metal (1 g) dissolved in absolute methanol (99.98 %, 100 ml) in a round bottomed flask. The mixture was heated to reflux temperature (70 °C) for 1 hour under Ar in the dark. The reaction mixture turned from yellow to deep orange. After 1 hour, evolution of $Fe(CO)_5$ (yellow vapour) ceased, indicating completion of the reaction. The reaction mixture was filtered, and the solvent removed under reduced pressure. The filtrate was dissolved in anhydrous diethyl ether (40 ml). Half the volume of *p*-xylene (20 ml) was added. Diethyl ether was then removed under reduced pressure, until such time as $[Fe(CO)_3NO]^-Na^+$ precipitated. The mixture was then filtered under Ar, and $[Fe(CO)_3NO]^-Na^+$ collected. This process was repeated. Typical yield was in the range 80-90 %.

Spectroscopic data for $[Fe(CO)_3NO]^-Na^+$:- IR (methanol): ν_{CO} 1995, 1895 cm^{-1}; ν_{NO} 1658 cm^{-1}.

3.3.2 Synthesis of $(\eta^3\text{-}C_3H_5)Fe(CO)_2NO$

The synthesis of $(\eta^3\text{-}C_3H_5)Fe(CO)_2NO$ was carried out according to the method of Knox and Pauson with a few minor alterations.[2] Typically allyl bromide (0.7 ml, 7.7.mmol) dissolved in anhydrous diethyl ether (10 ml) was added to $[Fe(CO)_3NO]^-Na^+$ (1.5 g, 7.7 mmol) in diethyl ether (50 ml). The mixture was heated to 40 °C for 24 hours. The solution turned from orange to red. The mixture was filtered, and the solvent removed under reduced pressure, yielding a dark red oil. The oil was chromatographed on alumina. Elution with pentane yielded a deep red oil, $(\eta^3\text{-}C_3H_5)Fe(CO)_2NO$. Typical yield was in the range 70-80 %.

Spectroscopic data for $(\eta^3\text{-}C_3H_5)Fe(CO)_2NO$: IR (cyclohexane): ν_{CO} 2035, 1980 cm^{-1}; ν_{NO} 1756 cm^{-1}; ^1H NMR (d-chloroform, δ/ppm): 3.12 (d, 2H), 3.95 (d, 2H), 4.3 (m, 1H).

3.3.3 Synthesis of $(\eta^3$-2-chloroallyl$)Fe(CO)_2NO$

The synthesis of $(2\text{-}\eta^3\text{-}C_3H_4Cl)Fe(CO)_2NO$ was carried out according to the method of Cardaci with some minor modifications.[3] Typically equimolar amounts of 2,3-

dichloropropene (0.9 ml, 12 mmol) dissolved in anhydrous diethyl ether (10 ml) and $[Fe(CO)_3NO]^-Na^+$ (1.5 g, 7.7 mmol) were allowed to react in diethyl ether (50 ml). Reaction progress was monitored using IR spectroscopy. The mixture was heated to reflux for 24 hours. Subsequently, the mixture was filtered, and the solvent removed under reduced pressure, yielding a dark red oil. The oil was chromatographed on alumina. Elution with pentane yielded a deep red oil. Typical yield was in the range 65-70 %.

Spectroscopic data for (2-η^3-C_3H_4Cl)$Fe(CO)_2NO$: IR (cyclohexane): ν_{CO} 2045, 1993 cm^{-1}; ν_{NO} 1760 cm^{-1}; ^1H NMR (d-chloroform, δ/ppm): 3.80 (s, 2H), 4.36 (s, 2H).

3.3.4 Synthesis of (η^3-allyl)Fe(CO)NO(PPh_3)

The synthesis of (η^3-C_3H_5)Fe(CO)NO(PPh_3) was carried out according to the method of Knox and Pauson with a few minor alterations.[2] Typically triphenylphosphine (1.5 g, 6 mmol) was added to (η^3-C_3H_5)$Fe(CO)_2NO$ (1.1 g, 6 mmol) in cyclohexane (50 ml). The mixture was heated to reflux temperature for 48 hours. The mixture was then filtered, and the solvent removed under reduced pressure. The residue was chromatographed on silica gel. (η^3-C_3H_5)$Fe(CO)_2NO$ was eluted with pentane. Elution with dichloromethane-pentane (1:4) yielded (η^3-C_3H_5)Fe(CO)NO(PPh_3) as a red solid. Typical yield was in the range 50-60 %.

Spectroscopic data for (η^3-C_3H_5)Fe(CO)NO(PPh_3): IR (cyclohexane): ν_{CO} 1945 cm^{-1}; ν_{NO} 1710 cm^{-1}; ^1H NMR (d-chloroform, δ/ppm): 2.80 (d, 2H), 3.59 (d, 2H), 5.2 (m, 1H), 7.39 (m, 15H).

3.3.5 Synthesis of (η^3-allyl)FeNO(PPh_3)$_2$

The synthesis of (η^3-C_3H_5)FeNO(PPh_3)$_2$ was attempted so as to investigate if the product observed from photolysis of (η^3-C_3H_5)Fe(CO)NO(PPh_3) with PPh_3 was indeed (η^3-C_3H_5)FeNO(PPh_3)$_2$. Triphenylphosphine (3.0 g, 12 mmol) was added to (η^3-C_3H_5)Fe(CO)NO(PPh_3) (2.5 g, 6 mmol) in *n*-heptane (50 ml). The mixture was heated to reflux temperature for 5 days. The progress of the reaction was monitored using IR spectroscopy until such time that most of the starting material had been consumed. The solvent was removed under reduced pressure. A portion of the residue was chromatographed on silica gel. Elution with dichloromethane-pentane (1:4) yielded (η^3-C_3H_5)Fe(CO)NO(PPh_3) as a red solid. Another darker red band was observed but could not be eluted. The product from photolysis experiments was insoluble in non-polar solvents. The remaining solid was washed with pentane a number of times, to isolate (η^3-C_3H_5)FeNO(PPh_3)$_2$. Identification of (η^3-C_3H_5)FeNO(PPh_3)$_2$ was determined by IR, ^1H and ^{13}C NMR spectroscopy. The recorded yield was less than 3 %.

Spectroscopic data for (η^3-C_3H_5)FeNO(PPh_3)$_2$: IR (chloroform): ν_{NO} 1717, 1669 cm^{-1}; ^1H NMR (d-chloroform, δ/ppm): 2.74 (s, 2H), 3.58 (s, 2H), 7.41 (m, 12H), 7.48 (d, 6H),

7.60 (q, 12H); ^{13}C NMR (d-chloroform, δ/ppm): 133.8, 133.6, 132.4, 129.8, 34.5, 22.8, 14.5

3.3.6 Attempted synthesis of (η^3-allyl)FeNO(DPPE)

The synthesis of (η^3-C_3H_5)FeNO(DPPE) (diphenyldiphosphinoethane) was attempted to investigate whether the photochemical reaction of (η^3-C_3H_5)$Fe(CO)_2NO$ with DPPE yielded (η^3-allyl)FeNO(DPPE) rather than the CO insertion product of but-3-enoyl Fe(CO)DPPE(NO), analogous to reported reactions of substituted (η^3-allyl)$Fe(CO)_2NO$ complexes.[3] DPPE (1.0 g, 2.5 mmol) was added to (η^3-C_3H_5)$Fe(CO)_2NO$ (0.45 g, 2.5 mmol) in cyclohexane (20 ml) in a round-bottomed flask which was continuously purged with Ar, to allow removal of evolved CO. The flask was placed in front of the xenon arc lamp (described below), fitted with a Corning filter ($\lambda_{exc.} > 300nm$). Water filters were used to prevent thermal reactions in the flask. The reaction was monitored using IR spectroscopy. The mixture was photolysed for 5 hours, as after such time the absorbance of the (η^3-allyl)$Fe(CO)_2NO$ bands had decreased completely, with no evidence for formation of (η^3-allyl)FeNO(DPPE).

3.4 Synthesis of $Fe(NO)_2(L)_2$ type complexes

3.4.1 Synthesis of $Fe(NO)_2(CO)_2$

The synthesis of $Fe(NO)_2(CO)_2$ was carried out according to the method of Hieber with some minor modifications.[4] $Fe(CO)_5$ (2.5 ml, 19 mmol) was added to an alkali solution of NaOH (100 ml, 1.25 M). An excess of $NaNO_2$ (1.85 g, 27 mmol) was added, and the mixture heated to reflux temperature. After 4 hours, the volatile $Fe(CO)_5$ was no longer observed in the reflux condenser, indicating completion of the reaction, forming $[Fe(CO)_3NO]^-$. The reaction flask was cooled to 30-40 °C. Acetic acid (0.625 M) was added until evolution of gas was observed. The reaction was left for 1 hour to allow complete evolution of CO and CO_2, and formation of $Fe(CO)_2(NO)_2$. $Fe(CO)_2(NO)_2$ was removed from the solvent by sublimation at reduced pressure at 0°C. Typical yield was in the range 80-90 %.

Spectroscopic data for $Fe(CO)_2(NO)_2$: IR (cyclohexane): ν_{CO} 2084, 2036 cm^{-1}; ν_{NO} 1811, 1768 cm^{-1}.

3.4.2 Synthesis of bis-*$Fe(NO)_2(PPh_3)_2$*

The synthesis of $Fe(NO)_2(PPh_3)_2$ was carried out according to the method of Malatesta with slight modifications.[5] Typically, a concentrated toluene (10 ml) solution of PPh_3 (2.6 g, 9.9 mmol) was added to $Fe(CO)_2(NO)_2$ in an inert atmosphere. The solution was

stirred at room temperature overnight, with evolution of CO gas. An equal volume of absolute methanol (10 ml) was added and $Fe(CO)_2(PPh_3)_2$ precipitated. This product was filtered off and chromatographed on silica gel. PPh_3 was eluted with toluene-pentane (1:9). Elution with toluene-pentane (1:4) yielded $Fe(NO)_2(PPh_3)2$. Yield was typically in the range 50-60 %.

Spectroscopic data for $Fe(NO)_2(PPh_3)_2$: IR (cyclohexane): ν_{NO} 1727, 1685 cm^{-1}; ^1H NMR (d-acetone, δ/ppm): 7.08 (2H), 7.18 (2H), 7.25 (1H).

3.4.3 Synthesis of $Fe(NO)_2(DPPE)$

$Fe(NO)_2(DPPE)$ was synthesised according to the method of Stafford, with some modifications.[6] This involved the equimolar reaction of $Fe(CO)_2(NO)_2$ (0.5 g, 3 mmol) and DPPE (1.2 g, 3 mmol) in cyclohexane at 40 °C for a period of 12 hours. Formation of $Fe(NO)_2(DPPE)$ was not observed. The mixture was then heated to reflux temperature for 6 hours. The solvent was removed at reduced pressure. The residue was chromatographed on silica gel. $Fe(NO)_2(DPPE)$ was eluted with acetonitrile-pentane (1:9). Yield was in the range 10-20 %.

Spectroscopic data for $Fe(NO)_2(DPPE)$: IR (acetonitrile): ν_{NO} 1714, 1668 cm^{-1}; ^1H NMR (d-chloroform, δ/ppm): 2.17 (s, 2H), 7.35 (m, 12H), 7.39 (s, 8H).

3.5 Laser flash photolysis –sample preparation

Laser flash photolysis samples were prepared in a specially designed, sealable degassing bulb attached to a fluorescence cell. Samples are prepared by dissolution in the appropriate spectroscopic grade solvent, such that the absorbance at $\lambda_{exc.}$ (532, 355, or 266 nm) was between 0.6 and 1.0 AU. The sample was then degassed by three cycles of the freeze-pump-thaw procedure to a pressure of 10^{-3} torr. Subsequently, liquid pumping of the sample is carried out to ensure that any trace impurities such as water are removed.

The atmosphere of interest, either CO or Ar is then placed over the sample The pressure of CO admitted into the flash photolysis cell at this point determines the concentration of CO. The solubility of the CO in cyclohexane was taken to be 9.0×10^{-3} in 1 atm. of CO.[7] Spectra were recorded before and after degassing the sample to ensure that no changes had taken place. Additionally, spectra were recorded throughout the flash photolysis experiments in order to monitor spectral changes, should they occur.

3.6 Laser flash photolysis instrumentation

The excitation source was a neodymium yttrium aluminium garnet (Nd-YAG) laser from Spectron Laser, operating at 1064 nm. Nd atoms are implanted in the host YAG crystals at a rate of approximately one per hundred. The YAG host material has the advantage of

having a high thermal conductivity to remove the wasted heat. This allows the crystals to be operated at high repetition rates of the order of many pulses per second. The frequency of 1064 nm may be doubled, tripled, or quadrupled using non-linear optics to generate a second, third or fourth harmonic frequency of 532 nm, 355 nm, or 266 nm respectively. The different harmonics may allow different atomic processes to be selected preferentially. The power of the laser may be amplified by applying different voltages across the amplifier flash tube. The duration of the laser pulse is in the region of 10ns. The energy of the pulse generated for the 266 nm, 355 nm and 532 nm frequencies is typically approximately 55 mJ, 45 mJ and 25 mJ respectively.

The circular laser pulse is directed onto the sample cuvette. As the pulse passes through the power meter, situated directly before the sample, the oscilloscope is triggered. The monitoring light source is an air-cooled Applied Photophysics medium pressure xenon arc lamp (300 W). This is arranged at right angles to the laser beam. The monitoring beam passes through the sample and is directed to the entrance slit of an Applied Photophysics f/3 monochromator via a circular lens. Generally UV/vis filters (Corning) are used to block higher energy photons, thus preventing excessive photo-degradation of the sample, and allowing wavelength selection. A Hamatsu 5 stage photomultiplier tube operating at 850 V was placed at the exit slit of the monochromator. The changes in absorbance were measured by a transient digitiser via a variable load resistor. The digitiser, a Hewlett Packard HP 54510A oscilloscope was interfaced to a personal computer. The signals were recorded and interpreted using a purpose designed software program which has been previously described.[8]

A typical transient signal was recorded in the following manner; the sample was placed in the cuvette holder and the amount of light transmitted through the solution by the monitoring beam before the flash, I_o, was recorded. This is the voltage corresponding to the amount of light detected by the photomultiplier tube when the source shutter opens, less the voltage due to stray light. The monitoring source is opened while simultaneously firing the laser pulse through the sample cuvette and the amount of transmitted light is recorded, I_t. As I_o/I_t = absorbance, the change in the intensity of the monitoring beam transmitted through the sample may be recorded as a function of time and/or wavelength.

By recording transient signals over a range of wavelengths, absorbance readings may be calculated at any time after the flash to generate a difference absorption spectrum of the transient species. Spectra are obtained as a result of point-by-point build up manually changing the wavelength of the monochromator. It is necessary that the solution is optically transparent for the monitoring light beam, hence solvents such as cyclohexane and pentane, which are spectroscopically transparent, are used. A schematic diagram of the laser flash photolysis apparatus is shown below in Figure 3.1.

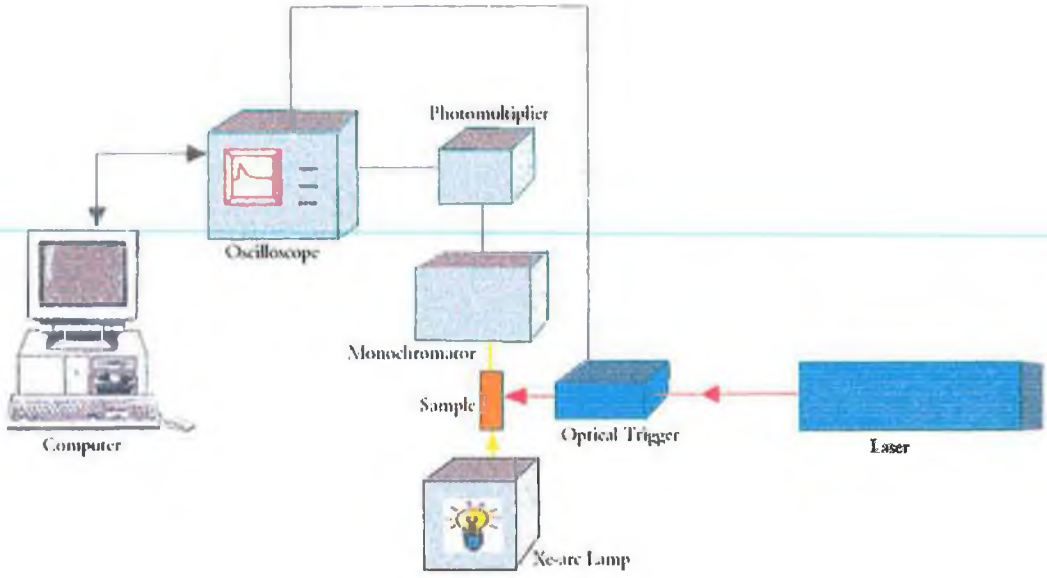

Figure 3.1 Schematic diagram of the instrumentation set-up used in laser flash photolysis experiments.

3.7 Matrix isolation instrumentation

As previously explained in Section 1.3, matrix isolation involves the trapping of molecules or atoms in a solidified inert gas, a technique which by definition requires very low temperatures. Matrix isolation as a technique for the study of organometallic intermediates offers a number of advantages. The complete transparency from the far infrared to the near vacuum ultraviolet, and rigidity at a suitably low temperature (4-20 K) are the two main advantages, along with chemical inertness. Molecules that might have as low a lifetime as 10^{-8} s under standard conditions are stable in matrices in their ground electronic and vibrational states. The instrumentation required is described in more detail elsewhere,[9] however a brief explanation is given here.

Pimentel was the first to carry out matrix isolation experiments in solidified noble gasses,[10] superseding the earlier method of Lewis and co-workers in the 1930's of using low temperature organic glasses.[11] These glasses were made up of a mixture ethanol, ether and *iso*-pentane and formed glasses at 77 K using liquid nitrogen. The glasses formed were transparent throughout the ultraviolet/visible region. Unfortunately the organic glasses are not chemically inert to reactive species such as metal atoms and they also absorb over the complete infrared region. The technique of matrix isolation has evolved into an analytical tool suited to a vast expanse of applications, depending on detection mode employed.

In matrix isolation the matrix is formed by deposition from the gas phase onto a cold window, held at typically 12 K. There are 2 ways of mixing the guest species with the host gas. If the guest species has a convenient, measurable vapour pressure, it can be mixed with the host gas on a vacuum line by standard manomeric techniques. This produces a gas mixture of known proportion. The ratio of host to guest is known as the matrix ratio. The gas mixture is then passed into the vacuum chamber of the cold cell at a controlled rate and is deposited onto the cold cell window as a solid matrix.
If the guest has a low volatility, as is generally the case for metal carbonyls and nitrosyls, it is usual to evaporate it from a side arm attached to the vacuum chamber of the cold cell, while simultaneously allowing the host gas into the chamber at an appropriate rate. This allows the guest to condense on the cell window with the host gas being deposited simultaneously.

For matrix isolation studies equipment essential for construction of a system is as follows:

- refrigeration system
- vacuum chamber
- vacuum pumping system
- sample holder
- gas handling system
- method for generation of the species of interest e.g. UV lamp
- method for analysis of species generated.

3.7.1 The refrigeration system

The refrigerator consists of a compressor unit connected to a compact expander unit or head module by high pressure (feed) and low pressure (return) helium. The head module is small and light enough to be incorporated into matrix cells for use with a wide variety of instrumentation. The helium is compressed and then allowed to expand within the head module. The expansion of the helium causes the cooling effect. The choice of coolant gas and choice of host gas control the temperature limits of the matrix system. A cryostat from APD Cryogenics Inc. was used in the experiments described.

3.7.2 The vacuum chamber; the shroud.

With the matrix sample held at 12 K, it needs to be enclosed in a vacuum chamber, the shroud. The shroud must have the following features:

- at least one inlet port to facilitate deposition of matrix must be provided
- external windows appropriate to the spectroscopic technique being used
- the shroud should fit into the sample compartment of the spectrometer being used
- the interior of the shroud should be conveniently accessible at standard pressure, to facilitate cleaning of the sample window and surrounding parts
- the head module should be attached to the shroud using a seal, which can be rotated, allowing the sample window to be rotated within the shroud
- the shroud must be connected the vacuum system.

3.7.3 The vacuum system.

The shroud enclosing the head module of the refrigerator must be evacuated to insulate the cold sample from warming by convection and conduction (Dewar vacuum). Pressures around 10^{-3} millibarr are sufficient to provide an efficient vacuum, however to minimise contamination, the highest achievable vacuum is required. A vacuum system of about 10^{-7} torr inside the sample chamber, when the cold window is at its experimental temperature (12 K) is required in all experiements. This vacuum was achieved by using an oil defusion pump backed by a 5 stage rotary pump from Edwards High Vacuum International.

3.7.4 The sample holder

The sample holder is connected to the lower heat station of the refrigerator. It is crucial that the sample holder is made of a material that will be a good conductor at very low temperatures. Copper is the most cost-effective material for the metal part of the sample holder. In these experiments the window onto to which the matrix is deposited was made from CaF_2. Other materials used are CsBr, CsI, NaCl or KBr. The caesium based windows are less brittle, and so do not deform as easily.

3.7.5. Gas handling system

The gases used were of very high purity from standard metal cylinders, supplied by Cryoservice Ltd. These were connected to regulators suitable for high purity gases, fitted with a flow control valve on the outlet, also supplied by Cryoservice Ltd. This allowed deposition of the matrix host at a controlled rate. Gas mixtures may be made up using a subsidiary gas handling line, increasing the risk of error, but greatly reducing the preparation time.

3.7.6 Generation of transients

The most common methods of generating reactive species are photolysis and pyrolysis. Photolysis was the chosen method in this study. A variety of light sources have been reported from tungsten filament bulbs to lasers The most versatile light sources are probably high or medium pressure mercury arc lamps, with outputs in the range 200-1000 W and 150-200 W respectively. The monitoring light source used was an air-cooled Oriel Instruments medium pressure xenon arc lamp (300 W), similar to that used in the laser flash photolysis experiments.

3.7.7 Analysis of species generated

As previously mentioned, a wide range of detection methods have been applied to the study of matrices, including IR, UV/vis , Raman, electron spin resonance, magnetic

circular dichromism, fluorescence, and Mössbauer spectroscopy. In this study, only IR spectroscopy was used to analyse the species generated, with spectra recorded on a Perkin Elmer Spectrum One spectrometer.

3.7.8 Preparation of typical sample

As the samples were oil based or solids, they were dissolved in a minimum of spectroscopic grade pentane and transferred a glass side arm. The solvent was then removed under reduced pressure. The side arm was then attached to the lower part of the shroud, close to the cold window. The spray-on gas line is then connected to the shroud. The system is brought to the required vacuum (~10^{-5} torr.) and deposition temperature (12 K). A specific volume of the required matrix gas is allowed into the gas handling line. This is then co-condensed onto the cold window with the sample. A gauge on the gas handling line controls the rate of deposition of the matrix gas. Varying the temperature of the sample in the side arm controls the rate of sample deposition. The amount of sample deposition was monitored periodically, using IR spectroscopy, until the maximum absorbance of the sample was between 0.8 and 1.0 AU in the carbonyl region.

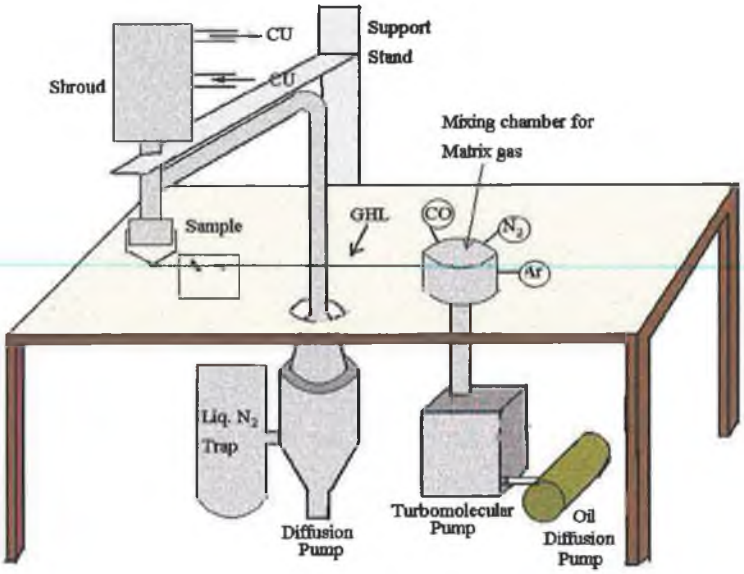

Figure 3.2 Schematic diagram of Matrix instrumentation. **CU** is Compressor Unit. **GHL** is Gas Handling Line. Pirani and other pressure gauges are not shown.

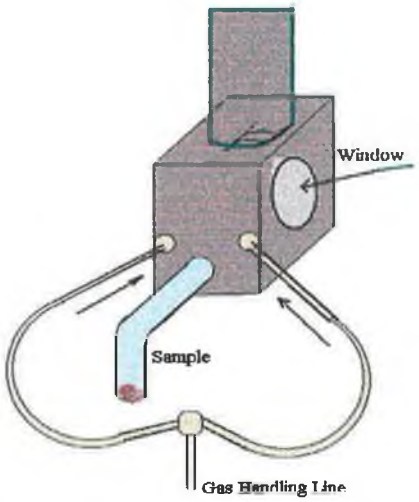

Figure 3.3 Schematic diagram of the matrix isolation cold cell.

3.8 Bibliography

[1] Hieber W.; Beuttner H. *Z. Naturforsch.* **1960**, *15b*, 101.

[2] Chaudhari F. M.; Knox G. R.; Pauson P. L.; *J. Chem. Soc. (C)* **1967**, 2255.

[3] Cardaci G.; Foffani A. *J. Chem. Soc. Dalton Trans.* **1974**, 1808.

[4] Hieber W.; Beuttner H. *Z. Anorg. Allg. Chem.* **1963**, *320*, 101.

[5] Malatesta L.; Araneo A. *J. Am. Chem. Soc.* **1957**, *79*, 3803.

[6] McBride D. W.; Stafford S. L.; Stone F. G. A. *Inorg. Chem.* **1962**, *1*, 386.

[7] Makrancy J. Megyery-Balog K.; Rosz L.; Patyt D. *J Ind. Chem.* **1976**, *4*, 269.

[8] Crocock B. *PhD. Thesis*, Dublin City University, **1994.**

[9] Duncan I. R. *"Matrix Isolation Techniques, A Practical Approach"*, Oxford University Press:London, **1998.**

[10] Whittle E.; Dows D. A.; Pimentel G. C. *J. Chem. Phys.* **1954**, *22*, 1943.

[11] Lewis G. N.; Lipkin D. *J. Am. Chem. Soc.* **1942**, 64, 2801.